An integrated proteomic and metabolomic approach to investigate cerebral ischemic preconditioning

Thesis

An integrated proteomic and metabolomic approach to investigate cerebral ischemic preconditioning

Thesis submitted for the Degree of Doctor of Philosophy

at the Open University, UK

Discipline of Life and Biomolecular Sciences

Giacomo Scornavacca

Personal identifier: A9813566

Degree in Pharmaceutical Chemical Technologies

IRCCS-Istituto di Ricerche Farmacologiche "Mario Negri"

Milan, Italy

September, 2013

The molecular mechanism that leads to ischemic preconditioning and hence to ischemic tolerance, are not completely understood although it is clear that multiple effectors and pathways contribute to the instauration of this neuroprotective profile. To study the mechanism/pathway involved in the ischemic tolerance, brain proteins, plasma proteins and plasma metabolites were analyzed in preconditioning stimulus (7'Middle Cerebral Artery occlusion or 7'MCAo), in severe stroke (permanent Middle Cerebral Artery occlusion or pMCAo) and in preconditioned (7'MCAo/pMCAo) mouse model.

A conventional 2-DE approach was used to study technical replicates of pooled brain proteins revealing an involvement of energy metabolism, mitochondrial electron transport, synaptic vesicle transport and antioxidant processes; moreover network analysis suggested an involvement of the androgen receptor that was validated on technical replicates of pooled brain proteins by western blot analysis revealing an increased expression in preconditioned stimulus animals (7'MCAo).

Plasma proteins were analyzed using a 1-DE LC-MS/MS approach on technical replicates of pooled plasma proteins revealing decreased levels of epidermal growth factor receptor (EGFR) and increased levels of insuline like growth factor acid labile subunit (IGFALS), which expression was paralleled by increased insulin like growth factor 1 (IGF1) plasma concentration, as validated by ELISA on biological replicates, in preconditioning stimulus animals (7'MCAo).

Finally an untarget metabolomics analysis was applied to technical replicates of pooled plasma proteins revealing fatty acid oxidation and branched-chain aminoacid metabolism as the main biological processes modulated in ischemic tolerance and highlighted an involvement of the aminoacid leucine, carnitine esters and adenosine.

The correlation of all the omics data obtained, indicates androgen receptor as an important mediator able to interact with brain and plasma proteins and plasma metabolites involved in brain ischemic tolerance.

The results described in this thesis represents the first application of both proteomic and metabolomic approaches in cerebral ischemic sets, highlighting the cross-talk between proteins and metabolites and adding new evidence to the current knowledge on ischemic preconditioning that may represent a starting point for future experiments on investigating candidate pathways that relate to Androgen receptor.

INDEX

LIST OF FIGURES

LIST OF TABLES

ABBREVIATIONS

1-DE	one-dimensional electrophoresis
2-DE	bi- dimensional electrophoresis
7'MCAo	7' transient middle cerebral artery occlusion (preconditioning stimulus)
7'MCAo/pMCAo	combination of preconditioning and severe ischemia
ALDOC	Fructose-biphosphate aldolase C
AR	Androgen receptor
CID	collision induced dissociation
DLDH	Dihydrolipoyl dehydrogenase
EGFR	Epidermal growth factor receptor
ESI	electrospray ionization
GLNA	glutamine synthetase
GSTM1	Glutathione *S*-transferase M1
GSTP1	Glutathione *S*-transferase P1
ICAT	isotope-coded affinity tags
IEF	isoelectrofocusing
IGF-1	Insuline like growth factor 1
IGFALS	Insuline like growth factor binding protein complex acid labile subunit
HSP70	Heat shock protein 70
IPC	ischemic preconditioning
IT	ischemic tolerance
iTRAQ	isobaric tags for relative and absolute quantitation
LC-MS/MS	liquid chromatography-tandem mass spectrometry

LTQ	linear quadrupole trap
MW	molecular weight
pMCAo	permanent middle cerebral artery occlusion (severe ischemia)
SILAC	stable-isotope labeling in cell culture
SOD2	Superoxide dismutase 2
DHSA	Succinate dehydrogenase
TIA	transient ischemic attack

CHAPTER 1

INTRODUCTION

1.1. ISCHEMIC STROKE

Ischemic stroke is characterized by a sudden interruption of the cerebral blood flow due to an occlusion of a cerebral vessel, and accounts approximately for 80% of all cases of stroke (Stoll, Kleinschnitz *et al.* 2008). The ischemic brain injury is a global health problem, representing the third leading cause of morbidity and mortality in Western countries. Globally there are 50 million survivors of stroke and transient ischemic attack, of whom 20% will suffer a subsequent stroke in the following 5 years, and 15-20% suffer permanent disability (Adams 1993; Lloyd-Jones, Adams *et al.* 2010).

Ischemic brain injury results from a complex sequence of pathophysiological events that evolve over time and space. The main pathogenic mechanisms include excitotoxicity, peri-infarct depolarisations, inflammation and apoptosis (Dirnagl, Iadecola *et al.* 1999) (Figure.1.1).

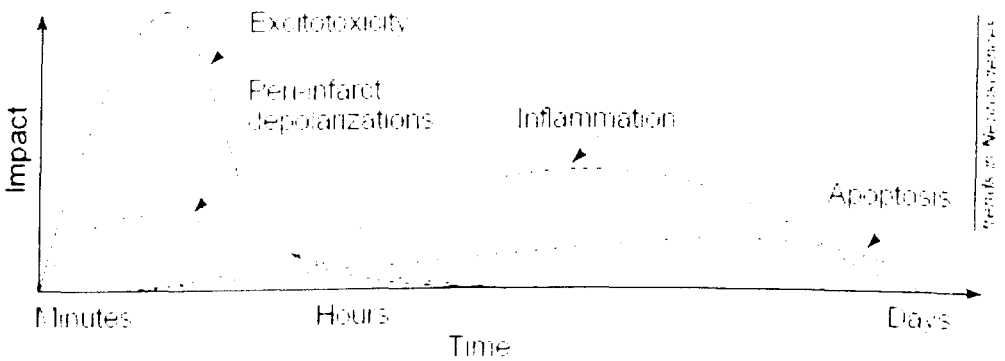

Figure 1.1. Temporal cascade of the main pathogenic events in stroke (adapted from Dirnagl, Iadecola *et al.* 1999).

1.1.1. Mechanisms of ischemic stroke

1.1.1.1. Excitotoxicity

A large amount of oxygen is required by the brain to generate sufficient ATP by oxidative phosphorylation to maintain and restore ionic gradients. When blood flow is reduced, there is

an inhibition of ATP synthesis that leads to ionic deregulation and neuronal plasma membrane depolarization. This depolarisation causes the release of the excitatory neurotransmitter glutamate, the activation of *N*-methyl-D-aspartate (NMDA), alpha-amino-3-hydroxy-5-methyl-4-isoxazolepropionic acid (AMPA), metabotropic glutamate receptors, and an increase in the level of intracellular calcium with the activation of many calcium-dependent proteases. These enzymes degrade cytoskeletal and extracellular matrix proteins, and also activate phospholipase A2 and cyclooxygenase. This leads to the generation of free-radical species that overwhelm endogenous scavenging mechanisms, producing lipid peroxidation, membrane damage, mitochondrial impairment, and finally activation of inflammatory system and induction of apoptosis (Figure1.2).

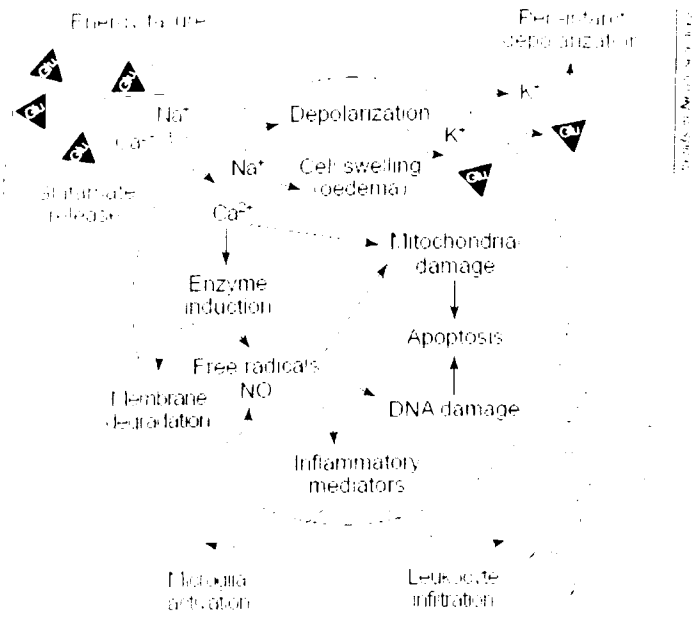

Figure 1.2. Simplified scheme of pathophysiological mechanisms of stroke (adapted from Dirnagl, Iadecola *et al.* 1999).

Peri-infarct depolarizations are spontaneous waves of depolarization that propagate through the penumbra following focal stroke. Peri-infarct depolarization may be caused by the release of potassium and excitatory amino acids from the ischemic core and are associated with

increased ischemic injury. Fabricius and colleagues (Fabricius, Fuhr *et al.* 2006) demonstrated the existence of peri-infarct depolarization in the acutely injured human brain, suggesting the therapeutic use of hypothermia or glutamate receptor antagonism to limit the development of ischemic injury within the penumbra.

Inflammation contributes to stroke-related brain injury. The inflammatory response is a composite process that involves many different cell types, inflammatory mediators and extracellular receptors.

Increased levels of Ca^{2+}, and free-radical species, activate pro-inflammatory genes that induce the synthesis of transcription factors and hence the production of mediators of the inflammations, such as cytokines.

Cytokines and chemokines, in turn, contribute to stroke-related brain injury (Gong, Qin *et al.* 1998).

During ischemia a variety of activated cell types (*i.e.* endothelial cells, microglia, neurons, platelets, leukocytes, fibroblasts) induces the production of cytokines (IL-1, IL-6, TNF-α, TGF-β) and chemokines such as CINC and MCP-1 (Huang, Upadhyay et al. 2006) (Figure 1.3). After permanent or transient cerebral ischemia in microglia, astrocytes, and neurons there is an increased production of IL-1. The exact role of IL-1 in propagating tissue damage is unclear, although it's possible deleterious effects include fever, arachidonic acid release, enhancement of NMDA-mediated excitotoxicity, and stimulation of nitric oxide synthesis (Huang, Upadhyay *et al.* 2006). The biological activity of IL-6 overlaps with that of IL-1, and data from human studies suggest a pro-inflammatory role for IL-6 in stroke. The level of IL-6 in peripheral blood is higher in stroke patients and detectable within a few hours of stroke onset. Further, higher CSF and serum levels of IL-6 correlate with larger infarct size and poorer clinical outcome (Huang, Upadhyay *et al.* 2006). However, IL-6 also has anti-inflammatory properties due to its ability to induce IL-1 receptor antagonist synthesis (Relton, Martin *et al.* 1996) therefore the

role of IL-1 in the context of stroke is still unclear. Up-regulation of TNF-α mRNA parallels that of IL-1 and IL-6 mRNA within the first hours after ischemia (Huang, Upadhyay *et al.* 2006). Both experimental and human data indicate a positive correlation between TNF-α and the extent of ischemic injury. Like IL-1, TNF-α induces the expression of adhesion molecules in cerebral endothelial cells and promotes the accumulation and transmigration of neutrophil. In addition, TNF-α stimulates the production of acute-phase proteins, disrupts the blood-brain barrier and stimulates the induction of other inflammatory mediators in rats. It was observed that the administration of TNF-α neutralizing antibody reduces brain injury after focal ischemia suggesting a TNF-α-targeted therapies for stroke treatment (Nawashiro, Martin *et al.* 1997). Growing evidence suggests that TGF-β plays a neuroprotective role in the pathogenesis of stroke (Huang, Upadhyay *et al.* 2006). It is likely that the neuroprotective effect of TGF-β is the concerted result of the activation of several neuroprotective pathways. Cytokines induces the expression of three classes of cell adhesion molecules: selectins, integrins, and immunoglobulins (Huang, Upadhyay *et al.* 2006). These adhesion molecules mediate the transmigration of neutrophils in the brain as early as 30 min after permanent middle cerebral artery occlusion (MCAo). The recruitment of neutrophils to the ischemic brain begins with neutrophil rolling on activated endothelial blood vessel walls, mediated by selectins, followed by neutrophil activation and adherence, mediated by integrins and immunoglobulins (Figure 1.3). When adhered to cerebral blood vessel walls, neutrophils transmigrate into the cerebral parenchyma, a process facilitated by disruption of the blood-brain barrier (BBB). The recruitment of neutrophils can obstruct the microcirculation and prevent complete restoration of cerebral blood flow after reperfusion. This blockage may cause further tissue damage after ischemia and is described as the ischemic no-reflow phenomenon (Huang, Upadhyay *et al.* 2006). Once neutrophils penetrate into the ischemic brain they cause tissue damage by releasing reactive oxygen species and proteolytic enzymes. Lymphocytes also appear to be responsible for mediating damage in response to brain ischemia. Although lymphocytes are

ordinarily excluded from the CNS, they appear within 24h in post ischemic brain (Schroeter, Jander *et al.* 1994). While the mechanism producing their infiltration into the brain remains unclear, it is likely that disruption of the BBB plays a major role in the influx, either by directly allowing the free movement of lymphocytes, or by leakage of brain antigens resulting in the transmigration of activated lymphocytes that could contribute to development of the lesion.

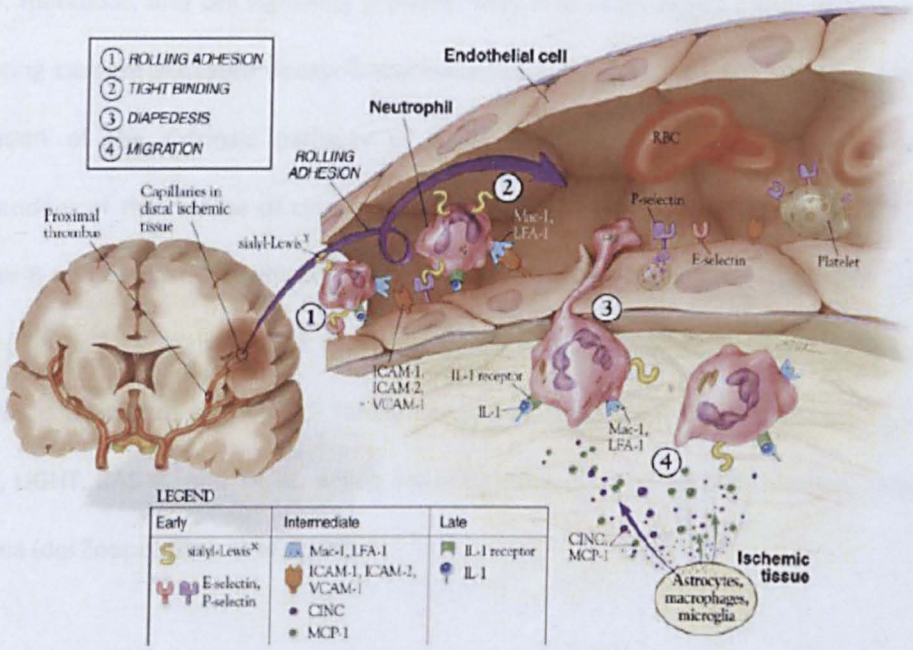

Figure 1.3. Inflammatory cascades following vessel occlusion (adapted from Huang, Upadhyay *et al.* 2006). Abbreviations used: Integrins macrophage-1 antigen (Mac-1); lymphocyte function-associated-1 antigen (LFA-1); intercellular adhesion molecule-1 and -2 (ICAM-1, ICAM-2), vascular cell adhesion molecule-1 (VCAM-1); neutrophil chemoattractant (CINC), interleukin-1(IL-1), Monocyte chemoattractant protein-1(MCP-1).

1.1.1.4. Apoptosis

Mild ischemic injury preferentially induces cell death via an apoptotic-like mechanism rather than necrosis. Because the ischemic penumbra sustains milder injury and preserves ATP, apoptosis predominates in this region (Kerr, Wyllie *et al.* 1972). Triggers of apoptosis include reactive oxygen species, death receptor ligation, DNA damage, protease activation and ionic imbalance. Subsequent to mitochondrial impairment, Cytochrome C is released and enters the

cytosol from its location on the external side of the inner mitochondrial membrane, and in presence of dATP activates an apoptosome complex [apoptosis-activating factor (APAF1) plus pro-caspase 9] (Green and Reed 1998). The formation of the apoptosome complex, which is suppressed by Bcl-xL, a protein of the Bcl-2 family, promotes clipping and activation of caspases 3 and 7, which are aspartate-specific cysteine proteases that exist as zymogens in cells. These caspases induce the dismantling of the cell by cleaving homeostatic, cytoskeletal, repair, metabolic, and cell signalling proteins; they also cause further DNA fragmentation by activating caspase-activated deoxyribonuclease (CAD) by cleaving the inhibitor protein ICAD. Activation of the extrinsic pathway of death receptors can induce caspase activation independent of the release of cytochrome C. Death receptor ligation results in activation of caspase-8 and caspase-10, which in turn can activate effector caspase 3 (Namura, Zhu *et al.* 1998) (Figure 1.4). Activation of death receptors such as Fas/CD95, TNFR1, and the TRAIL receptor is promoted by the TNF family of ligands, including FASL, TNF, LT-alpha, LT-beta, CD40L, LIGHT, RANKL, and TRAIL, which are released as part of the inflammatory response to ischemia (del Zoppo, Ginis *et al.* 2000).

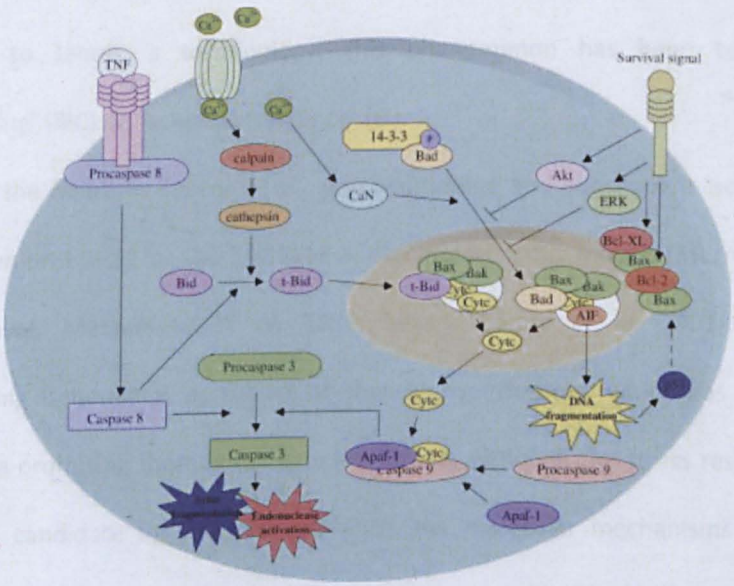

Figure 1.4. Apoptosis pathway activated during stroke (adapted from Doyle, Simon et al. 2008).

1.2. PRECONDITIONING

In 1964 Janoff introduced the terms 'tolerance' and 'preconditioning', referring to an organism that responds with protective mechanisms to potentially recurring challenges (Janoff 1964). Practically any stimulus capable of causing injury can, when applied close to (but below) the threshold of damage, protect the brain against subsequent ischemia (Figure 1.5).

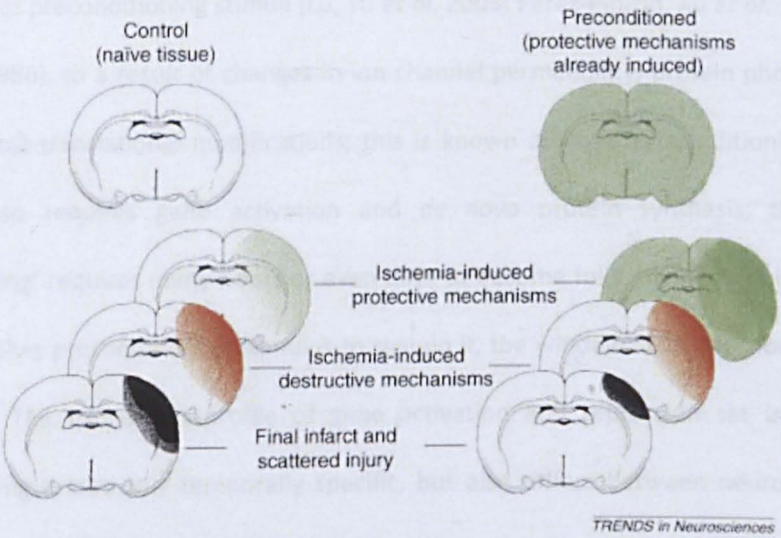

Figure 1.5. Brain preconditioning (adapted from Dirnagl, Simon *et al.* 2003).

By analogy to Janoff 's terminology, this phenomenon has been termed 'ischemic preconditioning' (IPC) or 'ischemic tolerance' (IT).

Identified in the heart by Murry *et al.*, preconditioning and subsequent ischemic tolerance were then demonstrated for the first time in cerebral ischemia models (Murry, Jennings *et al.* 1986; Kitagawa, Matsumoto *et al.* 1990; Kirino, Tsujita *et al.* 1991). The effect of preconditioning ischemia is as robust as that of hypothermia, which has attracted much attention as a promising therapy for ischemic stroke. Although the stress response had been considered a candidate for induced tolerance, the molecular mechanisms underlying this phenomenon are much more complex than initially expected (Kirino 2002; Dirnagl, Simon et al. 2003; Dirnagl, Becker et al. 2009; Gidday 2006). Amongst various brain regions, the

hippocampus, cerebral cortex, basal ganglia and thalamus were often reported to acquire ischemic tolerance (Kitagawa, Matsumoto *et al.* 1991).

Preconditioning triggers a fundamentally different adaptive response and, in mammals, this response is characterized by at least two distinct time frames of induced tolerance relative to the preconditioning stimulus and the subsequent ischemia: a rapid phase and a delayed phase (Figure 1.6). A short-lasting protective phenotype (rapid phase) can be induced within minutes of exposure to preconditioning stimuli (Lu, Yu *et al.* 2005; Perez-Pinzon, Xu *et al.* 1997; Schurr, Reid *et al.* 1986), as a result of changes in ion channel permeability, protein phosphorylation and other post-translational modifications; this is known as rapid preconditioning. Ischemic tolerance also requires gene activation and *de novo* protein synthesis; this 'classical preconditioning' requires many hours or even days to become fully manifest (delayed phase). Without another preconditioning stimulus to sustain it, the window for protection also wanes within days. The expression profile of gene activation and repression set in motion by preconditioning is not only temporally specific, but also differs between neurons, glia and endothelial cells (Dirnagl, Becker *et al.* 2009).

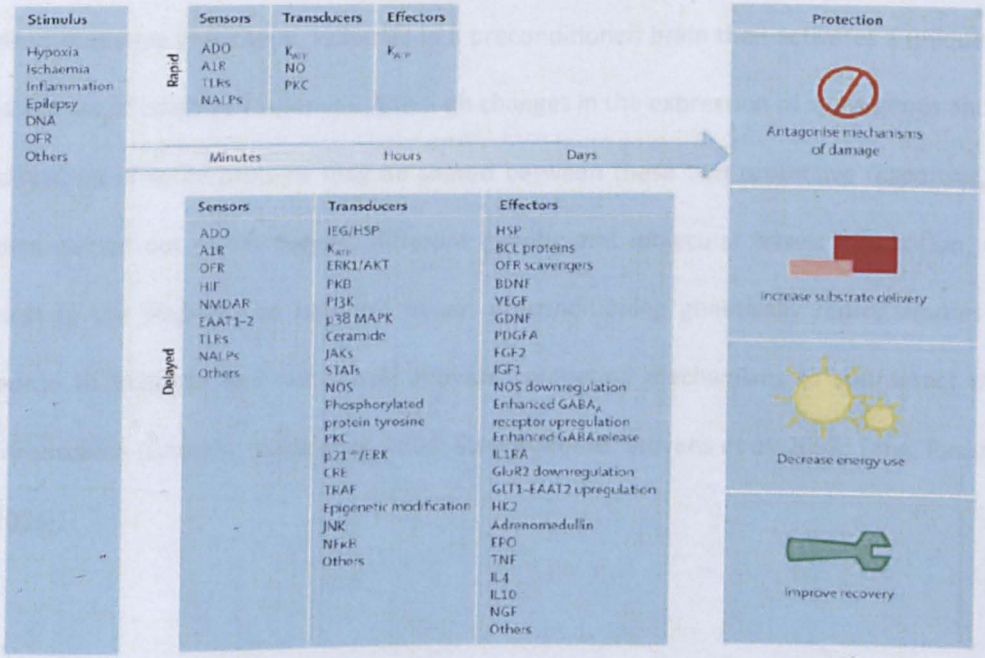

Figure 1.6. Signalling cascades of preconditioning (adapted from Dirnagl, Becker *et al.* 2009).

The overall implication is that different families of pro-survival genes are activated which encode proteins that serve to enhance the brain's resistance to ischemia. Protection is achieved by attenuation of injury-inducing mechanisms like excitotoxicity, ion/pH imbalance, oxidative and nitrosative stress, metabolic dysfunction, inflammation, necrotic and apoptotic cell death (Dirnagl, Becker *et al.* 2009). Protection is also manifested by engaging innate survival mechanisms and enhancing endogenous repair processes (for example, the proliferation and mobilization of bone marrow and other stem cells) that lessen the overall extent of injury and concomitantly facilitate the recovery of brain function (Sommer 2009). The acquisition of the ischemia-tolerant phenotype involves particular adaptation response cascades to specific stimuli occurring over distinct time frames (Bernaudin, Tang *et al.* 2002), (Stenzel-Poore, Stevens *et al.* 2003). Whether the triggering stimulus is preconditioning alone, ischemia alone, or ischemia with prior preconditioning, each of the cascades can be characterized by gene-dependent responses involving a unique family of sensors, transducers and transcription factors that activate them and the effector proteins that are produced. Gene-independent, post-translational modifications of existing proteins also contribute concomitantly to the response (Figure 1.7) leading to the establishment of a 'latent' cerebroprotective phenotype. Ischemia in a preconditioned brain then activates a unique and separate set of adaptive responses. Although changes in the expression of some genes and the modification of some proteins may be shared between these two protective responses, the studies carried out so far suggest different genetic and molecular bases. In addition, with respect to the response to ischemic injury, preconditioning genetically reprogrammes the response to ischemia and not simply activate competing mechanisms to counteract these injury cascades (Dhodda, Sailor *et al.* 2004; Stenzel-Poore, Stevens *et al.* 2003; Tang, Pacary *et al.* 2006).

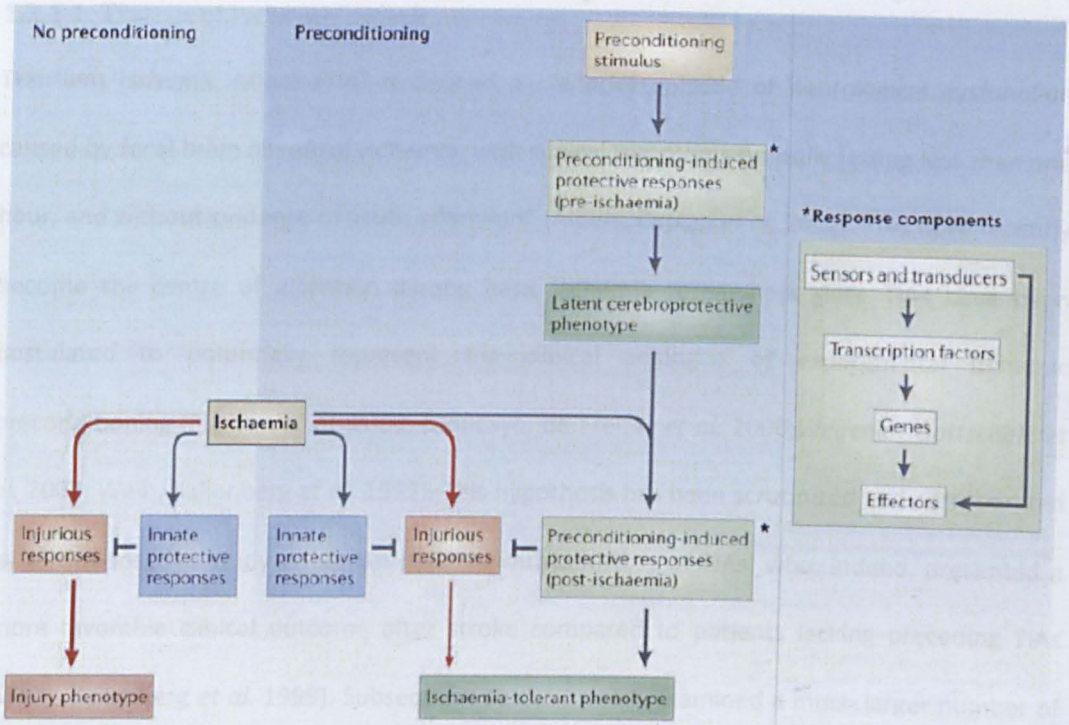

Figure 1.7. Cerebroprotection by preconditioning. (adapted from Gidday 2006).

1.2.1. Preconditioning stimulus

Many stimuli, stressors, and chemicals can serve to induce resistance in the brain to ischemic injury: hyperthermia, hypothermia, hypoxia, reactive oxygen species, inflammatory cytokines, spreading depression, mitochondrial inhibition, resveratrol, volatile anaesthetics, K-ATP channel openers, antibiotics, myelin basic proteins, E-selectin and also the transient ischemic attack . Therefore, "cross-tolerance," in which one stressor promotes resistance to another, can be induced in the brain. The sheer variety of stimuli capable of inducing an ischemia-resistant phenotype in the brain indicates that the signalling pathways activated by these different triggers converge downstream on some common, fundamental mechanisms that ultimately account for the protection.

Transient Ischemic Attack (TIA) is defined as "a brief episode of neurological dysfunction caused by focal brain or retinal ischemia, with clinical symptoms typically lasting less than one hour, and without evidence of acute infarction" (Albers, Caplan *et al.* 2002). TIAs have recently become the centre of attention among basic ischemia researchers since TIAs have been postulated to potentially represent the clinical analogue of experimental ischemic preconditioning (Fu, Sun *et al.* 2008; Moncayo, de Freitas *et al.* 2000;*Wegener, Gottschalk et al.* 2004; Weih, Kallenberg *et al.* 1999). This hypothesis has been scrutinized and corroborated by a retrospective study on stroke patients with a history of TIAs, who, indeed, presented a more favorable clinical outcome after stroke compared to patients lacking preceding TIAs (Weih, Kallenberg *et al.* 1999). Subsequent studies, which examined a much larger number of patients, impressively corroborated these findings (Wegener, Gottschalk *et al.* 2004). In a retrospective study, Schaller clearly demonstrated that stroke patients only showed a more favourable neurological outcome when the preceding TIAs occurred 1–7 days prior to stroke and the duration of TIAs did not exceed 20 min (Schaller 2005). Therefore, TIAs would provide neuroprotection only for a limited period. A plethora of changes after TIAs have to be expected, at both the functional and structural level. In this thesis, a TIA was used as trigger of ischemic preconditioning.

The induction of ischemic tolerance is accompanied by changes in gene expression conferring cytoprotection and survival to cells. Preconditioning changes the expression of genes involved in the suppression of metabolic pathways, immune response, ion-channel activity and blood coagulation (Stenzel-Poore, Stevens *et al.* 2007). Gene expression is regulated by transcription factors like response elements binding protein (CREB) that is activated after preconditioning,

inducing an up regulation of Bcl-2 an important gene against cell death; the nuclear factor NF-κB, a key regulator of apoptosis and inflammation, is activated after preconditioning and is linked to an up-regulation of key survival regulators such as superoxide dismutase or proteins that inhibits apoptosis. Following ischemic preconditioning, the activation of the mitogen-activated protein kinase (MAPK) induces an increase of the binding activity of the protein AP-1 but this was not demonstrated to be involved in the induction of tolerance. p53 is a transcriptional factor historically associated to the promotion of cell death and in models of preconditioning/severe ischemia, it is down-regulated in such conditions (Stetler, Zhang *et al.* 2009). Gene expression is also regulated by epigenetic mechanisms such as DNA methylation and histone modification, which modify the structure of chromatin thereby controlling the access of transcription factors to regulatory loci. These findings indicate that genomic reprogramming is closely involved in ischemic tolerance and suggest that metabolic down-regulation underlies the common pathways of neuroprotection seen in ischemic tolerance, hibernation, and hypothermia (Yenari, Kitagawa *et al.* 2008). The hypometabolic state, under all three conditions seems to occur, appears to be mediated in part by covalent attachment of the small ubiquitin-related modifier (SUMO) to a large number of substrates (Lee, Miyake *et al.* 2007; Lee, Castri *et al.* 2009; Yang, Ma *et al.* 2009). Most of the SUMO targets are in the nucleus, including transcription factors, transcriptional coactivators, and chromosome remodelling regulators (Hay 2005). SUMOylation of a wide range of transcription factors is likely to attenuate its activity and result in a hypometabolic state.

One of the latest discoveries in post-translational regulation was the miRNAs (microRNA), single-stranded RNA molecules approximately 21–23 nucleotides in length that regulate gene expression by the degradation or translational repression of target mRNAs. In the brain, miRNAs are abundant and play important roles in development, function and synaptic plasticity. Based on the discovery that almost the same numbers of mRNA species are up- and down-regulated under ischemic tolerance, miRNA microarray analysis showed both up- and

down-regulation of multiple miRNA profiles in the brain after ischemic preconditioning (Dharap and Vemuganti 2010; Saugstad 2010).

One of the most important key regulators of the genomic response after a preconditioning stimulus is the transcription factor named Hypoxia-inducing factor (HIF). The α-subunit of HIF (HIFα) is unstable and is hydroxylated by prolyl-4-hydroxylase, an oxygen sensor, and processed for proteasomal degradation. Under hypoxic conditions, the inactivation of prolyl-4-hydroxylase increases the amount of HIF, which can then bind the hypoxia-responsive elements (HREs) in the promoter region of a number of genes, including erythropoietin (EPO), vascular endothelial growth factor (VEGF), angiopoietin 2, insulin-like growth factor (IGF), and glucose transporters. The expression of the isoform HIF-1α was increased after hypoxic preconditioning in neonatal rat and adult mice brains (Bergeron, Gidday *et al.* 2000). Among the genes whose transcription is mediated specifically by HRE, erythropoietin (Ruscher, Isaev *et al.* 1998; Bernaudin, Nedelec *et al.* 2002), adrenomedullin (Tixier, Leconte *et al.* 2008), VEGF (Wick, Wick *et al.* 2002), Na-Ca exchanger (Valsecchi, Pignataro *et al.* 2011), and sphingosine kinase 2 (Wacker, Park *et al.* 2009) have been shown to be involved in ischemic or hypoxic tolerance. However, the role of HIF-1α remains controversial, because hypoxic tolerance was preserved in neuron-specific HIF-1α-deficient mice (Baranova, Miranda *et al.* 2007). Furthermore, ischemic injury after transient global ischemia was mitigated, not augmented, in neuron-specific HIF-1α-deficient mice (Helton, Cui *et al.* 2005). Therefore, the involvement of HIF-1α-mediated gene expression in brain ischemic tolerance does not appear to be robust. HIF might actively down-regulate oxidative metabolism by lowering mitochondrial biogenesis, augmenting glycolysis, decreasing metabolite entry into the citric acid cycle, promoting removal of free-radical-generating mitochondria by autophagy (Tracy and Macleod 2007),

(Zhang, Li *et al.* 2008) and optimising respiratory efficiency by the differential regulation of cytochrome oxidase subunits (Fukuda, Zhang *et al.* 2007).

Tolerance mechanisms, working at the level of endoplasmic reticulum function, result in improved rates of recovery of neuronal protein synthesis (Paschen and Mies 1999); specifically, better preservation of the initiation and elongation steps of transcription, and increased levels of the chaperone heat shock protein 70 (HSP70) are realized (Hayashi, Saito *et al.* 2003). HSP70 contributes to preconditioning maintaining mitochondria physiology, inhibiting intrinsic and caspase independent apoptosis; inhibiting programmed necrosis; contributing to initiation of the inflammatory response acting by "danger signal" for the toll like receptors; suppressing the up-regulation of matrix metalloproteinases, involved in the inflammatory response.

In addition during preconditioning, post-ischemic protein aggregation, redistribution and conjugation are reduced. The rate of repair of oxidative DNA damage is also enhanced (Li, Luo *et al.* 2006). Overall, many facets of ischemic mitochondrial dysfunction, including changes in the redox activity of the respiratory chain components, oxidative phosphorylation deficits (Dave, Saul *et al.* 2001), calcium overload and the initiation of apoptosis, are abrogated in ischemic tolerance (Zhang, Du *et al.* 2003). Compared with the naive brain, the preconditioned brain also shows post-ischemic increases in the Mn and CuZn isoforms of superoxide dismutase (Garnier, Demougeot *et al.* 2001), glutathione peroxidise and glutathione reductase (Arthur, Lim *et al.* 2004), uric acid (Glantz, Avramovich *et al.* 2005), and heme oxygenase-1 (Garnier, Demougeot *et al.* 2001), which enhance the tissue's capability to scavenge free radicals, contributing to the protective phenotype.

Glutamate is an excitatory neurotransmitter well known for its capability to kill neurons through the *N*-methyl-D-aspartic acid (NMDA) receptor –mediated mechanism. Some evidence (Bond, Lodge *et al.* 1999), (Grabb and Choi 1999) suggests that a mild activation of the NMDA receptor is involved in the protective effect of the ischemic tolerance and this neuroprotection could be achieved by two different mechanisms. One is a rapid calcium adaptation that may alleviate the neuronal damage caused by calcium overload (Shimazaki, Nakamura *et al.* 1998); the other is the rapid release of the brain-derived neurotrophic factor (BDNF), which activates its cognate tyrosine kinase B (TrkB) receptors. Both NMDA and TrkB activate NF-κB, which protects against oxidative stress-induced apoptosis. Brain ischemic preconditioning results in a robust release of the gamma-aminobutyric acid (GABA), an inhibitory neurotransmitter, and the GABAα receptor seems to be the receptor activated during neuroprotection (Dave, Lange-Asschenfeldt *et al.* 2005). Adenosine (an endogenous neuroprotectant that can inhibit the release of excitatory amino acids), adenosine A1 receptors and ATP-sensitive K^+ channels play an essential role in the ischemic preconditioning (Heurteaux, Lauritzen *et al.* 1995). In fact after ischemia, adenosine increases and inhibits synaptic transmission, decreases K^+-stimulated glutamate release, and inhibits presynaptic calcium fluxes via adenosine A1 receptors.

Activation of the innate immune response is a consequence of stroke, and preclinical data indicate that inflammation contributes to ischemic brain injury (Wang, Tang *et al.* 2007). Inflammatory stimuli can also induce ischemic tolerance. The production of pro-inflammatory cytokines is initiated by signalling cascades involving Toll-like receptors (TLR), which recognise host-derived molecules released from damaged tissue as well as common molecular motifs of invading pathogens. These proteins can exacerbate ischemic injury (Lehnardt, Lehmann *et al.* 2007; Tang, Arumugam *et al.* 2007; Kilic *et al.* 2008) or, as in the case of TLR 2, 4, and 9, could

mediate ischemic tolerance in the brain (Stevens and Stenzel-Poore 2006; Hua, Ma *et al.* 2008; Stevens, Ciesielski *et al.* 2008) and others might be involved (Kariko, Weissman *et al.* 2004). Although the genomic reprogramming induced by Toll-like receptors differs from the gene expression pattern induced by ischemic preconditioning, the degree of protection is similar. Cerebral ischemia might activate adaptive immunity and innate immunity. The adaptive immune response is characterised by lymphocytes that recognise and respond to specific antigens; however, this response depends on the environment in which the lymphocytes initially encountered the antigen, driving the differentiation into different effectors cell types (Weaver, Harrington *et al.* 2006). Because inflammation seems to worsen stroke outcome, induction of regulatory T cells to limit CNS inflammation presents a new opportunity for stroke treatment. Although these cells are activated in an antigen-specific way, they could control the immune response in an antigen non-specific way, an event referred to as bystander suppression (Miller, Lider *et al.* 1991). Stroke induces dynamic changes in brain cytokines such as tumour necrosis factor (TNF-alpha), interleukin (IL-1b and IL-6), suggesting that different types of T-effector cells and regulatory T cells could emerge depending on the timing of the lymphocyte-antigen encounter. Experimental data indicate an upregulation of the endogenous regulatory T-effector cells after stroke (Becker, Kindrick *et al.* 2005; Offner, Subramanian *et al.* 2006) and recently were reported to be cerebroprotective immunomodulators against stroke (Liesz, Suri-Payer *et al.* 2009).

Vascular remodelling could contribute to reducing the severity of the subsequent test ischemia by improving collateral blood supply in stroke models, thereby complementing the possible adaptation of energy metabolism and brain cell membrane ionic homeostasis (Obrenovitch 2008). There is convincing evidence that the cerebrovascular system has such an adaptive capability through arteriogenesis (Heil and Schaper 2005) and angiogenesis (Greenberg and Jin

2005). When both carotid arteries are ligated in rats to produce a chronic hypoperfusion, cerebral blood flow (CBF) drops sharply right after the occlusion, but then increases gradually during the following weeks (Farkas, Luiten *et al.* 2007; Otori, Katsumata et al. 2003), and recent studies confirmed that both arteriogenesis and angiogenesis may contribute to this adaptive process (Choy, Ganesan *et al.* 2006; Ohtaki, Fujimoto *et al.* 2006). Ischemic preconditioning in rats improved CBF during the reperfusion that followed the subsequent 30-min forebrain ischemia, and this functional effect was associated with reduced brain oedema (Vlasov, Korzhevskii *et al.* 2005). An up-regulation of endothelial nitric oxide synthase (eNOS) may also contribute to improved recirculation in tolerant brain regions, since increased expression of eNOS mRNA was associated with ischemic tolerance induced by ischemic preconditioning (Hashiguchi, Yano *et al.* 2004).

The BBB is anatomically defined by the tight junctions between adjacent endothelial cells lining the lumen of cerebral microvessels, but the BBB function also involves astrocytes, pericytes, neurons, and the extracellular matrix (Wolburg and Lippoldt 2002; de Vries, Kuiper *et al.* 1997). The latter constitutes the basement membrane underlying the vasculature, and its disruption is strongly associated with increased BBB permeability in pathological states (Hawkins and Davis 2005). BBB breakdown with associated vasogenic oedema is an important and early feature of ischemic brain damage and appears as a precursor and good predictor of poor outcome (Latour, Kang *et al.* 2004). Several studies have shown that ischemic tolerance includes a better preservation of the BBB and reduced oedema formation during the test ischemia (Masada, Hua *et al.* 2001; Zhang, Chen *et al.* 2006; Gesuete, Orsini *et al.* 2011; Gesuete, Packard *et al.* 2012). It is difficult to determine whether the preservation of BBB integrity contributes to, or is a consequence of, reduced ischemic damage. From mechanistic point of view, it is clear that a reduction of the brain inflammatory responsiveness is likely to

help maintain BBB integrity. However, preservation of BBB integrity may be a primary and important feature of ischemic tolerance, given that it is the interface between damaged/vulnerable tissue and circulating inflammatory cells during recirculation.

1.3. MASS SPECTROMETRY AS CORE-TECHNOLOGY FOR PROTEOMIC AND METABOLOMIC ANALYSES

This project utilized mass spectrometry both for proteomic and metabolomic analyses of cerebral ischemic preconditioning. It is therefore appropriate to review some of the underlying principles to provide the reader with a comprehensive overview of the studies.

1.3.1. Principle of Mass Spectrometry

Mass spectrometry (MS) is an analytical technique that measures the mass to charge ratio (*m/z*) of a charged species based on its response to electric and/or magnetic fields (Baldwin 2004; Domon and Aebersold 2006). As shown in figure 1.8, mass spectrometers consist of three basic components: an ion source, a mass analyzer and a detector. The ion source converts sample molecules into ions in gas phase, the mass analyzer separates the various ionised species according to their *m/z* ratios, and the detector records signal intensity at each *m/z* value. Conventionally, mass spectra are presented as a plot of *m/z* value against relative intensity. In proteomics, it is possible to use several types of mass spectrometers that differ in their physical principle, performance standards, mode of operation and ability to support specific analytical strategies (Guerrera and Kleiner 2005; Guerrero, Tagwerker *et al.* 2006; Wysocki, Resing *et al.* 2005).

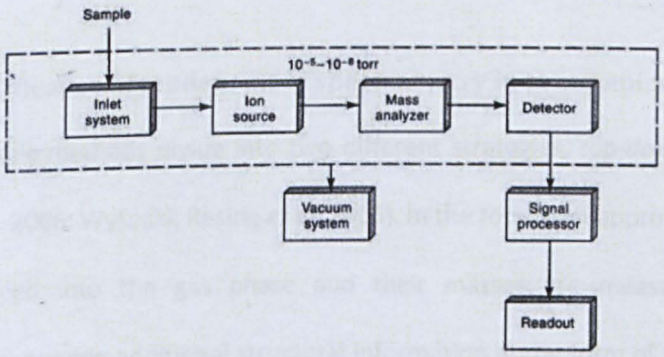

Figure 1.8. A block diagram indicating the main regions of a mass spectrometer (http://people.stfx.ca/tsmithpa/Chem361/labs/ms.html).

The two most common ionisation methods used at the moment in the analysis of peptides and proteins are matrix assisted laser desorption ionisation (MALDI) and electrospray ionization (ESI) (Wysocki, Resing *et al.* 2005), while the four basic types of mass analysers are ion trap, quadrupole, time-of-flight, and Fourier-transform ion cyclotron analysers.

For the work described in this thesis, two different mass spectrometers were used: the first was an HPLC-Chip coupled to an ESI-IT (ion trap) MS/MS (Agilent Technologies) (Figure 1.9a), used to identify the proteins separated on 2-DE gels; the second one was an LC-LTQ Orbitrap XL™ (Thermo Scientific) (Figure 1.9b), which was used to identify the proteins separated by the 1-DE analysis and to perform untargeted metabolomic analyses.

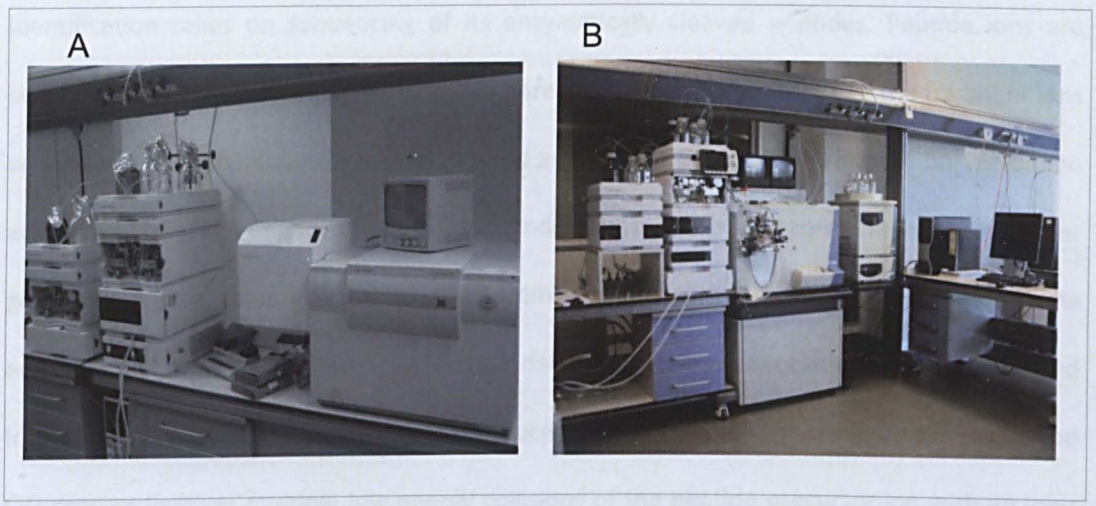

Figure 1.9. An overview of our Agilent 1200 Series HPLC-Chip/MS system (A) and our Thermo LTQ Orbitrap XL™ (B).

1.3.1.1. The significance of tandem mass spectrometry in proteomics

MS-based proteomic methods divide into two different strategies, *top-down* and *bottom-up* (Millea, Krull *et al.* 2006; Wysocki, Resing *et al.* 2005). In the top-down approach, intact protein ions are introduced into the gas phase and their masses are measured. Subsequent fragmentation may provide additional structural information in the form of partial amino acid sequences. In the bottom-up approach, proteins are cleaved with a proteolytic enzyme and

the resulting peptides are analyzed in the gas phase by MS. This approach is more widely used since MS of whole proteins is less sensitive than peptide MS, and the mass of an intact protein by itself is often insufficient for identification (Aebersold and Mann 2003). In this study a bottom-up approach was used. Currently, there are two major methods for proteins identification by MS analysis in the bottom-up proteomics approach: peptide mass fingerprinting and peptide sequencing by tandem MS (also known as MS/MS analysis). In peptide mass fingerprinting, the masses of the intact peptides in a protein digest are determined, and protein identification is based on the comparison of the experimentally determined peptide mass values with the predicted molecular mass of the peptides generated by a theoretical digestion of each protein in a database In MS/MS analysis, instead, protein identification relies on sequencing of its enzymatically cleaved peptides. Peptide ions are separated in a first mass analyser. Selected parent ions are fragmented, and the fragment ions are separated in the same/or a second mass analyser to produce information on the amino acid sequence of the peptide. The resulting tandem mass spectra are compared with computer generated fragmentation models derived from all the tryptic peptides computed from the entries in a protein or translated nucleic acid database. Various dissociation methods are used to fragment ions, but gas phase collision induced dissociation (CID) is the most common. The CID process involves multiple low energy collisions of the peptide precursor ion with an inert gas, which converts translational energy into vibrationally excited states, eventually resulting in bond cleavage. The fragments produced are the result of N-terminal and C-terminal fragmentations across the peptide bond to give sequence ions with charge retention on either the acylium ion fragment, which retains the original N terminal residue (*b*-type ion), or ammonium ion fragments retaining the C-terminus (*y*-type ion) (Figure 1.10) (Roepstorff and Fohlman 1984). Tryptic peptides by definition have readily protonated arginine or lysine residues at the C-terminus, which favour charge retention on the C-terminal containing fragment. Therefore, in their low energy CID spectra, *y*-type ions usually predominate, though

internal lysine or arginines resulting from incomplete tryptic cleavage, or histidines towards the N-terminus, can increase the incidence of *b*–type cleavages. Instrument type and geometry can also exert a significant influence on detailed fragmentation patterns (Steen and Mann 2004).

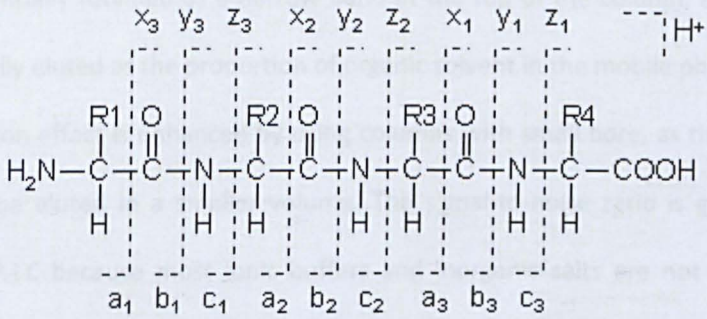

Figure 1.10. Peptide fragmentation nomenclature.

Other fragments, derived from loss of water or ammonia from these ions, are commonly observed. B-ions can eliminate carbon monoxide, forming *a*-ions. Other common ions in the mass spectra are immonium ions (H_2N=CHR, where R is the amino acid side chain) and internal fragments containing neither the original N- or C-terminal residue.

1.3.1.2. Sample introduction into the mass spectrometer

The choice of sample introduction method depends on the mode of ionization employed, and on the complexity/purity of the sample. Samples that are well desalted, and that contain relatively few components of reasonable abundance, may be infused directly. In most cases, however, online liquid chromatography is the preferred introduction method, particularly in the case of ESI which, being a solution-phase technique operating at atmospheric pressure, is intrinsically compatible with liquid chromatography. The experiments reported in this work are based on reversed phase liquid chromatography (RP-LC) coupled to MS. In this technique, the stationary phase is less polar than the mobile phase and hydrophobic interactions are the main

mechanism of analyte retention on the column. The RP-LC columns most commonly used in peptide separations are packed with a stationary phase composed of non-polar C18-alkyl chains covalently attached to silica particles. RP-LC usually achieves a considerable increase in the concentration of samples entering the ionisation source, since relatively large volumes of diluted sample in aqueous solution can be pumped through the column, with the analytes of interest being initially retained as a narrow band at the top of the column, and components being sequentially eluted as the proportion of organic solvent in the mobile phase is increased. This concentration effect is enhanced by using columns with small bore, as the same amount of sample will be eluted in a smaller volume. The signal-to-noise ratio is generally further improved by RP-LC because most ionic buffers and inorganic salts are not retained on RP columns, and so they can be diverted to waste. Reversed phase chromatography generally increases the number of peptides detected in complex mixtures because fewer separate components enter the source at any one time, so the duty cycle of the mass spectrometer can be more efficiently exploited.

1.3.2. Ion sources

All the mass spectrometers used in my studies were equipped with ESI sources. ESI was first described by Dole and was developed as a practical ionization source for mass spectrometry, initially on quadrupole instruments, by John Fenn (Fenn, Mann *et al.* 1989). The mechanism of electrospray is visualized in Figure 1.11. ESI is an atmospheric pressure ionization technique in which the sample solution is sprayed from a fine capillary (usually around 10 µm in diameter), which is maintained at a high potential difference with respect to the ion source orifice of the mass spectrometer. This voltage is applied either via direct contact with an electrode, or through a (metallic) coating on the spray tip. The potential difference generates a force extending the liquid to form a cone at the capillary tip (the Taylor cone) from which a fine mist of electrically charged droplets emerges. Positive charge is conferred by the presence of

protons or other cations. These droplets rapidly become smaller, due to evaporation of solvent molecules until Coulombic repulsion causes fission, forming smaller droplets with reduced charge density.

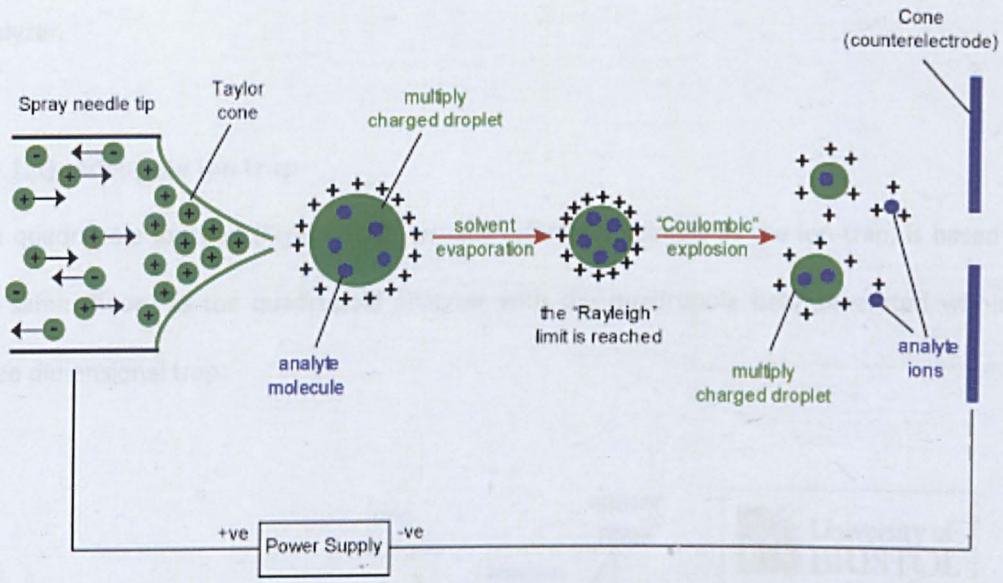

Figure 1.11. Schematic view of ESI (adapted from web source University of Bristol).

There are two mechanisms proposed for the desolvation and charging of analytes within the droplets: ion evaporation and charge residue models (IEM and CRM, respectively). The IEM was the first mechanism to be proposed. This model states that when the droplets become smaller, the electric field will become strong enough to expel ions into the ambient gas. Evaporated ions can remain somewhat solvated. This model applies mainly to small ions. For the ionization and evaporation of proteins, i.e. considerably large ions, the CRM is more applicable. In this model large droplets dissociate via a sequence of Rayleigh instabilities, called Coulombic explosions, into successively smaller ones until eventually only one analyte molecule per droplet remains. Further evaporation of solvent results in fully desolvated charged protein molecule. The charges are statistically distributed over the analyte's potential charge bearing sites, enabling the formation of multiply charged ions.

1.3.3. Mass analyser

The mass spectrometric analyses reported in this thesis were obtained using an Agilent MSD XCT Ultra (quadrupole ion trap mass analyzer) and an LTQ Orbitrap XL™ (Thermo Scientific), which is a hybrid mass spectrometer, composed of a linear ion trap and an orbitrap mass analyzer.

3.3.1. Quadrupole ion trap

The quadrupole ion trap (Figure 1.12), usually referred to simply as the ion-trap, is based on the same theory as the quadrupole analyzer with the quadrupole field generated within a three dimensional trap.

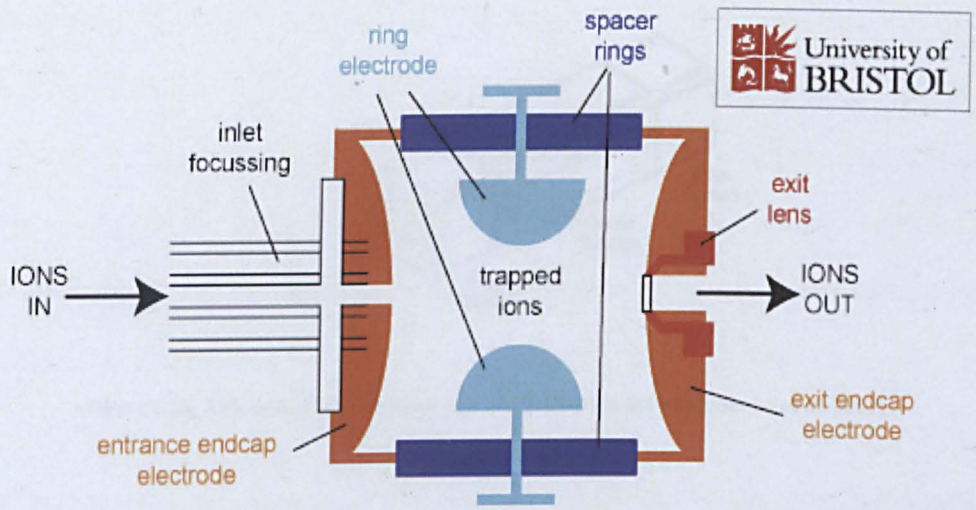

Figure 1.12. A schematic cutaway view of a Quadrupole Ion Trap Mass Analyser (adapted from web source University of Bristol).

The ion trap itself is filled with helium and comprises a ring electrode and two end cap electrodes, creating the electric field by applying a large frequency (RF) voltage to the ring electrode. The orbiting motion of the ions in the trap is governed by the large RF voltage and the cooling effects of collisions with the helium gas (that reduces the kinetic energy of the ions and helps focus the ions in the centre of the trap). A mass spectrum is acquired by sequentially

ejecting fragment ions from low *m/z* to high *m/z*. This is performed by scanning the RF voltage to make ion trajectories sequentially become unstable, the mass selective instability mode developed by Stafford's group (March 2009). A product ion MS/MS spectrum is obtained via resonance excitation. The precursor ion is isolated by the application of a waveform signal to the endcap electrodes. Fragmentation of the precursor ion is caused by the application of a small voltage across the endcap electrodes and collision with helium gas.

The linear ion trap is a MS analyser that can store, isolate, and fragment ions. The basic design of the linear ion trap, composed by a square array of hyperbolic rods, is shown in Figure 1.13.

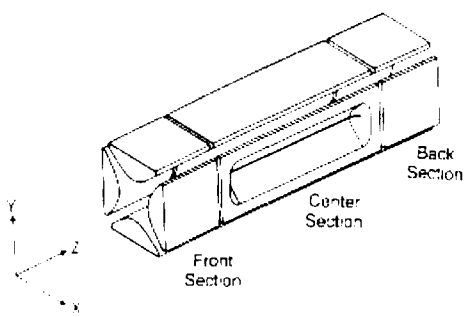

Figure 1.13. A picture of the linear ion trap (adapted from Schwartz, Senko *et al.* 2002).

The LTQ XL uses three direct current (dc) axial trapping voltages, one for each rod section, that establish axial (Z-axis) trapping by lowering the potential of the center section below the potential of the front and back sections. (http://www.thermo.com/eThermo/CMA/PDFs/Various/File_26638.pdf)

The ion isolation waveform voltage, resonance excitation RF voltage, and resonance ejection RF voltage are ac voltages that are applied to the exit rods to stimulate motion of the ions in the direction of the ion detection system. The voltages applied to the exit rods are equal in amplitude but are 180° out of phase to one another. When the ac frequency applied to the

rods equals the resonance frequency of a trapped ion (which depends on its mass) the ion gains kinetic energy and is ejected from the mass analyzer in the direction of the ion detection system (X direction). The ion isolation waveform voltage consists of a distribution of frequencies containing all resonance frequencies except for those corresponding to the ions to be trapped. The ion isolation waveform voltage, in combination with the main RF voltage, ejects all ions except those of a selected mass-to-charge ratio or narrow ranges of mass-to-charge ratios. During the collision-induced dissociation step, the resonance excitation RF voltage is applied to the exit rods to fragment parent ions into product ions. The resonance excitation RF voltage is not strong enough to eject an ion from the mass analyzer. However, ion motion in the radial direction is enhanced and the ion gains kinetic energy. After many collisions with the helium damping gas, which is present in the mass analyzer, the ion gains enough internal energy to cause it to dissociate into product ions. The product ions are then mass analyzed. During ion scan out, the resonance ejection RF voltage facilitates the ejection of ions from the mass analyzer and thus improves mass resolution. The resonance ejection RF voltage is applied at a fixed frequency and increasing amplitude during the ramp of the main RF voltage. Only when an ion is about to be ejected from the mass analyzer cavity by the main RF voltage is it in resonance with the resonance ejection ac voltage. When an ion approaches resonance, it moves farther away from the centre of the mass analyzer, where the field generated by the main RF voltage is zero (and space-charge effects are strong), into a region where the field produced by the main RF voltage is strong (and space-charge effects are small). As a result, the ejection of the ion is facilitated, and mass resolution is significantly improved.

A limitation on the use of linear ion traps is represented by the low stability of fragment ions with an *m/z* values less than 30% of the *m/z* for the precursor ion selected for fragmentation during MS/MS analyisis; this limitation, also known as one-third rule, is particularly important on low molecular weight metabolites analisys due the unreliable MS/MS detection of the metabolites fragment ions.

1.3.3.3. The Orbitrap mass analyser

The orbitrap is an axially-symmetrical mass analyser composed of a spindle-shape central electrode surrounded by two bell-shaped outer electrodes, using the principle of orbital trapping in electrostatic field (Hu, Noll *et al.* 2005) (Figure 1.14).

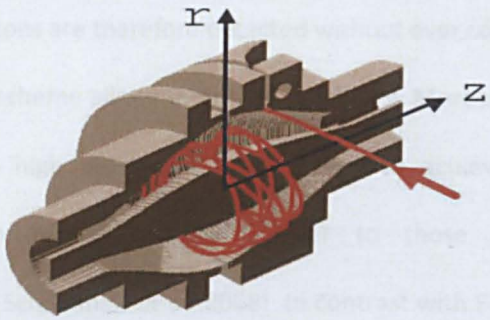

Figure 1.14. Cutaway view of the orbitrap mass analyser. Ions are injected into the Orbitrap at the point indicated by the red arrow. (adapted from Hu, Noll *et al.* 2005).

Ions beams are injected in the Orbitrap with a velocity perpendicular to the long axis of the Orbitrap (the z-axis) so that ions start coherent axial oscillations without the need for any additional excitation cycle. During ion injection a rapidly changing electric field is created by shaping the electrodes appropriately to prevent collision of the ions with electrodes and ions are trapped around the inner electrode. The electrostatic attraction towards the central electrode is compensated by a centrifugal force that arises from the initial tangential velocity of ions. After ions have entered the Orbitrap, a stable electrostatic field is achieved, and image current detection is subsequently performed. During ion detection, stable ion trajectories rotate around the axial central electrode with harmonic oscillations along it. The frequency ω of these oscillations along the z-axis depends only on the ion mass-to-charge ratio m/z and the instrumental constant ω:√(z/m)*k. Two split halves of the outer electrode of the Orbitrap detects the image current produced by the oscillating ions. By Fast Fourier Transformation (FFT) of the image current, the instrument obtains the frequencies of these axial oscillations and therefore the mass-to-charge ratios of the ions. During ion detection the outer electrode is split in half at z=0 by an insulating ceramic ring. Moving from one half outer electrode to the

other, packets of positive ions characterised by a precise mass-to-charge ratio induce opposite currents on these halves, thus creating a signal to be detected by differential amplification (Hu, Noll *et al.* 2005). The amplitude of the created current is proportional to the number of ions in the analyser cell, while its frequency is the same as the frequency of ion axial oscillations. Because the frequency of axial oscillation is function of m/z, it is possible to obtain a spectrum as a function of m/z. The ions are therefore detected without ever colliding with the electrodes and this non-destructive scheme allows improved sensitivity. Moreover, since frequencies can be measured with very high precision, it is possible to achieve a high-accuracy mass measurement and high resolving power similar to those achievable with FT-ICR instrumentation (Schenk, Schoenhals *et al.* 2008). In contrast with FT-ICR, which is also based on Fourier-Transform principle, the Orbitrap does not require a superconducting magnet and supplies of liquid helium.

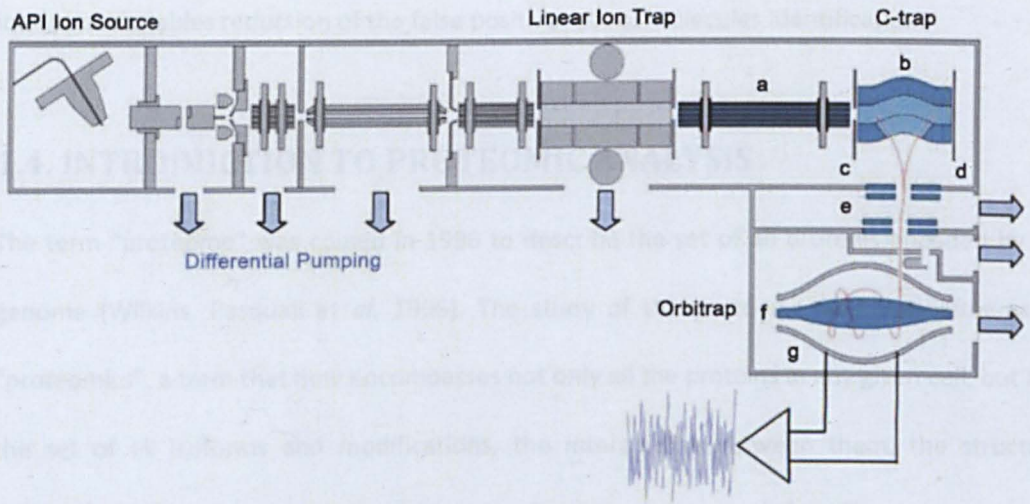

Figure 1.15. Schematic view of the LTQ orbitrap (adapted from www.thermo.com).

Depending on the requirements for the analysis, the two analysers (LTQ and Orbitrap) that form the hybrid LTQ Orbitrap XL™ (Thermo Scientific) (Figure 1.15) instrument can be used independently or in concert. There are in fact several possible ways of operation in the linear ion trap hybrid system. In my experiments the two mass analysers were configured as follows:

ions generated by API were collected in the LTQ XL followed by axial ejection into the C-shaped storage trap, which was used to store and collisionally cool ions before injection into the orbitral trap. In the orbitrap mass analyser I performed the measurement of the precursor ions, while the linear ion trap was used to perform MS/MS experiments. The benefit of this configuration is that both mass analysers work in parallel, while a high resolution/high mass accuracy spectrum of the precursor ion is acquired in the orbitrap, the fast linear ion trap carries out fragmentation and detection of MS/MS spectra of selected ions. Parallel operation is achieved because the initial small part of the high resolution spectrum can be used for data-dependent selection of precursors, which are then fragmented while the high resolution mass spectrum is still being acquired. It has been shown that one orbitrap spectrum acquired at the resolving power 60 000 and 3-5 linear ion trap fragmentation spectra are obtained within 1 second (Yates, Cociorva *et al.* 2006). This configuration is particularly convenient for proteomic and metabolomic studies, because the very accurate and resolved measurement of precursor ion masses enables reduction of the false positive rate of molecules identification.

1.4. INTRODUCTION TO PROTEOMIC ANALYSIS

The term "proteome" was coined in 1996 to describe the set of all proteins encoded by the genome (Wilkins, Pasquali *et al.* 1996). The study of the proteome was thereafter called "proteomics", a term that now encompasses not only all the proteins in any given cell, but also the set of all isoforms and modifications, the interactions between them, the structural description of proteins and their higher-order complexes, and for that matter almost everything "post-genomic" (Tyers and Mann 2003). The greatest challenge for proteomics technology is the inherently complex nature of cellular proteomes. A proteome is a highly dynamic entity: protein expression in a biological system changes with the state of development, in response to environmental stimuli, with the progression of a disease, etc. In addition, different cells within a multicellular organism have different proteomes. Moreover,

the dynamic range of protein expression spans seven or eight orders of magnitude and, consequently, proteins are present in vastly different quantities. With its ever-growing array of analytical, biochemical and bioinformatic tools and approaches, proteomics has now the power to identify the protein profile of different cell types, to assess differential expression between healthy and diseased tissues, and to discover their specific functions and interactions (Yarmush and Jayaraman 2002). Accordingly, an improved knowledge of ischemic preconditioning IP/IT should help to identify neuroprotective strategies potentially capable of suppressing multiple, parallel pathophysiological events that cause ischemic brain damage. In the brain, ischemic preconditioning triggers several adaptive molecular responses of cells to injury, characterized by different time frames during which proteins seem to play a relevant role. For instance, a rapid and short-lasting protection can be established within minutes of exposure to ischemic attack, as a result of post-translational modification of proteins. A second phase develops more slowly and requires gene activation and *de novo* synthesis of proteins (Barone, White *et al.* 1998).

A previous proteomic analysis of adult ischemic preconditioning rat brain showed increased expression of stress proteins such as chaperones, the intracellular "cleaning" molecules that contribute to the induction of tolerance (Dhodda, Sailor *et al.* 2004). The authors performed a combined genomic and proteomics analysis showing the induction of putative neuroprotective transcripts such as heat shock proteins. Further, proteomic profile investigated by the 2-DE combined with MALDI-TOF analysis, confirmed the protein increased expression of the transcripts at 24 h after preconditioning suggesting also a temporal relationship between gene expression and neuroprotection (Dhodda, Sailor *et al.* 2004).

Moreover proteomics profiling of cortical neuronal culture showed that the proteosomal degradation of structural proteins after their ubiquitination results in a morphological phenotype change of neurons rendering them resistant to excitotoxicity (Meller, Thompson *et al.* 2008).

So far, only a few studies in experimental models of IT, both *in vivo* and *in vitro,* have taken advantage of proteomic approaches though discovery-driven proteomic studies focused on finding mediators of IP and brain injury are still limited (Stapels, Piper *et al.* 2010; Dhodda, Sailor *et al.* 2004).

In this study I applied two different proteomic approaches (Figure 1.16):

1. Classical two-dimensional gel electrophoresis (2-DE) and liquid chromatography-tandem mass-spectrometry (LC-MS/MS) for the identification of differentially expressed proteins in various experimental conditions;
2. One-dimensional gel electrophoresis (1-DE) in conjunction with LC-MS/MS for the identification and semi-quantitation by spectral counts of proteins present in different experimental conditions.

As indicated in Figure 1.16, these approaches have some common steps (in-gel digestion, MS/MS analysis, proteins identification and pathway analysis) that will be described in detail.

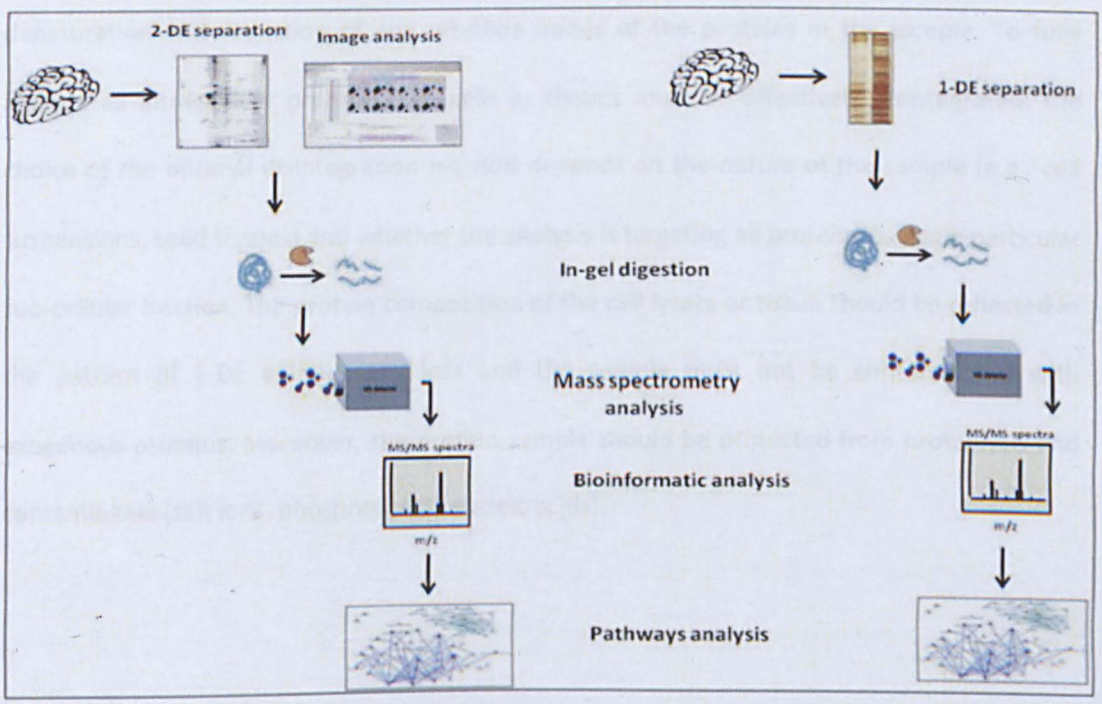

Figure 1.16. Proteomic workflows used in this study.

1.4.1. Two-dimensional gel electrophoresis analysis (2-DE)

This approach comprises six main steps: (1) sample preparation, (2) protein separation by two-dimensional gel electrophoresis (2-DE), (3) gel image analysis and statistical analysis, (4) in-gel digestion of spots with differentially expressed proteins and extraction of peptides, (5) separation of tryptic peptides by LC-MS/MS analysis, (6) identification of proteins by database searching. 2-DE and mass spectrometric analyses need both appropriate statistical and bioinformatics tools to minimize experimental artifacts and to avoid false positives or negatives in MS/MS protein identification.

1.4.1.1. Sample preparation

Sample preparation is a key step for good 2-DE results. Because of the great diversity of protein sample types and origins, the best sample preparation procedure has to be determined empirically. An efficient and reproducible method is essential to get reliable analysis results. Ideally, the process will result in the complete solubilisation, disaggregation, denaturation and reduction of any disulfide bonds of the proteins in the sample. To fully analyse all intracellular proteins, the cells or tissues must be effectively disintegrated: the choice of the optimal disintegration method depends on the nature of the sample (e.g., cell suspensions, solid tissues) and whether the analysis is targeting all proteins or just a particular sub-cellular fraction. The protein composition of the cell lysate or tissue should be reflected in the pattern of 2-DE without any loss and the sample must not be contaminated with exogenous proteins. Moreover, the protein sample should be protected from proteolysis and contaminants (salt ions, phospholipids, nucleic acids).

1.4.1.2. Protein separation by electrophoresis

2-DE electrophoresis is the oldest technology used in proteomics, having first been described in 1975 by O'Farrell and (separately) by Klose (O'Farrell 1975; Klose 1975),. It is a powerful and widely used method to analyze complex protein mixtures extracted from different biological samples, since it allows the simultaneous separation of thousands of proteins according to two independent properties in two different steps. The first-dimension step, isoelectric focusing (IEF), separates the proteins according to their isoelectric point (pI). Proteins are amphoteric molecules, with acidic and basic buffering groups, that can become protonated or deprotonated depending on the pH of the environment: in basic environment the acidic groups become negatively charged, on the contrary, in acidic environment they become positively charged. The net charge of a protein is the sum of all negative or positive charges of its amino acid side chains; obviously, each protein has an individual net charge. The isoelectric point represents the pH at which the net charge of the protein is zero; proteins are positively charged at pH values below and negatively charged at pH value above their pI. When an electric field is applied, a protein will start to migrate towards the electrode of the opposite sign of its net charge, until it will reach the pH of its isoelectric point, in which it has not net charge anymore and stops migrating. This is called the "focusing effect", which concentrates proteins at their pIs and allows proteins to be separated based on very small charge differences.

In the second-dimension step, sodium dodecyl sulfate-polyacrylamide gel electrophoresis (SDS-PAGE), the proteins are separated according to their molecular weights (MW), due to the ability of SDS to denature the proteins by wrapping their hydrophobic 'tails' around the polypeptide backbone. SDS also disrupts hydrogen bonds, blocks hydrophobic interactions and substantially unfolds the molecules, minimizing differences in the molecular shape by eliminating the tertiary and secondary structures. Moreover, the proteins can be totally unfolded when a reducing agent such as dithiothreitol (DTT) is employed, since DTT cleaves

any disulfide bonds between cysteine residues. When an electric field is applied, the SDS-denatured and negatively charged polypeptides move through a sieving polyacrylamide gel toward the anode, and thus they are separated by their molecular weights. Using 2-DE, proteins thus migrate to a co-ordinate on a 2D-gel defined by their molecular mass and pI. Thousands of different proteins can thus be separated, and information such as the protein pI, the apparent molecular weight and the relative amount of each protein can be obtained. Visualisation of proteins after their separation can be done with different staining techniques. Organic dyes like Coomassie R250 or Coomassie G250 (colloidal Coomassie) are widely used. Coomassie staining has a linear response of three orders of magnitude, but it suffers from low detection sensitivity in protein, though the colloidal version is somewhat better in this respect. Despite this limitation, colloidal Coomassie staining is still widely used, because of its low price, ease of use and compatibility with most subsequent protein analysis. Other visible staining methods include silver staining, which is generally more sensitive than Coomassie, though individual proteins are quite variable in their response and the range of linearity is rather limited. Moreover, some silver staining protocols show poor compatibility with MS analyses. Fluorescent dyes, such as Sypro Ruby, have a sensibility that is comparable to silver staining but their response is linear over a greater range of protein concentration (at least three orders of magnitude). Being end point stains the protocol is very simple, and they are highly compatible with in gel digestion and mass spectrometric analysis (Gevaert and Vandekerckhove 2000; Scheler, Lamer *et al.* 1998), but they are unfortunately rather expensive. It is very important to know that different staining techniques stain protein differently: indeed, silver staining often produces a pattern different from the pattern achieved with Coomassie blue and other staining procedures like with Sypro Ruby (Gorg, Obermaier *et al.* 2000).

An alternative to the classic 2-DE electrophoresis approach is represented by the difference gel electrophoresis (DIGE), introduced by Unlu *et al.* (Unlu *et al.* 1997). The DIGE consist in the

covalent labelling of proteins with different cyanine dyes (Cy2, Cy3 and Cy5) prior to IEF. After the SDS PAGE separation, the gels were acquired using the excitation wavelight of each cyanine dyes. This technique overcomes the inter-gel reproducibility problems of the 2D-page since the proteins of the different samples are run on the same gel and can be compared each other. A cyanine labelled pool of all the samples is run on all gels for the normalization and the use of cyanine labelled internal standard allows the proteins quantification.

1.4.1.3. Differential gel image analysis

The reliable evaluation and the comparison of the complex 2-DE pattern by eye is impossible. Therefore, the gel images have to be converted into digital data with a scanner and compared using image analysis software. For an optimum computational analysis it is important to obtain a high resolution grey scale image ideally with a bit depth of 16 to maximise the number of distinguishable gray levels. The success of differential expression analysis depends critically on the accuracy and the reliability of the analytical software used for image processing. The software and the parameters chosen may have a profound effect on the interpretation of the protein pattern obtained and the amount of user intervention demanded during the analysis. Currently, several 2-DE image analysis software packages are commercially available. These programs have been continuously improved and enhanced over the years in terms of faster matching algorithms with less manual intervention and greater automation. Novel algorithms offering more reliable spot detection, quantitation and matching have been introduced together with the inclusion of flexible statistical tools for a more robust differential expression analysis. This is the case of the state-of-the-art Progenesis SameSpots image analysis software (NonLinear Dynamics, UK), which provides fully automated gel image processing (spot detection, gel alignment, spot matching and spot quantification). Indeed, SameSpots gel image analysis consists of a fast and streamlined 2D workflow, which includes an innovative visual tool for highly advanced and automated image alignment. The images are first aligned by

localised warping to an image selected as a master image. Then spots are detected simultaneously across all the images leading to one spot map, which is then overlaid on each warped gel image in the dataset leading to an identical spot outline across the gel series. After the alignment, SameSpots automatic analysis includes spot detection, background subtraction, normalisation and matching. The result is perfectly aligned images at the pixel level, with 100% matching and no missing values, which radically reduces the need for editing spot detection and re-matching. This method attempts to reduce the subjectivity of user matching and address the issue of missing values, which are a problem for data analysis as many techniques in multivariate analysis cannot be used with incomplete datasets. Results are then ready for validation and statistical analysis. This was the method used to calculate the protein abundance in the 2-DE brain analysis.

1.4.1.4. 2-DE: strength and limitations

The combination of 2-DE, MS and bioinformatics tools has been utilized extensively for proteomics research in industry and academia. The power of the 2-DE-based technology was early recognized by the research community and scientists from various disciplines were attracted to the field of proteomics. The 2-DE-based approach has several characteristics that are currently unmatched by other proteomics methodologies:

- Hundreds of proteins can be resolved and visualized simultaneously on a single 2-DE gel; for each protein, the isoelectric point, the molecular weight and the relative quantity can be measured.
- High-resolution capabilities of 2-DE allow the separation and visualization of post-translationally modified (PTM) proteins. In many instances, PTM proteins can be readily located in 2-DE gels because they appear as distinctive horizontal or vertical clusters of spots. In addition, modified proteins can be revealed by MS analysis, when multiple spots of the

same protein are identified. On the other hand, several limitations and problem issues have been recognized to 2-DE proteomics approach:

- The most important drawback of the 2-DE based proteomics is that it is not possible to analyze the entire proteome. Membrane proteins are not readily amenable to 2-DE (Santoni, Molloy *et al.* 2000), because of their poor solubility in standard extraction solution. Moreover, proteins displayed in a single 2-DE gel represent only a portion of all the proteins that are present in the sample. Generally, proteins that are visualized in 2-DE gels by conventional staining methods are high-abundance proteins. The limit for the detection of proteins with Sypro-Ruby is approximately 1 ng (i.e., 20 fmol for a 50 kDa protein). Low-abundance proteins, which are not detected by conventional staining, include regulatory proteins, receptors and other proteins that play roles in cellular responses.

Poor reproducibility of 2-DE patterns often results in difficulties during the spot matching. Correct identification of differentially expressed proteins can also be hindered by co-migrating proteins in a single spot, making it difficult to determine which protein is differentially expressed. The sources of variability that influence 2-DE results can mostly be grouped into two categories: biological and technical variability. The biological variability is due to genetic and/or environmental factors, differences in the physiological conditions of individual at the moment of sample collection. Technical variation can ensue not only from any stage of the experimental procedure, but also from reagents quality or handling variation.

An important issue is the need to reduce technical and biological variation gaining increased power to detect treatment differences. A biological replicate is obtained analysing different samples from the same experimental group and any significant change in protein expression is considered significant above biological noise. A technical replicate is obtained when the same sample is analyzed multiple times. This allows the establishement of analytical technique variability. An ideal experiment design would always consist of a mix of biological and technical replicates, of which the biological replicates bear more weight for answering the underlying

biological questions. However, the reality of budget and sample limitations for biological variability assesment often force to compromise as in the case of this Thesis. To overcome resource constraints, often sample pooling is performed. Because pools represent averages, the dominant differences and similarities between experimental groups might be easier to find (Kendzioniski *et al* 2005; Diz *et al* 2009; Karp *et al* 2009). The assumption of biological averaging is usually met in animal models where the source of bias (subject-to-subject variation) are small and can be neglected (Karp *et al* 2009). However when sample pooling is performed, it is important to known that an artificially low variation has been created and consequently the p-values will look "better" than they might be if a biological variation was also included.

Nevertheless, the identification of up- and down-regulated protein expression from pooled samples does not mean that the proteins are not interesting with the respect to the underlying biological population. It just means that there is no statistical confidence and the use of additional methods of validating the findings is highly recommended.

1.4.2. One dimensional gel electrophoresis analysis (1-DE)

To overcome 2-DE drawbacks, a large effort has been focused not only on improving the capabilities of 2-DE-based proteomics, but mainly on the developing of alternative approaches that significantly expand the array of tools available for proteome research. One of the most used and innovative is the 1-DE gel approach for protein prefractionation coupled to high-accuracy mass spectrometry for protein identification (1-DE-LC-MS/MS). Extracted proteins are quickly and broadly separated by 1-DE gel to decrease the complexity of the samples, the gel is stained and cut into gel slices. The gel slices are then digested with trypsin, peptides extracted and identified by LC-MS/MS. The intensity of the resulting LC-MS/MS features is then used for relative quantification of peptides and proteins (details are reported in paragraph 1.4.2.4.

Quantitative approaches in proteomics). This workflow is capable of accurately identifying and quantifying thousands of peptides simultaneously. Advantage of this approach includes a comprehensive protein profile with relative quantitative information for all the proteins identified in a sample.

1.4.2.1. 1-DE and 2-DE approaches

1-DE and 2-DE approaches represent different ways to separate complex mixtures of proteins, and provide different information at different level of the proteome. Only a limited subset of proteins is amenable to 2-DE, since this technique favours the detection of high abundant proteins with medium-size and medium hydrophobicity. However 2-DE allows the visualization of protein isoforms as multiple protein spots on 2-DE maps with either slightly different pI or molecular weight or both, as results of post-translational modifications (PTM). The 1-DE-LC-MS/MS method overcomes some 2-DE drawbacks providing a more complex protein repertoire and allowing a direct relative quantitation using the mass spectral output, but it cannot easily provide information on the presence of a protein PTM.

1.4.2.2. Protein identification by Mass-Spectrometry

Proteolytic digestion of proteins (Matherials and Methods, page 90) is particularly useful in both 2-DE and 1-DE based workflows, since in-gel digestion provides a simple and efficient way of recovering the stained gel-entrained protein for subsequent characterization by MS. The most widely used enzyme is trypsin, which hydrolyzes the proteins on the C-terminal side of lysine and arginine, unless the following amino acid is proline. This is advantageous as every peptide other than the one including the original C-terminus has at least two sites for efficient protonation, the N-terminal amino group and the C-terminal basic residue, so peptides are readily ionized and detected as positive ions. Moreover, the presence of a basic residue at the C terminus favours simple and easily interpretable fragmentation pathways in collision-induced dissociation experiments.

1.4.2.3. Protein identification and database searching

The final stage is bioinformatic analysis of mass spectrometric data in order to allow identification and characterization of the proteins under study. Several search algorithms have been developed that compare the tandem mass spectra to a known *in silico* generated database of peptide spectra and identify the closest match or matches. The identified peptides are then used to derive their parent proteins. MS/MS search algorithms can be broadly classified in heuristic and probabilistic search algorithms (Omenn, States *et al.* 2005). The first category correlates the experimental MS/MS spectrum with a theoretical spectrum and calculates a score based on the similarity between the two spectra. These search algorithms are often based on the notion of "shared peak count" (SPC) since they simply count the number of peaks common to the two spectra. Sequest, Spectrum Mill, X!Tandem belong to this category. Probabilistic algorithms, such as Mascot, model the peptide fragmentation and calculate the probability that a particular peptide sequence produced the observed spectrum by chance. Although different search engines processing the same input spectra often produce comparable outputs, subtle differences remain (Fitzgibbon, Li *et al.* 2008). An analysis can therefore benefit from the use of multiple search algorithms for consensus scoring (Wenger and Coon 2013; Omenn, States *et al.* 2005).

In this work, I have used three different search algorithms: Phenyx, Mascot and X!Tandem. The Phenyx search engine applies a two-stage analytical strategy (see Table 2 in Material and Methods section). The initial search typically uses stringent parameters with an extended database to obtain a filtered list of candidate proteins while minimising the computational overhead associated with too many combinatorial possibilities. In the second round a much more comprehensive search is performed on a limited database consisting only of the candidate proteins. This can encompass nonspecific cleavages and consider a wide selection of posttranslational and artefactual modifications. A search of a randomized version of the database enables estimation of the false-positive rate. The final assignments and associated

confidence levels calculated from the scores and the chosen database are then reported. The Mascot algorithm (http://www.matrixscience.com) is based on the MOWSE scoring algorithm. For each identified peptide, Mascot reports a probability-based ion score which is defined as -10*log10(p) where p is the probability that the observed match between the experimental data and the database sequence is a random event. Knowing the size of the sequence database being searched it becomes possible to provide an objective measure of the significance of a result. Mascot also reports an expectation value (E-value) that is the number of matches with equal or better scores that are expected to occur by chance alone. Similar to Mascot, X!Tandem uses score distributions but extrapolates empirical Evalues to assess the significance of a peptide match, using cyclic permutations of all peptide candidates that are scored. Search algorithm mistakes in interpreting mass spectrometric data should lead to false positive identification of the protein/gene from which the peptide derives. False positive identification can arise for several reasons such as poor quality fragmentation, poor signal to noise ratio, amino acid sequence that do not produce a unique fragmentation pattern, but share enough of the same fragment ions to be indistinguishable from one another. In particular, small peptides, less than eight amino acids in length, may not produce a fragmentation pattern that achieves a unique result. To complicate this process there is the fact that often a peptide sequence exists in multiple proteins and without additional peptide data it would be impossible to determine which protein produced the peptide that generated the tandem mass spectrum (Sadygov, Cociorva *et al.* 2004). A useful means to reduce the number of false positives is to perform a decoy search. During a decoy search, every time a protein sequence from the target database is tested, a random sequence of the same length is automatically generated and tested. The number of matches that are found from the "decoy" database is an excellent estimate of the number of false positives that are present in the results from the real or "target" database and allows an estimation of the quality of the obtained data (Elias and Gygi 2007).

1.4.2.4. Quantitative approaches in proteomics

Earlier proteomic research was merely focused on the identification of proteins, but nowadays the quantitative and comparative aspects of proteomics increasingly attract the interest of researchers. Approaches employed in quantitative proteomics range from 2-DE to the more recent gel-free quantification methods (Ross, Huang *et al.* 2004). In the 2-DE approach differences between samples are estimated by statistical analysis performed with image analysis software able to merge and compare a number of replicate sets of gels for controls and samples. In the last decade, in order to overcome the limitations of 2-DE related approaches (reported in the preceding section on 2-DE: strength and limitations), gel-free protein quantification methods alternative quantitative approaches were developed. These alternative quantitative approaches not only circumvent the 2-DE approach, but they significantly expand the spectrum of tools available for proteomic research. The numerous reported strategies to derive quantitative information from MS analysis can be classified into:

1. Stable isotope labelling, based on the chemical tagging of proteins/peptides, followed by relative quantification of protein sample by LC-MS/MS analysis;
2. Label free approaches.

In protein-labelling approaches, different protein samples are combined together once labelling is finished and the pooled mixtures are then taken through the sample preparation step before being analyzed by a single LC-MS/MS experiment (Figure 1.17). In contrast, with label-free quantitative methods, each sample is separately prepared, then subjected to individual LC-MS/MS runs (Figure 1.17).

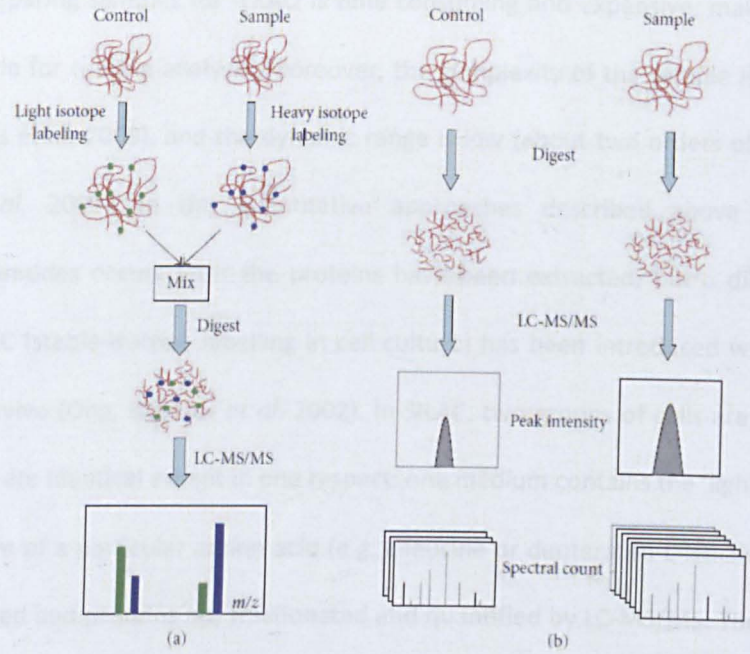

Figure 1.17. General approaches of quantitative proteomics. (a) Shotgun isotope labelling method, (b) label free quantitative proteomics.

1.4.2.4.1. Stable isotope labelling approaches

The stable isotope labelling strategies were first to emerge in the field of proteomics (Turck, Falick *et al.* 2007). The prototypical stable-isotope labelling is isotope-coded affinity tags (ICAT) technology (Gygi, Rist *et al.* 1999). Proteins from two samples to be compared are labelled at cysteine residues with light and heavy tags carrying a biotin moiety, used for purification purposes. Light and heavy tags contain respectively hydrogen and deuterium atoms. A number of limitations to the prototypical ICAT technique has been reported (Patton 2002) and some of these have been solved by the new cleavable ICAT (cICAT) reagent, which employs C 13 isotopes and an acid-cleavable biotin group (Hansen, Schmitt-Ulms *et al.* 2003). Recently, a new quantitative method, isobaric tags for relative and absolute quantitation (iTRAQ), was developed (Ross, Huang *et al.* 2004). iTRAQ technology employs a 8-plex set of amine reactive isobaric tags to derivatize peptides at the N-terminus and the lysine side chains, thereby labelling all peptides in a digest mixture. iTRAQ consists of three components, a balance group, a peptide reactive group, and a reporter group that have different masses (from 113.1 to

121.1). Preparing samples for iTRAQ is time consuming and expensive, making this approach less suitable for routine analysis. Moreover, the complexity of the sample is increased (Patel, Thalassinos *et al.* 2009), and the dynamic range is low (about two orders of magnitude) (Ow, Salim *et al.* 2009). In the quantitative approaches described above the labelling of proteins/peptides occurs after the proteins have been extracted, but a different technique called SILAC (stable-isotope labelling in cell culture) has been introduced where proteins are labelled in vivo (Ong, Blagoev *et al.* 2002). In SILAC, two groups of cells are grown in culture media that are identical except in one respect: one medium contains the 'light' and the other a 'heavy' form of a particular amino acid (e.g. L-leucine or deuterated L-leucine). Then samples are combined and proteins are fractionated and quantified by LC-MS/MS. The SILAC approach has some interesting advantages, for example it does not require additional purifications to remove excess labelling reagent, nor does it involves multistep labelling protocols. SILAC enables discrimination between proteins derived from cells and those derived from other sources, such as serum. However, to obtain accurate quantitation the labelling process must be long enough to allow full incorporation of the heavy label (Ong, Foster *et al.* 2003) and to guarantee a more complete sequence coverage in identification, the use of two labelled amino acids is advisable.. SILAC is quite impractical for the routine labelling of large organisms such as rats and mice, as the labelled amino acids are so expensive. Limitations of these labelling methods are mainly related to their high cost (Kuhner and Gavin 2007; Vandenbogaert, Li-Thiao-Te *et al.* 2008).

1.4.2.4.2. Label free approaches

The label free approaches have received increasing attention as alternative strategy of lower complexity and cost without the limitation in the number of compared samples. Free from the requirement of sample mixing, the analysis can include data sets obtained at different time (Ackermann, Berna *et al.* 2008). Protein quantification is generally based on the measurement

of ion intensity changes (such as peptide peak areas or peak heights in chromatography) or on spectral counting of identified proteins after MS/MS analysis (Yan and Chen 2005; Zhu, Smith *et al.* 2010). Peptide peak intensity or spectral counting is measured for individual LC-MS/MS runs and changes in protein abundance are calculated via a direct comparison between different analyses. Due to advances in instrumentation, specifically the stability and control of most of the physical properties of the analytical platform, it is possible to compare ion intensities of tryptic peptides without the need of labelling techniques. In LC-MS, an ion with a particular *m/z* is detected and recorded with a particular intensity, at a particular time. It has been observed that signal intensity from electrospray ionization (ESI) correlates with ion concentration (Voyksner and Lee 1999). In this study a label free approach was used to analyze the plasma proteome.

1.4.2.4.3. Ion Intensity Changes

The label-free quantification of the peptide/protein via peak intensity in LC-MS was first studied in 2002 on myoglobin peptides (Chelius and Bondarenko 2002), when the peak areas were found to increase with the increased concentration of injected peptides. Although this study showed that the relative quantification of the peptides could be achieved via direct comparison of peak intensity of each peptide ion in multiple LC-MS datasets, applying this method on the analysis of changes in protein abundances in complex biological samples had some practical constraints. First, experimental variations (sample preparation or sample injection) can lead to differences in the peak intensity of the peptides belong to the same sample from run to run. Thus, normalization is required to account for this kind of variation. Second, any experimental drifts in the retention time and *m/z* will significantly complicate the accurate comparison of multiple LC-MS datasets. Unaligned peak comparison will result in large variability and inaccuracy in quantification. Thus, highly reproducible LC-MS and careful chromatographic peak alignment are required and critical in this comparative approach. Last,

the large volume of data collected during LC-MS/MS analysis of complex protein mixtures requires the data analysis of these spectra to be automated. Therefore, several algorithms have been developed to automatically compare the peak intensity data between LC-MS samples with high throughput, such as those integrated in Scaffold (Proteome Software Inc, Portland, OR) or in MSQuant (Center for Experimental Bioinformatics, University of Southern Denmark).

1.4.2.4.4. Absolute and relative proteins quantification

A label free approach can be used to perform not only relative protein quantification but also an absolute quantification (Silva, Denny *et al.* 2006).

The Protein Abundance Index (PAI), was initially defined as the number of identified peptides divided by the number of theoretically observable tryptic peptides for each protein, (Rappsilber, Ryder *et al.* 2002) and was then later converted to exponentially modified PAI (emPAI, the exponential form of PAI minus one) (Ishihama, Oda *et al.* 2005). emPAI, as well as most of other label-free methods, has been shown to correlate well with protein abundance in complex samples (Ishihama, Oda *et al.* 2005). emPAI takes into account the number of identified peptides, normalized against the number of identifiable peptides for a given protein. The formula is $emPAI=10^{N\ observed/N\ observable}-1$, where N observed is the number of experimentally observed peptides and N observable is the calculated number of observable peptides for each protein. Ishihama (Ishihama, Oda *et al.* 2005) estimated the number of observable peptides by performing in silico digestion of protein sequences. The peptide list was then filtered to exclude peptides outside the mass spectrometer scan range and the observed nano-LC retention time range. The values of emPAI can be calculated easily with a simple script and do not require additional experimentation in protein identification, it can be routinely used for reporting approximate absolute protein abundance in a large-scale analysis.

Recently, an alternative approach was developed termed absolute protein expression (APEX) profiling. This measures the absolute protein concentration per cell from the proportionality between the protein abundance and the number of peptides observed (Lu, Vogel *et al.* 2007). The key to APEX is the introduction of appropriate correction factors that make the fraction of expected number of peptides and the fraction of observed number of peptides proportional to another. The protein's absolute abundance is indicated by an APEX score, which is calculated from the fraction of observed peptides mass spectra associated with one protein, corrected by the prior estimate of the number of unique peptides expected from a given protein during a MudPIT (multidimensional protein identification technology) experiment. The MudPIT technology is a non-gel approach for the identification of proteins from complex mixtures that consists of a 2-dimensional liquid chromatography separation, prior to electrospray mass spectrometry). Another strategy is represented by the normalized spectral abundance factor, NSAF that divides counts by the protein length, analogously to the Fabb index, that normalizes by the protein molecular weight (Cappadona, Baker *et al.* 2012). Absolute protein copy numbers have been recently reported based on precursor ion currents (Schwanhausser, Busse *et al.* 2011) and the technique, called intensity-based absolute quantification (iBAQ), proposes the sum of peak intensities of all peptides matching to a specific protein, normalized by the number of theoretically observable peptides, as an accurate proxy for protein levels (Cappadona, Baker *et al.* 2012).

In the spectral counting approach, relative protein quantification is achieved by comparing the number of identified MS/MS spectra from the same protein in each of the multiple LC-MS/MS datasets. This is possible because an increase in protein abundance typically results in an increase in the number of its proteolytic peptides, and vice versa. This increased number of tryptic digests then usually results in an increase in protein sequence coverage, the number of identified unique peptides and the number of identified total MS/MS spectra (spectral counts) for each protein (Washburn, Wolters *et al.* 2001). Liu *et al.* studied the correlation between

relative protein abundance and sequence coverage, peptide number and spectral count. It was demonstrated that among all factors of identifications, only spectral count showed strong linear correlation with protein abundance with a dynamic range over 2 orders of magnitude (Liu, Sadygov *et al.* 2004). Moreover, it has been demonstrated that spectral counting yields good reproducibility between replicate experiments (Old, Meyer-Arendt *et al.* 2005). Therefore, spectral count can be used to provide a semi-quantitative measure of protein abundance (Ishihama, Oda *et al.* 2005; Lu, Vogel *et al.* 2007; Old, Meyer-Arendt *et al.* 2005). In contrast to the chromatographic peak intensity, which requires delicate computer algorithms for automatic LC-MS peak alignment and comparison, no specific tools or algorithms have been developed specially for spectral counting due to its ease of implementation. However, normalization and statistical analysis of spectral counting datasets are necessary for accurate and reliable detection of protein changes in complex mixtures. Overall spectral counting proved to be more sensitive method for detecting proteins that undergo changes in abundance, whereas peak area intensity measurements yielded more accurate estimates of protein ratios (Old *et al.* 2005). A problem with the spectral counting approach could be the low sensitivity with the low abundant proteins, but as reported by Hoehenwarter (Hoehenwarter and Wienkoop 2010) this problem could be resolved using high mass accuracy mass spectrometer (like Orbitrap), minimizing redundant MS/MS acquisition and maximizing the resolution of the proteome by accurately measured m/z ratiosFrom these considerations, the spectral counting approach was the label-free method chosen for quantifying the proteins in the plasma samples of this study.

1.5. INTRODUCTION TO METABOLOMIC ANALYSIS

Metabolomics is a scientific discipline that aims to identify and quantify the metabolome, which is the total quantitative collection of small molecular compounds present in an organism or biological sample. Metabolomics was first discussed in 1998 by Stephen Oliver, who not only coined the term but saw the enormous potential of the application of metabolomics for functional genomics (Oliver, Winson *et al.* 1998).

Metabolites are the reactants and products of a metabolic network; therefore, the quantification of the metabolome provides a direct method for the analysis of internal metabolism kinetics (Buchholz, Hurlebaus *et al.* 2002). Metabolomics is a logical progression from the analyses of genes, RNA and protein at the systems level. It provides the correlation between genes and the functional phenotype of an organism, which is the ultimate purpose of a functional genomics approach. In contrast to transcriptomics and proteomics, metabolomics can provide direct evidence rather than indications of changes in biochemical pathways (Heijne, Kienhuis *et al.* 2005). Metabolomics is considered to be a downstream analysis, in that the changes occurring in the metabolome reflect amplifications of the changes that occurred in the transcriptome and the proteome (Kell 2005). Another benefit of metabolomics is that, unlike a transcript or protein, a given metabolite is the same in every organism that contains it. Although the development of metabolomic methods and technologies is progressing rapidly, there are still issues and drawbacks that must be considered. DNA, RNA and proteins all have some structural properties in common, allowing the development of analytical methods that apply to basically all members of the class. On the other hand, metabolites within a cell have no shared chemical features on which a single general isolation, separation or identification method can be developed (Fridman and Pichersky 2005). The number of metabolites and derivatives of known metabolites expected in mammals, plants and bacteria is still largely unknown. Moreover it is difficult to assign changes in metabolite levels to changes in the

expression of specific genes and/or proteins. The metabolome is made up of very diverse compounds, ranging from ionic inorganic species to hydrophobic lipids, in a dynamic range of concentrations (Villas-Boas, Rasmussen *et al.* 2005). Many major advances in the design and applications of analytical instrumentations for metabolomics have been made over the past few decades, allowing a broader and more comprehensive study of small molecules. However, in order for the true potential of metabolomics to be realized, efforts must be focused on improving sensitivity as a truly comprehensive analysis of the metabolome is not yet technically possible.

Since the cerebroprotection by ischemic preconditioning requires a complex response cascades that involves many genes, proteins and their products (metabolites) responsible for establishing the ischemia-tolerant phenotype, I decided to integrate my PhD project with a metabolomics investigation aimed at defining whether changes in circulating metabolites might have a link with brain and plasma proteomic profiles in my experimental model of ischemic preconditioning.

The use of an integrated proteomics and metabolomics analysis allowed me to obtain a more comprehensive picture of the molecular changes that occur during ischemic preconditioning.

1.5.1. Metabolomics approaches

There are two fundamental approaches that can be used when analyzing metabolites: targeted and un-targeted.

A targeted approach is restricted to the analysis of defined groups of chemically characterized compounds. Targeted metabolomic approaches are commonly driven by a specific biochemical question or hypothesis that motivates the investigation of a particular pathway. A robust improvement of this method had been made using triple quadrupole (QqQ) mass spectrometry. In the triple quadrupole (QqQ)-based targeted metabolomic workflow, standard

compounds for the metabolites of interest are first used to set up selected reaction monitoring methods. Here, optimal instrument voltages are determined and response curves are generated for absolute quantification. After the targeted methods have been established on the basis of standard metabolites, metabolites are extracted from tissues, body fluids or cell cultures and analysed. The data output provides quantification only of those metabolites for which standard methods have been built (Patti, Yanes *et al.* 2012). The untargeted approach is the comprehensive analysis of all measurable analytes in a sample with no prior knowledge about their structure. The power of the non-targeted approach allows for the generation of a data-driven hypothesis, whereas a targeted approach is intended to address a hypothesis and not to generate a new one. To date there is not a single analytical method capable of detecting and quantifying all metabolites in a system. This is largely due to the chemical complexity of compounds that comprise the metabolome. However, there have been many advances made in metabolomics analyses and the combination of these technologies may make the detection of all metabolites attainable in the near future.

1.5.2. Metabolomics technologies

There are numerous technologies available for studying the metabolome, each with advantages and limitations. Mass spectrometry (MS) and nuclear magnetic resonance (NMR) are the most commonly applied analytical technologies in metabolomics studies.

NMR is a powerful technique and is particularly useful in the structure elucidation of unknown organic compounds. The main limitations of this approach are the complex computational requirements to resolve complex mixtures, the low sensitivity, and the cost of the NMR equipment that can be significantly more expensive than MS-based technologies (Villas-Boas, Mas *et al.* 2005). MS is a widely applied technology in the study of metabolites as it provides a system which is both sensitive and capable of identifying and quantifying a wide range of metabolites (Dunn, Bailey *et al.* 2005).

Traditionally, gas chromatography-mass spectrometry (GC-MS) and liquid chromatography-mass spectrometry (LC-MS) have been used to study metabolites in a biological system. GC-MS can be used for the simultaneous separation, identification and quantification of volatile and non-volatile metabolites. The advantages of using GC-MS for the analysis of biological metabolites are the high chromatographic resolution and the ability to simultaneously analyze different classes of metabolites (Villas-Boas, Mas *et al.* 2005). The major drawbacks of this technology are that non-volatile compounds must be derivatized before they can be analyzed, large thermally-labile compounds cannot be detected due to their limited volatility, and that electron impact causes fragmentation (Dunn, Bailey *et al.* 2005; Villas-Boas, Mas *et al.* 2005). MS is a widely applied technology in the study of metabolites as it provides a system which is both sensitive and capable of identifying and quantifying a wide range of metabolites (Dunn, Bailey *et al.* 2005). LC-MS is also capable of separating, identifying and quantifying a broad range of metabolites, especially metabolites with similar molecular masses. The advantages of this approach are that derivatization is not needed and thermo-labile metabolites can be analyzed; however, the potential for identification can be a limitation unless a MS-MS fragmentation approach is used (Dunn, Bailey *et al.* 2005). Fourier Transform Ion Cyclotron Resonance-Mass Spectrometry (FTICR-MS) is a mass spectrometry platform, which is highly attractive for non-targeted metabolic profiling as it offers the highest mass accuracy and resolution of any other mass spectrometry technology. Although this analytical technique is very powerful, and extremely useful in metabolomic studies, it does have a few limitations that must be overcome in order for it to be a stand-alone metabolomic tool. These include the inability to discriminate between isomers, and a lower mass limit of approximately 100 Da. These limitations can be dealt with through the use of a targeted mass spectrometry platform, such as a liquid chromatography tandem mass spectrometer (LC MS/MS), which can be optimized to detect lower weight masses and discriminate between isomers. One of the new type of mass analyzer is the Orbitrap (Makarov 2000) in which a FTICR

ion detection is followed by a fast Fourier transform to convert the recorded time domain signal into a mass/charge spectrum and is characterized by an high mass accuracy (2-5 ppm) that make this kind of mass analyzer very useful for a metabolomic study.

1.5.3. Mass-spectrometry based-metabolomic data analysis

1.5.3.1. Data preprocessing

Raw data acquired by MS are typically pre-processed to provide structured data in an appropriate format for data analysis. The data are pretreated to reduce noise and background, alignment of mass spectra or mass chromatograms, automated picking and annotation of mass spectrometric or total-ion/extracted ion chromatographic peaks of metabolic features. Currently several public and proprietary software tools exist to implement data export and subsequent data analysis.

In this thesis I report the main characteristics of the commercially available software I used to analyze my metabolomics data. The software is SIEVE from Thermo Fisher, Cambridge, MA, US.

The mass spectra obtained by non-target approach are analyzed using SIEVE v2, a software package that allows the semi-quantitative differential expression analysis. The first step in data elaboration is the alignment of all the raw chromatograms to make them comparable. The SIEVE software performs a chromatographic alignment using full scan spectra shape (no peaks). User-defined peak threshold like minimum height, signal to noise, width etc. are applied to detect MS peak. Alignment of drift (retention time and accurate mass) in data related to run order is performed and ensures that a chromatographic peak is identified with the same parameters in each sample. The second step is finding peaks, also called *features*. A metabolic feature is defined as a detected chromatographic peak with associated retention time and unique accurate *m/z*. An important issue is to relate peaks to individual ions and then to molecular species. A single metabolite is often detected as multiple metabolic

features, each having the same retention time, but a difference in *m/z*. The difference in *m/z* relates to different derivative ions of the same metabolite. Each molecule produces many ions (molecular fragments, adducts formation), even under the most gentle ionization conditions. As a result, a typical ESI LC-MS data set from a body fluid sample may contain tens of thousands of peaks (millions if one considers noise) that represent only hundreds of compounds. The SIEVE software uses a new signal detection algorithm called *component extraction* for automatic matching of the metabolic features derived from the same metabolite. Metabolic features derived from the same metabolite are identified, annotated and grouped together using accurate *m/z*, *m/z* differences, adduct relationship, retention time similarity, peak shape similarities. Consequently, metabolite identification for one metabolic feature is linked to all other derived metabolic feature for that metabolite.

For identification of the features of interest, the SIEVE software provides a web services query Application Program Interface that links the software directly to metabolic spectral library databases such as ChemSpyder or others by Internet connection .

1.5.3.2. Metabolite identification

The effort required for identification of metabolites depends on the scope of the study, be it targeted or untargeted. If the search is for known metabolites the identification involves comparing the experimental data with that of pure standards. If the metabolites can be predicted, then the metabolic identification involves finding representative standards and searching for the predicted metabolites. If nothing is known about the metabolites in the experimental data, as in the untargeted strategy, the metabolite identification is much more complicated and does not provide 100% coverage. This approach is widespread in mass spectrometry-based metabolomics due to MS high sensitivity and hereby the possibility to discover new and low-abundant metabolites. The identification strategy takes advantage of the accurate mass measurement and fragmentation pattern obtained from up-to-date

instrumentations such as the Orbitrap mass analyser that has high resolving power and excellent mass accuracy (1-5 ppm). Usually, identification by MS uses the accurate mass to define molecular formulae and to query electronic resources (metabolomic databases and mass-spectral libraries). The accuracy of the *m/z* measurement defines the number of molecular formula matches; the greater the accuracy the lower the error range and the lower the number of molecular formula matches (Kind and Fiehn 2006).

Usually, an experimentally determined accurate mass, within a specific mass error for a single metabolic feature, is matched to the theoretical accurate mass related to a single or multiple molecular compounds searching for molecular formulae in the databases to define putative metabolic identification. Various public mass-spectral libraries exist so far such as the Human Metabolome Database (HMD); METLIN; ChemSpyder; NIST; MassBank. However these repositories suffer from some intrinsic limitations. This is because the metabolome (e.g. human metabolome) has not been completely and experimentally characterized yet and therefore the libraries used for identification do not yet reflect all known metabolites. Moreover, not all metabolites of those known to be present can be synthesized or purchased to construct mass spectral libraries to aid identification processes. A further constraint exists for LC-MS libraries insofar as fragmentation spectra vary between different type of mass analyzer (Bristow, Webb *et al.* 2004, Jansen, Lachatre *et al.* 2005). Thus the creation of universal libraries for LC-MC is impeded. Therefore, definitive identification of all detectable metabolites is not currently achievable and is a significant limitation in metabolic profiling.

1.5.3.3. Network and pathway analysis of proteomic and metabolomic data

The increasing amount of data derived from global gene, protein and metabolite expression measurements necessitates the use of computational technologies to store, analyze, correlate and interpret this information. A major challenge of contemporary biology is to embark on an integrated theoretical and experimental program to map out, understand and model in

quantifiable terms the topological and dynamics proprieties of the various networks that control the behaviour of the cell (Barabasi and Oltvai 2004). The main aim of the network biology is to study and understand the interactions among molecules in a living cell. This is important since it is now clear that a discrete biological function cannot be ascribed to an individual molecule. Currently, several different pathway databases and network building tools are available, allowing the visualization of cellular components as networks of signalling, regulatory and biochemical interactions. Although most of these techniques were developed to accommodate the huge amount of data derived from gene microarray experiments, they have been applied to proteomic/metabolomic data more recently. Mapping of up- and/or down-regulated proteins or metabolites onto known pathways, combining functional enrichment and transcription regulation analysis, is indeed a useful means to provide information to supplement the conventional approach of linking proteins and metabolites to biological process via review of the literature. This may allow a richer interpretation of proteomic and metabolomic experiments, suggesting pathways involved in pathological processes and helping formulate new hypotheses to be tested and validated with different ad-hoc approaches.

In this thesis two different bioinformatic tools were used to understand the biological significance of proteomics and metabolomics data: the commercially available Metacore software package, and the public available MetaboAnalyst software.

1. MetaCore (Thomson Reuters, NY, USA) is an integrated analytical suite of algorithms, based on a manually annotated and regularly updated databases of human and rodent protein-protein interactions, transcriptional factors, signalling, metabolism and bioactive molecules linked to functional processes (www.genego.com). The databases consist of millions of relationships between proteins and metabolites that are derived from literature publications on proteins and small molecules. The content of MetaCore's underlying database is packaged into pathway maps or networks that describe a biological function, then further organized into

ontologies, such as biological process or disease. GeneGo's biological process ontology consists of about 1000 networks that summarize regulatory functions. Networks provide a clear representation of complicated relationships between large numbers of elements (genes/proteins). These elements represent the nodes, often graphically depicted as small circle. Nodes are connected by links, called edges (Figure 1.18).

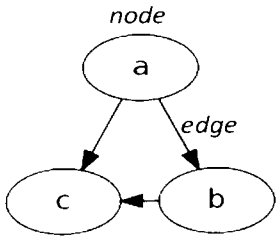

Figure 1.18. Schematic representation of the relationships provided from networks.

Edges represent functional relationships or physical interactions between nodes. Depending on the nature of interaction, an edge can also have associated numerical values corresponding to the strength, or weight, of the relationship. In addition to representing a wealth of diverse data as a coherent and synthetic picture, networks can also be dissected according to the rules of network analysis, which helps extracting biological insights. MetaCore contains many options for network building. It currently has many network building algorithms (Analyze Network, Analyze transcriptional regulation, Analyze transcription factors, Analyze receptors, Shortest Paths, and Self Regulations, Direct Interactions, Auto Expand and Expand by One Interaction) as well as many options to modify these algorithms. Analyze network creates a large network and breaks it up into smaller sub-networks which can be built separately. The resulting networks are ranked by a p-Value. Analyze transcription regulation works similar to analyze network, but the subnetworks created are centered on transcriptional factors. The other two additional "Analyze" network algorithms (transcription factors and receptors) focus on the presence of either start-nodes or end-nodes of a certain pathway in the submitted list

of genes/proteins. As reported in the MetaCore user manual (https://portal.genego.com/help/MetaCore_Advanced_Training_Manual_5.0.pdf) the Direct interactions algorithm creates a network only from the objects in the original list; no other objects from the database will be added. This algorithm is good to start with because it can show if any of the objects in the list "cluster" together by interacting with each other. The Auto expand algorithm adds objects until it creates a fairly dense network; this is best used to see the neighboring interactions and objects around a few nodes. Finally, Expand by one interaction simply adds all the one-step interactions around each node from the list. In MetaCore, different networks and pathways modules can be prioritized based on their statistical significance. Significance is evaluated based on the size of the intersection between user's dataset and MetaCore set of genes/proteins corresponding to a network module/pathway in question. MetaCore software calculates p-values on the basis of hypergeometric distribution probability test. The resulting networks are evaluated for which algorithm have succeeded in creating modules that have higher than random saturation with the protein of interest.

2. MetaboAnalyst (www.metaboanalyst.ca) is an integrated web-based platform for comprehensive analysis of metabolomic data. MetaboAnalyst version 2 is designed to perform a variety of complex metabolomic data analysis tasks that includes data processing, normalization, statistical analysis and high-level functional interpretation. In this thesis, this last function has been particularly used for elucidating possible biological mechanisms. MetaboAnalyst presents the following types of enrichment analysis:

- Over-representation analysis (ORA): a list of compound names obtained by multivariate analysis is subjected to a hypergeometric test and the p-value obtained indicates the possibility of observing at least a particular number of metabolites from a certain metabolite set in a given compound list.

- Simple-sample profiling (SSP): the method first identifies those metabolites with concentrations in biological fluids deviating significantly from the reported normal reference ranges and then subjects this metabolites to ORA

- Quantitative enrichment analysis (QEA): a compound concentration table is analyzed with the globaltest algorithm and the p-value obtained indicates the probability that none of the matched compounds in the metabolite set is associated with the class label

Current analytical technologies offer a partial metabolome coverage, which makes metabolomic studies intrinsically biased toward metabolite sets containing compounds that are more abundant or more easily detected by a given technology platform. MetaboAnalyst supports application of a platform-specific reference metabolome to correct for this potential bias (Xia and Wishart 2011)

1.6. STATISTICAL MULTIVARIATE APPROACHES USED IN PROTEOMIC AND METABOLOMIC ANALYSIS

Proteomics and metabolomics data typically contains thousands of variables from each sample. The multidimensionality of this type of data is difficult to comprehend and visualise, and invoke for analytical techniques, which can extract the relevant information. Chemometric methods are here an obvious choice due to their ability to decompose complex multivariate data into simpler and potentially interpretable structures (Wold 1991). Depending on the aim of the analysis, unsupervised or supervised methods may be applied and assist in obtaining an overview of data, in variable selection, in group classification or to relate the data set to a reference value for construction of prediction models.

To this purpose two main tools are generally used: principal component analysis (PCA) and/or partial least square regression (PLS).

1. Principal component analysis (PCA) can be generally described as a method that reveals the internal structure of a data set in a way that best explains the variance in the data. Mathematically a PCA model can be written as: $X = T P' + E$ where X is the data matrix representing samples and variables decomposed into a score matrix (T) and a transposed loading matrix (P'). The E matrix contains the residuals, the part of the data not 'explained' by the principal component model. In this way, the score and loading matrix contains the systematic variation with respect to samples and variables, leaving the unsystematic variation in the residual (Wold 1991). PCA offers a reduced dimensional model that summarises the major variation in the data into few axes, and in this way, systematic variation is captured in a model that can be used to quickly visualise which samples in the data set are similar or dissimilar to each other. From this, possible spectral loadings causing any treatment-related separation may be identified.

2. Partial least square regression is a powerful algorithm that can analyse data with numerous strongly correlated X-variables (e.g. spectra) and also simultaneously model one or several Y-

variables (e.g. a response variable/biomarker) (Wold 1991). This enables establishment of a linear model that can predict Y from the measured spectra in X. Like PCA, PLS regression generates a linear model of the data, but where PCA models the major variation in the data itself, PLS derives a model that describes the correlation between the X variables and a feature (Y variable) of interest (Keun 2006). PLS is often used as a classification tool in metabolomics studies by applying the discriminant analysis approach (PLS-DA). For this analysis, a class vector is constructed of one variable of each class with a value of 1 if the sample belongs to a particular class and 0 if not. By regression against this class vector, latent variables can be derived that separate the classes from each other. It seems worth mentioning that PLS-DA can suffer severely from overfitting, since the number of samples used in metabolomics applications is usually much smaller than the number of variables, and this can easily lead to chance classifications. Consequently, the PLS-DA algorithm can separate two groups comprised completely of random data. Therefore, a focus on the validation process is particularly important in this analysis (Westerhuis 2008).

CHAPTER 2

AIM OF THE STUDY

2.1. RATIONALE

Ischemia indicates an insufficient influx of blood in a specific organ or tissue including the heart, muscle, kidney or brain. Among these, brain ischemia represents the primary cause of permanent invalidity and the third most common cause of death in industrialized states. The symptoms are consequences of a transient or permanent loss of some cerebral function and these are strictly dependent on the location of the damaged area. To date, an effective therapy to treat such injuries is still lacking.

A considerable body of evidence supports the hypothesis that a brief ischemic insult, below the threshold of damage, evokes endogenous defence mechanisms that confer protection against a subsequent severe ischemic attack (Dirnagl *et al.* 2003; Weih *et al.* 1999; Moncayo *et al.* 2000). This phenomenon is termed ischemic preconditioning (**IP**) and the resulting protection is known as ischemic tolerance (**IT**). IP and IT can occur in different tissues and organs and have been shown in experimental models and in humans too. These phenomena are attracting much attention because preconditioning-induced ischemic tolerance is an effective experimental probe to understand how the brain protects itself (Obrenovitch, 2008). To date, the molecular mechanisms that lead to IT are not yet completely understood, although it is clear that multiple effectors such as the activation of cellular defence mechanisms and reduced inflammatory responsiveness, contribute to IT (Schaller and Graf, 2003; Muramatsu *et al.* 2004; DeGracia and Montie 2004). In this complex scenario, proteomics and metabolomics represent powerful tools to identify the constellation of protein and metabolite alterations that occur during IT development, by exploring expression profiles globally. Moreover, the integration of these two strategies raises the possibility of detecting new biological mechanisms/pathways underlying neuro-protection, and could eventually lead to the discovery of a panel of protein and metabolite mediators that could serve as predictors for preconditioning traits and as putative diagnostic markers of brain injury.

2.2. AIMS OF THE PROJECT

Based on the above considerations, the principle aim of this project is to perform an exploratory analysis to investigate changes in the proteome profile of the brain cortex and plasma, together with changes in the profiles of metabolites in plasma, using a murine model of IT induced by TIA. Specifically, the project aims to:

(i) clarify the mechanisms of preconditioning and endogenous neuro-protection, identifying possible IT mediators that can be used as possible therapeutic tools and/or targets for acute brain injury.
(ii) search for a panel of candidate protein mediators in the plasma of the IT animal model. Particular attention will be made to evaluate the correlations between brain and plasma proteins, in order to discover a panel of protein candidates mediators for stroke progression and prognosis.
(iii) identify circulating metabolites that could be involved in ischemic preconditioning and might represent, together with plasma and brain proteins, an innovative array of candidate mediators.

To achieve the above-mentioned goals three different analytical strategies were used:

- a conventional 2-DE approach was applied to protein samples of right brain cortices to identify differentially expressed components.
- A 1-DE LC-MS/MS approach was applied to analyse qualitatively and quantitatively the protein repertoire of whole plasma.
- An untargeted metabolomics approach was applied to obtain a metabolic plasma profile that could be related to the proteomic changes in plasma and also to such changes in the brain cortex.

The three analytical strategies were performed on pooling samples due to budget constrains (e.g. expensive surgical procedure for the ischemic models) and sample limitations for biological variability assesment. The results of each experiment consist only of technical replicates and this means that the statistical analysis has weak relevance. Nevertheless, the identification of altered proteins expression and metabolites abundance from pooled samples

does not mean that these features are not interesting with the respect to the underlying biological population. It just means that the statistical confidence is limited and the use of additional methods of validating the findings is highly recommended.

CHAPTER 3

MATERIALS AND METHODS

3.1. ANIMALS

The ARRIVE guidelines have been followed in this study (Kilkenny *et al.* 2010).

C57Bl/6 mice (11 week-old male mice, Harlan Laboratories, Italy), housed in specific pathogen free *vivarium*, were used. Procedures involving animals and their care are conducted in conformity with the institutional guidelines that are in compliance with national (D.L. N. 116, G.U., Suppl. 40, 18 febbraio 1992, Circolare No.8, G.U., 14 luglio 1994) and international laws and policies (EEC Council Directive 86/609, OJ L 358, 1, Dec. 12, 1987; Guide for the Care and Use of Laboratory Animals, U.S. National Research Council, 1996).

3.1.2. Focal permanent cerebral ischemia

For permanent MCAo (pMCAo), a vertical midline incision was made between the right orbit and tragus (Gesuete, Orsini *et al* 2011; Storini *et al* 2005). The temporal muscle was excised, and the distal branch of the right MCA was exposed through a small burr hole in the right temporal bone. The dura mater was cut with a fine needle, and the MCA was permanently occluded by electrocoagulation just proximally to the origin of the olfactory branch (Figure 3.2). Intraoperative rectal temperature was kept at 37°C ± 0.5°C using a heating pad (LSI Letica, Spain). The mortality rate for this model is 13.5%. Sham-operated mice received an incision between the right orbit and tragus and the subsequent exposure of the temporal bone. The bone was drilled, but the dura mater and the middle cerebral artery were left intact. Similar to ischemic mice, sham-operated mice were maintained at 37°C during surgery.

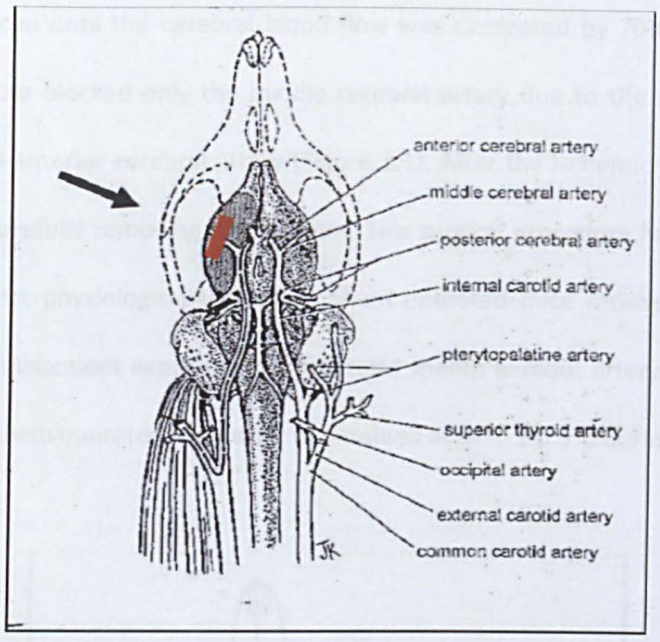

Figure 3.2. Permanent occlusion of the middle cerebral artery. Schematic drawing of ventral view of mouse cerebral vessels, showing permanent MCAo procedure.

3.1.1. Focal transient cerebral ischemia

Transient focal cerebral ischemia was achieved by middle cerebral artery occlusion (MCAo) as previously described (Gesuete, Orsini *et al* 2011), (Figure 3.1). Eleven week-old male mice were anesthetized by 5% isoflurane in N2O/O2 (70/30%) mixture and maintained by 1.5 to 2% isoflurane in the same gas mixture. To confirm the adequacy of the vascular occlusion in each animal, blood flow was measured by laser Doppler flowmetry (Perimed PF5010) using a flexible 0.5-mm optic fibre probe (type M, 0.5 mm diameter; Transonic) positioned on the brain surface and secured with impression material on the skull at the following coordinates: AP= -1 mm; L= -3.5 mm. The animals were placed supine on a homeothermic pad equipped with a rectal probe to maintain a constant *core* temperature of 37°C ± 0.5°C (LSI-Letica, Barcelona, Spain). A midline neck incision was made and the carotid sheath was exposed. The following surgical steps were performed under an operating microscope (Nachet, Dijon, France). The right common carotid artery was exposed and a siliconized monofilament (7-0, Doccol Corp., Redlands, CA, USA), was introduced in it to reach the middle cerebral artery

(MCA) and advanced until the cerebral blood flow was decreased by 70% compared to the baseline. The suture blocked only the middle cerebral artery due to the minor diameter of MCA compared to anterior cerebral artery (Figure 3.1). After the ischemic period, blood flow was restored by carefully removing the filament. This surgical procedure has been previously shown not to affect physiologic parameters. Sham operated mice received a midline neck incision, and the subsequent exposure of the carotid sheath without artery occlusion. Similar to ischemic mice, sham operated mice were maintained at 37°C ± 0.5°C during surgery.

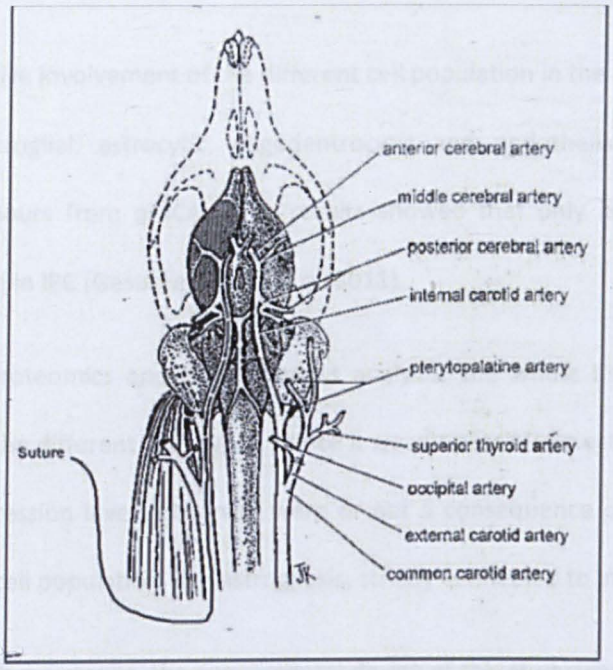

Figure 3.1. Transient occlusion of the middle cerebral artery. Schematic drawing of ventral view of mouse cerebral vessels, showing transient MCAo procedure.

3.1.3. Experimental design

The length of MCAo to mimic a TIA was setup testing 3 short periods (10', 7' and 5') and the neurological deficits were evalueted 48 hours later. Ten minutes of MCAo induce a small lesion in the striatum that wasn't present at 7' and 5' minutes. Since the 7'MCAo is the longest non-

injurious stimulus close to but below the threshold of damage (Dirnagl *et al* 2003), this time point was selected to mimic the TIA (Gesuete, Orsini *et al.* 2011).

Then different time point between the preconditioning stimulus and the severe ischemia (1,2,3,4 and 5 days) were evaluated to assess the neuroprotection. When pMCAo was performed after 1 or 2 days from 7'MCAo, the lesion volumes (12.91 ± 1.48 mm^3, 10 ± 2.2 mm^3 respectively) were similar to non-preconditioned mice (13.61 ± 0.8 mm^3) instead after 3 or 4 days a significant reduction was observed (8.95 ± 1.02 mm^3 and 8.45 ± 0.7 mm^3 respectively) that was not anymore present after 5 days of interval (Gesuete, Orsini *et al.* 2011)l.

To dissect the selective involvement of the different cell population in the IPC, gene expression for neuronal, microglial, astrocytic, oligodentrocytic and endothelial component were analyzed after 48 hours from pMCAo. The results showed that only astrocytic population seems to be involved in IPC (Gesuete, Orsini *et al.* 2011).

In this thesis, for proteomics and metabolomics analysis, the whole tissue was processed without fractioning the different cells types, hence it wasn't possible to establish if the protein and metabolite expression levels observed were or not a consequence of biological process related to a specific cell population, like astrogliosis, strictly connected to inflammation.

On the basis of the above results, the experimental design of this study was set-up as shown in Figure 3.3. Mice (five per group) were assigned to five experimental groups, in the following sets: SET 1a, mice receiving 7' middle cerebral artery occlusion (MCAo) (IPC stimulus); SET 1b, sham surgery, and killed by cervical dislocation 4 days later; SET 2a, mice receiving sham 7'MCAo followed, 4 days later, by pMCAo, and killed 7 days later (severe ischemia); SET 2b, mice receiving sham 7'MCAo followed, 4 days later, by sham pMCAo, and killed 7 days later; SET 2c, mice receiving 7'MCAo followed, 4 days later, by pMCAo (7'MCAo/ pMCAo), and killed 7 days later (ischemic tolerance). SET 2b served as sham control for SETS 2a and 2c.

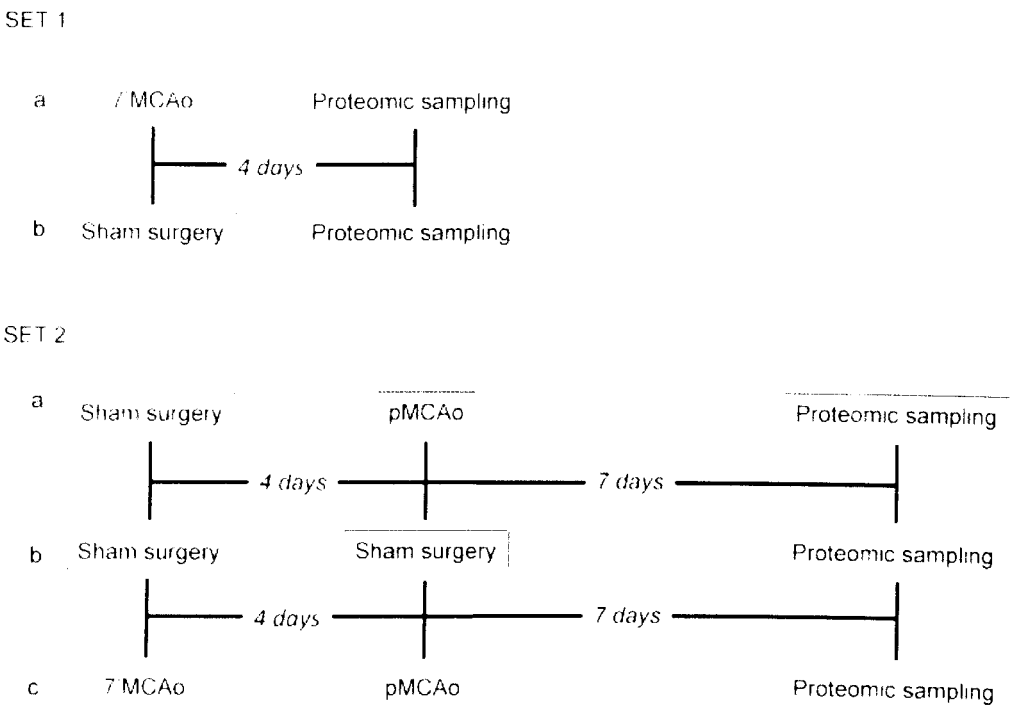

Figure 3.3. Experimental Design. *SET 1a*, Preconditioning stimulus: mice received 7'MCAo or *1b*, 7'MCAo sham surgery and were sacrificed 4 days later. *SET 2a*, Severe ischemia: mice received 7'MCAo sham surgery followed, 4 days later, by pMCAo and sacrificed 7 days later; *SET 2b*, 7'MCAo sham surgery and, 4 days later, pMCAo sham surgery, and were sacrificed 7 days later; *SET 2c*, Preconditioning/severe ischemia: mice received 7'MCAo and, 4 days later, pMCAo (7'MCAo/pMCAo), and were sacrificed 7 days later. SET 2b served as sham control for both SET 2a, and SET 2c.

3.2. BRAIN PROTEOMICS

3.2.1. Brain tissue collection and preparation

Brains were rapidly removed, right cortices dissected (De Simoni, Storini *et al.* 2003, Gesuete, Orsini *et al.* 2011), frozen on dry ice and stored at -80°C until proteomic analysis. For each animal proteins were extracted from frozen tissue by disintegrating about 90 mg of right brain cortex with Mikro-Dismembrator S (3000 rpm, 40 seconds). The powder obtained was resuspended in 1.8 mL of lysis buffer containing 5M urea, 2M tiourea, 2%(w/v) CHAPS, 2% (w/v) Zwittergent and a mixture of protease inhibitors, and homogenised for 1 minute. The samples were sonicated 3 minutes, and 250 Units of benzonase endonuclease were added in each sample. The homogenates were mixed for 30 minutes at 1000 rpm, at 25°C. The samples were then ultracentrifuged at 100,000xg, for 30 minutes at 15°C. The pellets were discarded and the supernatant collected.

3.2.2. Lipid removal and protein precipitation

Since cortex is a tissue rich in lipids that can dramatically interfere with protein extraction and with subsequent protein separation by 2-DE, their elimination is mandatory (Healthcare 1998). Lipids were therefore removed by performing a methanol/chloroform extraction. For each 100 µL of protein supernatant, 400 µL of methanol were added, the mixture was vortexed 30 seconds and centrifuged 1 minute at 9000xg. Then 100 µL of chloroform were added and the mixture was vortexed again and centrifuged 1 minute at 9,000xg. Then 300 µL H_2O were added and the mixture was centrifuged 5 minutes at 9,000xg. The top layer was removed (proteins were between layers), 300 µL methanol were added and centrifuged 5 minutes at 9,000xg, the methanol was immediately removed without disturbing the pellet. The protein pellets were resuspended in 50 µL of rehydration solution (5M urea, 2M thiourea, 2% CHAPS, 2%

Zwittergent), perfectly compatible with the next steps of bi-dimensional electrophoresis. Sample protein concentration was measured with the PlusOne 2-D Quant kit protein assay reagent (GE Healthcare, Italy) before and after precipitation. Protein recovery was more than 85% of the total protein extract. Proteins, delipidated by methanol/chloroform extraction, were quantified using PlusOne 2-D Quant Kit. This kit is designed for the accurate determination of protein concentration in samples to be analyzed by 2-D electrophoresis. Many of the reagents used in the preparation of such samples, (e.g. detergents, reductants, chaotropes and carrier ampholytes), are incompatible with the majority of commercially available protein quantification kits. The PlusOne 2-D Quant Kit works by quantitatively precipitating proteins while leaving interfering substances in solution. The assay is based on the specific binding of copper ions to protein. Precipitated proteins are resuspended in a copper-containing solution and unbound copper is measured with a colorimetric agent. The color density is inversely related to the protein concentration. The assay has a linear response to protein concentration in the range of 0-50 µg. The absorbance of each sample and standard is read at 480 nm using water as reference, by UltraSpect 2100 pro (Amersham Biosciences).

Due to budget and sample limitations for biological variability assesment , I adopted a samples pooling strategy to overcome the resource constraints . Pool cortices samples were prepared mixing equal amounts of protein (100µg proteins/animal) extracted from individual brain cortices (5 animals/experimental group). Five technical replicate gels were run for each pooled sample. Another limiting factor to consider is that two animal groups (7'MCAo/pMCAo and SHAM 7'MCAo/pMCAo) were processed and analyzed separately afterwards so the results obtained could be affected by the batch effect that can mask the underlying biology.

One hundred µg pooled proteins were diluted to a final volume of 130 µL with rehydration buffer containing also 100mM DeStreak reagent (GE Healthcare, Milan, Italy), added to protect

cysteinyl groups and prevent non-specific oxidation during the isoelectric focusing (IEF) run, and with 0.5% (v/v) IPG buffer (GE Healthcare, Milan, Italy) (Olsson, Larsson *et al.* 2002). The samples were loaded on 13 cm long strips, linear pH 3-10 gradient (IPG Strips, GE Healthcare, Milan, Italy). IEF was performed at 20 °C using an IPGphor apparatus (GE Healthcare, Italy) as previously described with minor modifications (Carpi, Korkalainen *et al.* 2009). Briefly, after a rehydration step for 16h at 30V, focusing was run over about 10h until about 46000 VhT were reached. After the first-dimension run, proteins were reduced and alkylated, the strips were then embedded in 0.6% agarose (w/v) on the top of 1mm thick acrylamide gels cast at 12%. Proteins were separated by apparent molecular mass at 10mA for 30 min and 35mA to completion.

3.2.2.1. 2-DE gel image analysis

After gel fixation and staining with colloidal Coomassie Blue (Pierce, Rockford, IL), the gel images were acquired at 16-bit resolution using an ImageScanner III (GE Healthcare). TIFF image analyses for spot quantification were performed using the Progenesis SameSpot (v4) and Progenesis Workstation (PG240, v2006) software (Nonlinear Dynamics Group, Newcastle upon Tyne, UK) to discriminate spots with a 1.5-fold or greater increases or decreased intensity across the experimental groups (reported in detail in the Introduction section, paragraph 1.4.1.3).

3.2.2.2. Statistical analysis

The Progenesis Stats Package (Progenesis Workstation PG240, v2006) integrated in the Progenesis SameSpot software was used to explore the differential expression of brain proteomics 2-DE data. This package allows multivariate and univariate analyses, including one-way ANOVA, and provides the q-value for each tested spot. The q-value controls for the false

discovery rate (FDR), as ANOVA does not take account of the multiple testing effect. Significant one-way ANOVA p-values and FDR (q-values) were set at < 0.05. As multivariate approach was used the principal component analysis (PCA) that allows a quickly visualization of similar and dissimilar samples in the given dataset. Between-groups comparisons were computed by a multiple comparison test (Tukey–Kramer honestly significant difference (HSD), $p < 0.05$) using JMP v8 software (SAS Institute, Inc., Cary, NC, USA).

3.2.2.3. Protein identification by tandem mass spectrometry

Protein identification is based on mass spectrometric analysis of peptides generated by proteolytic digestion. To this purpose, the protease of choice is generally sequencing-grade trypsin, which hydrolyzes the protein on the C-terminal side of lysine and arginine, unless the subsequent amino acid in the sequence is a proline.

3.2.2.4. Protein in-gel digestion

Protein spots with a significant modulation in their intensity were excised manually from the gel by pipette tip under laminar flow sterilized hood, wearing powder-free gloves, to avoid keratin contamination. Excised spots were placed into an Eppendorf tube and smashed by sterile surgical blades into small pieces to increase the surface area of proteins/peptides in the solution for improving trypsin accessibility. The gel pieces were then washed with 100 µL water and then dehydrated with 100 µL acetonitrile twice. Cysteine residues were reduced by incubating gel pieces 30 minutes at 56 °C with dithiothreitol (10 mM DTT/0.1 M NH_4HCO_3). Gel pieces were washed three times with acetonitrile and derivatized by treatment with iodoacetamide (55 mM IAA/0.1 M NH_4HCO_3) for 20 min at room temperature in the dark. The reduction and alkylation of cystein residues are intended to ensure maximum sequence coverage and to secure identification of proteins with a large number of disulphide bridges. Gel pieces were washed three times with 0.1 M ammonium bicarbonate, dehydrated three times with 100% acetonitrile and dried in a SpeedVac centrifuge. Twenty µL of digestion buffer

were added to the gel pieces and incubated one hour at 4°C. The digestion buffer consisted of 12.5 ng/µL sequencing-grade (i.e., modified by reductive methylation to reduce its susceptibility to autolysis) bovine trypsin (Roche, Switzerland) in 50mM ammonium bicarbonate with 5mM $CaCl_2$ (since calcium ions retard trypsin autolysis). Although trypsin is active over a wide pH range (pH 7-9), the optimum pH for digestion with modified trypsin is between 7.8 and 8.1, so the presence of ammonium bicarbonate (pH 8.1) is useful to improve trypsin activity. Once the gel plugs had become swollen with absorbed digestion buffer, the excess was removed and replace with the same buffer without trypsin, to ensure that the gel plugs were kept wet during the digestion process. In-gel protein digestion was performed overnight at 37 °C, shaking the tubes in a Thermomixer apparatus. To maximize peptide recovery, after collecting the peptide-rich supernatant, the gel plugs were extracted twice (37°C, 15 minutes) with 30 µL of acetonitrile. The two peptide supernatants obtained were collected, pooled, dried and dissolved in the supernatant previously collected. This final sample, hereafter referred to as "digest", containing all peptides recovered from the digestion of a single spot was directly analyzed by mass spectrometry.

3.2.2.5. Liquid chromatography- tandem mass spectrometry

Liquid chromatography-tandem mass spectrometry (LC-MS/MS) analysis was performed using a microfluidic chip-based technology for nanoelectrospray, whose functionality is equivalent to conventional nanospray LC/MS, coupled to an ion trap mass spectrometer (Agilent 1200 LC/MSD Trap XCT). Sample digest aliquots (6 µL, equal to one third of the total digest) were directly injected into a G4240-62001 HPLC-Chip (Agilent 1200 G4240A HPLC-Chip Cube), composed of a 40 nl enrichment column and a 75 µm x 43 mm separation column packed with Zorbax 300SB-C18 (5 µm) at a flow rate of 0.3 µL/min. The mobile phases consisted of 0.1% formic acid in water (eluent A) and 0.1% formic acid in CH_3CN (eluent B). The linear solvent gradient was as follow: from 5% of B to 30% of B in 28 min, then to 90% of B in 15 min and

finally re-equilibration to 5% of B for 10 min. The electrospray source operated in positive ion mode, with the following conditions: capillary voltage, -1750 V; Cap exit voltage 100V, skimmer voltage, 30.0 V; dry gas flow, 3 L/min; dry temperature, 300°C. Data were acquired sequentially in MS mode (scan range of 200 to 2000 amu) and in data dependent mode, automatically recording the MS/MS spectra of the four most abundant ions in every scan cycle. The MS/MS spectra were acquired with isolation width of 4 m/z and fragmentation amplitude of 1.3V.

3.2.2.6. Database searching and protein identification

Tandem mass spectra were analysed using the MS/MS search engine Phenyx version 2.1 (GenBio, Switzerland) (www.phenyx-ms.com, phenyx@genebio.com), against the UniProt_Swiss Prot database (version 54.6). The search was enzymatically constrained for trypsin, and allowed for one missed cleavage site. Further search parameters were: no restriction on molecular weight (MW) and isoelectric point; taxonomy: *mus musculus*; fixed modification carbamidomethylation of cysteine; variable modification: oxidation of methionine. Table 3.1 concisely restates the main submission parameters including algorithm, scoring models, thresholds. Protein identification has been considered valid when: *(i)* two or more peptides independently matched the same protein sequence, *(ii)* the peptide score was significant ($p < 0.05$), and *(iii)* the manual interpretation confirmed agreement between spectra and peptide sequence.

Table 3.1. Submission parameters to Phenyx MS/MS search engine.

Scoring model	ESI ion trap (HCT ultra)	
Parent charge	1,2,3 (trust=yes)	
Rounds	1	2
Modifications	Cys_CAM [fixed]	Cys_CAM [fixed]
	Oxidation_M [variable]	Oxidation_M [variable]
Enzyme	Trypsin	Trypsin
	missCleav=1	missCleav=2
	cleavMode=normal	cleavMode=half cleaved
AC score	10	10
Pept. Threshold	score>=8	score>=7
	p value<=1.00E-6	p value<=1.00E-5
	lenght>=6	lenght>=6
Conflict resolution	none	none
Parent Tol.	1.0 Da	2.0 Da
Turbo scoring	tolerance = 8000.0 ppm	no
	coverage>=0.2	
	series=b,b++,y,y++	

Scoring model refers to the algorithm that generates the score between experimental and theoretical masses, dependent upon the instrument type

Parent charge refers to the charge state of the parent ions, singly-, doubly-, triply-charged

Rounds sets of calculations carried out on the data. A second round of calculations is used to fine-tune the results obtained from the first round of scoring because only the accession numbers that fulfilled the first round criteria are processed during the second round

Modifications fixed chemical/post translational modification that occurs for every instance of the modifiable amino acid in the protein sequence, variable modification that may or may not occur

Enzyme the enzyme used to digest the protein. The error allowance for enzyme inefficiency is included as number of sites per peptide that were not cut (MissCleav) and as occurrence of the digestion according to the cleavage rules (one or both ends of protein) (CleavMode)

AC score refers to the minimum significant value for a protein's accession number score. Protein matches scoring lower than this value (set as 6) are rejected from the identified proteins

Peptide Thresholds refer to three parameters (i) minimum peptide z-score, the minimum distance from a random match, (ii) minimum peptide p-value, the probability of a peptide match in a database occurring by chance with the associated z-score or better. The lower the p-value, the more significant the match, (iii) minimum peptide length, peptides with less that the specified number of amino acids (6) are reported in the peptide match results but they do not contribute to the protein score

Conflict resolution conflicts arise when the scoring algorithm can match more than one peptide with acceptable z-score and p-value to a given spectrum. Phenyx resolves a conflict only if conflicting peptide matches are good enough quality, i.e. if they reach a minimum z-score and p-value. These thresholds are a function of the parent charge and are set by Phenyx. If the peptides' z-score and p-values are too low, then the conflict is not resolved and the matches rejected

Parent tolerance parent error tolerance, as amount of deviation allowed between experimental (observed) parent ion masses and the theoretical (calculated) masses

Turbo scoring a procedure that accelerates the searches by processing the data before submitting them to the main scoring calculation. A minimum percentage (20%) of the peptide sequence coverage by b+ (b), b2+ (b++), y+ (y) or y2 (y++) fragment series is looked for. If this percentage is not attained, the spectrum is not submitted for further scoring. In-depth explanations of each descriptor are available at www.phenyx-ms.com

In depth explanations of each descriptor are available at www.phenyx-ms.com

3.2.2.7. Western blot analysis of brain proteins

Pooled protein extracts (15 µg) were separated on NuPAGE 10% Bis-Tris Gels 1mm x 10 well (Invitrogen, CA, USA) using a Mighty Small II for 8x9 cm gels apparatus (Amersham Bioscience, MN, USA) at 200V for 1h. Each pool was run in triplicate (technical replicates). Resolved proteins were transferred to a nitrocellulose membrane (Bio-Rad) using the transfer buffer (10mM Tris-HCl pH 8, 150mM HCl, 0.05% (v/v) Tween-20) and blocked in TBS-T 5% (w/v) nonfat dried milk (Nestlé, Italy) for 2h. After transfer, membranes were incubated overnight with either of the following primary antibodies diluted in TBS-T 5% nonfat dried milk: heath shock protein 70 (3A3), superoxide dismutase-2 (A-2) (Santa Cruz Biotechnology, Santa Cruz, CA, USA, 1:1000) and mouse anti-Actin (Chemicon International, CA, USA, 1:2000) mouse monoclonal antibody; androgen receptor C-19 rabbit polyclonal antibody, (Santa Cruz, 1:1000). After washing with TBS-T, the membranes were incubated with secondary antibodies (goat anti-rabbit IgG-HRP and goat anti-mouse IgG-HRP, Santa Cruz Biotechnology) diluted 1:1000 in TBS-T 5% nonfat dried milk. The secondary antibody goat anti-mouse IgG-HRP used for anti-Actin was diluted 1:4000. Blots were detected by enhanced chemiluminescence (ECL-plus, GE Healthcare), visualized on autoradiography film (Hyperfilm ECL, GE Healthcare) and scanned at 16-bit images (ImageScanner III, GE Healthcare). The resulting TIFF images were analyzed using Progenesis software (PG240, v2006, Nonlinear Dynamics Group, UK). Expression data were normalized relative to actin.

3.3. PLASMA PROTEOMICS

Plasma proteomics analysis was performed using 1-DE for plasma protein prefractionation and subsequent LC-MS/MS for protein identification (1-DE-LC-MS/MS). This approach has been applied on all the experimental groups. Plasma samples were from the same animals used for brain proteomics analysis.

3.3.1. One-dimensional gel electrophoresis (1-DE) and in-situ digestion of gel slices

As already mentioned, due to budget and sample limitations for biological variability assesment, I adopted a samples pooling strategy to overcome the resource constraints .

Protein samples were prepared by pooling plasma protein from individual animals (20 µg proteins/animal) in each of the experimental group (5 animals/experimental group). Since plasma is a highly complex mixture of proteins/peptides with a high dynamic range, the first step was the depletion of high abundance protein species. The ProteoSpin plasma depletion kit (Norgen Biotek Corp, Ontario, Canada) was used. This kit allow the depletion of major serum proteins including albumin, α-antitrypsin, transferrin and haptoglobin and it is based on an ion-exchange mechanism and not on the use of specific antibodies. The kit can be used to deplete serum proteins from a wide variety of samples, including human and various animals. The complete procedure is available at: http://www.norgenbiotek.com/product_resources/abundant_serum_protein_depletion_kit_abundant_serum_protein_depletion_kit__protocol_17300_959.pdf. For each group, triplicates of pooled protein extracts (15 µg/replicate) were mixed with equal volume of Laemmli sample buffer (100mM Tris-Cl pH 6.8, 4% SDS, 20% glycerol, 0.2% bromophenol blue, 200mM DTT) and resolved on a manually cast 12% polyacrylamide SDS-PAGE using the Mini Protean II electrophoresis system at 90V, for 2 h (BioRad, Milan, Italy). The samples were loaded in the following order in each gel (from left to right) : 7'MCAo, pMCAo, 7'MCAo/pMCAo, SHAM

7'MCAo, SHAM 7'MCAo/pMCAo and a SHAM merge obtained mixing an equal amount of protein from the two SHAM samples (e.g Figure 4.7, page 123 section results).

Proteins were visualized after staining the gel with colloidal Coomassie Blue (Invitrogen, Carlsbad, CA, US). Each gel lane was manually cut with a sterile surgical blade into 24 bands of equal height (about 3 mm); in Figure 4.7, page 123 (Results chapter), the last lane from left to right represent an example of how were selected the 24 bands. Each band, placed into an Eppendorf tube and crushed into very small fragments, was submitted to the same in-gel digestion protocol applied for 2-DE approach (Matherials and Methods, page 90), but doubling the amount of each buffer.

3.3.2. Liquid chromatography-ESI-tandem mass spectrometry

An aliquot of each digest (2 µL) was directly analysed by liquid chromatography-tandem mass spectrometry (LC-MS/MS). All digests from triplicate gel samples were analysed (576 digests in total). HPLC-MS/MS analyses were carried out with an LTQ Orbitrap XL™ (Thermo Scientific, Waltham, MA, US), interfaced with a 1200 series capillary pump (Agilent, Santa Clara, CA, USA). Peptides were separated on a Thermo Scientific Biobasic 18 column (150x0.18mm, particle size 5 µm). LC condition were: column flow 2 µL/min; eluent A, H_2O and 0.1% formic acid; eluent B, CH_3CN and 0.1 % acid formic; gradient program: from 2% of B to 60% of B in 35 minutes, then 98% of B in 11 minutes for 4 minutes and re-equilibration to 2% of B for 24 minutes. MS conditions were: source DESI Omni Spray (Prosolia, Indianapolis, IN) used in nanospray mode with positive ions; ion spray voltage: 2100V; interface capillary temperature: 220°C; capillary voltage: 42V. MS spectra (*m/z* 400-2000) were acquired on the Orbitrap analyzer at 60,000 resolution, in parallel with low-resolution MS/MS scans of the four most abundant precursor ions being acquired in the LTQ, excluding single charged ions. The lock mass option was used to obtain the most accurate mass measurements in MS mode. The polydimethylcyclosiloxane ion generated in the electrospray process from ambient air

(protonated $(Si(CH_3)_2O)_6$, *m/z* 445.120025 was used for internal recalibration in real time. MS/MS analysis was performed in data-dependent mode using XCalibur software (Thermo Scientific), with dynamic exclusion and 30 seconds exclusion duration.

3.3.3. Database searching and criteria for protein identification

Tandem mass spectra were extracted and the charge states deconvoluted by BioWorks version 3.3.1 (Thermo Scientific, Waltham, MA, US). Deisotoping was not performed. For each sample, the MS/MS data from the 24 gel bands were merged and submitted as "mgf" file to the search engine Mascot (in-house version 2.2.06, Matrix Science, London, UK) to simplify the comparison of results between samples and to allow peptides from any protein that had not migrate exactly within a single (blindly cut) gel slice to be included in the same search, thus increasing the probability of its identification. Mascot searches were performed against the Swiss-Prot database, version 57.8. Search parameters were: no restriction on molecular weight; Taxonomy: Mus Musculus; enzyme: trypsin (one missed cleavage allowed); fixed modification: carbamidomethylation of cysteine; variable modification: deamidation of glutamine and oxidation of methionine; experimental mass values: monoisotopic; peptide mass tolerance: ±2 ppm (our experimental mass accuracy was constantly better than 1 ppm); MS/MS mass tolerance: 1 Da; peptide charge: 2+,3+. Decoy search: active, so that this type of search was performed automatically. In this way during the search, every time a protein sequence from the target database is tested, a random sequence of the same length is automatically generated and tested. The average amino acid composition of the random sequences is the same as the average composition of the target database. The number of matches that are found from the decoy database is an excellent estimate of the number of false positives that are present in the results from the real or target database (Elias and Gygi 2007). If TP is true positive matches and FP is false positive matches, the number of matches in the target database is TP + FP and the number of matches in the decoy database is FP. The

quantity that is reported is the False Discovery Rate (FDR) = FP / (FP + TP). False positive peptide identification is widely acknowledged to be a problem (Keller, Purvine *et al.* 2002; Elias and Gygi 2007), so the knowledge of FDR is very important since it allows to estimate the quality of the results (Keller, Purvine *et al.* 2002; Elias and Gygi 2007). To further validate the proteins lists generated by Mascot search, Scaffold software (version 3.00.02, Proteome Software Inc., Portland, OR, US) was used. All MS/MS data were analyzed using both Mascot (Matrix Science, London, UK; version 2.2.06) and X! Tandem (**www.thegpm.org**; version 2007.01.01.1). Mascot was set up to search both the forward and reversed sequences of the SwissProt_2010 database (version 57.8, taxonomy Mus musculus) assuming the digestion enzyme trypsin (1 missed cleavage allowed). X! Tandem was set up to search a subset of the uniprot_sprot database also assuming trypsin (2 missed cleavages allowed). Mascot and X! Tandem were searched with a fragment ion mass tolerance of 1.00 Da and a parent ion tolerance of 2.0 ppm. Iodoacetamide derivative of cysteine was specified in Mascot and X! Tandem as a fixed modification. Deamidation of asparagine and glutamine and oxidation of methionine were specified in both Mascot and X!Tandem as variable modifications. Peptide identifications were accepted if they could be established at greater than 95.0% probability as specified by the Peptide Prophet algorithm (Keller *et al.*, 2002). Protein identifications were accepted if they could be established at greater than 99.9% probability and with a least 2 identified peptides. Protein probabilities were assigned by the Protein Prophet algorithm (Nesvizhskii, Keller *et al.* 2003). Proteins which contained similar peptides and could not be differentiated based on MS/MS analysis alone were grouped to satisfy the principles of parsimony. These filtering criteria established a protein false positive identification rate (FDR) of 0% for the mouse proteome dataset based on the reported decoy database search strategy.

3.3.4. Protein quantification by spectral counting

Identified proteins were quantified using spectral counts directly computed by Scaffold software, where the number of MS/MS spectra are grouped into "counts" associated to a

specific protein. Spectral counts normalization was performed by Scaffold averaging the spectrum counts across the samples within an experimental group, followed by averaging the spectral counts across all experimental groups, and then multiplying the spectrum counts in each sample or experimental group by the average divided by the individual sample or experimental group sum. Since one or two spectra identifications are often irreproducible and, as such, finding of significant difference based on their presence are highly suspect, a minimum value of 3 was set for spectral counting. For each identified protein, the number of spectral counts was exported to Excel and normalized counts were averaged for replicate samples. Subsequently estimation of differential protein abundance was expressed as fold-change.

3.3.5. Statistical analysis

Statistical comparisons of the individual protein abundance in the experimental groups (one-way ANOVA) and between-groups comparisons (multiple comparison test, Tukey-Kramer honestly significant difference (HSD), $p < 0.05$) were computed using JMP v8 software (SAS Institute, Inc., Cary, NC). Proteomic data were analyzed by multivariate techniques. The analysis was performed with Simca-P 13 software (Umetrics AB, Umea, Sweden). The data was mean-centered and Pareto-scaled prior to multivariate statistical analysis. The dataset was examined using Partial-Least Square-Discriminant Analysis (PLS-DA). In this pattern recognition technique, a regression model is formed between the expression value of features and class membership (*e.g.* sham and/or 7'MCAoplasma samples). The loadings plot was examined to identify which feature (variable) was significant in classifying the data. Differential variables (features) responsible for the clustering were then selected based on a threshold of variable importance in the projection (VIP) value (VIP>1). This threshold is based on the fact that the sum of squares of all VIP values is equal to the number of terms in the model, hence the average VIP is equal to 1.

3.3.6. IGF-1 validation by ELISA

The complete ELISA procedure is available at http://www.rndsystems.com/pdf/mg100.pdf. Briefly, 10 microL of plasma for each animal in each experimental group (three biological replicates for sample) were diluted 1:500 with the Calibrator Diluents, loaded in the plate and after the incubation with the Substrate Solution, the optical density was assessed at 450 nm using the Tecan I-control microplate reader (Tecan Group Ltd, Mannendorf, Switzerland). The IGF-1 concentration in each animal was obtained from the standard curve, the statistical comparison of the IGF-1 concentration in the experimental groups (one-way ANOVA) and between each group (multiple comparison test, Tukey-Kramer honestly significant difference, $p < 0.05$) were obtained using Prism 6.01 (GraphPad Software, Inc).

3.3.7. Protein network and pathways analyses

The lists of differentially expressed proteins were analysed by network and pathway analysis using the MetaCore analytical suite version 5.3 (GeneGo, MI, US). Metacore is an integrated analytical suite of algorithms, based on a manually annotated and regularly updated databases of human and rodent protein-protein interactions, transcriptional factors, signalling, metabolism and bioactive molecules linked to functional processes and diseases (www.genego.com/). MetaCore's *default background* was used as background dataset for two main reasons: *(i)* my protein identification was potentially "proteome-wide", meaning that my global workflow was not restricted to predetermined protein sets (as it happens, for example, with the genes on a microarray); *(ii)* in statistical evaluation the use of larger backgrounds (*e.g.*, all genes in the genome) gives in general more solid results (as indicated by the lower P-values) as compared to a restricted set of genes (*e.g.*, the genes existing on a microarray) (Huang da, Sherman *et al.* 2009). Once the list of significantly differently expressed proteins (with Uniprot-

Swiss Prot ID and fold-changes values) was uploaded to MetaCore, the size of their intersection between the subset of uploaded proteins and the proteins on all the possible pathways mapped in the MetaCore database was computed using the hypergeometric distribution probability test, where the p-value represents the probability that a process appears in the data set relative to that expected by chance. A p-value <0.05 was used to identify pathways that are assumed to be affected by treatment. Subsequently, networks of proteins from our experiment against the default background were built using two different algorithms: 1) *the analyze network algorithm* generating sub-networks ranked by a P-value and interpreted in terms of Gene Ontology processes to deduce top scoring process that are regulated by differentially expressed proteins; and 2) *the standard Dijkstra's shortest path algorithm* to map the shortest path for interaction. The resulting networks were evaluated to determine which algorithm succeeded in creating modules that have higher than random saturation with the protein of interest. Networks were then visualized graphically as nodes (proteins) and edges (relationship between proteins) alongside the expression pattern.

3.4. PLASMA METABOLOMICS PROFILING

3.4.1. Plasma samples preparation

As already mentioned, due to budget and sample limitations for biological variability assesment, I adopted a sample pooling strategy to overcome the resource constraints. I pooled plasma samples from individual animals (20 µg proteins/animal) in each of the experimental group (5 animals/experimental group)and run technical replicates .

I am aware that results based solely on technical replicates might have a limited statistical relevance. Neverthless the identification of metabolites with different abundance from pooled samples does not mean that these metabolic species are not interesting with the respect to the underlying biological population. It just means that the statistical confidence is limited and the use of additional methods of validating the findings is highly recommended.

Metabolites were extracted by adding four volumes of cold methanol to the plasma sample; samples were vortexed and incubated at -20°C for 1h. They were then centrifuged 10 min at 14,000 x *g*, and the supernatant (rich in small-molecule analytes) was collected, dried in a SpeedVac and resuspended in 20 µL of 0.1% formic acid.

3.4.2. Metabolomic profiling by LTQ-Orbitrap mass spectrometry

A portion (2 µL) of metabolite extract from each groups was directly analysed by LC-MS/MS, using an LTQ Orbitrap XL™ (Thermo Scientific, Waltham, MA, US), interfaced with a 1200 series capillary pump (Agilent, Santa Clara, CA, US). The MS instrument was operated in positive (POS) and negative (NEG) ionization modes and the analyses were run in triplicate. Metabolites were separated on an Agilent Technologies Zorbax C18 SB column (150 x 0.5 mm ID, particle size 5 Tm). Flow rate 10 µL/min with mobile phases: water containing 0.1% formic acid (A) and acetonitrile (B) for the positive ion. For negative ion mode, 2 mM of ammonium acetate was substituted for the 0.1% formic acid. The gradient consisted of 5% B for 5 min, followed by a

linear gradient to 95% B over 45 min, hold at 95% B for 5 min, and re-equilibration at 5% for 2 min. MS conditions were: source DESI Omni Spray (Prosolia, Indianapolis, IN) used in nanospray mode with positive and negative ion modes; ion spray voltage 2100 V; capillary temperature 220°C; capillary voltage, 42 V. MS spectra (*m/z* 100-1000) were acquired in the Orbitrap analyzer at 60,000 resolution, in parallel with the low-resolution MS/MS scans of the four most abundant precursor ions being acquired in the LTQ, selecting singly charged ions. The lock-mass option was used to obtain the most accurate mass measurements in MS mode. The polydimethylcyclosoloxane ion generated in the electrospray process from the ambient air (protonated (Si(CH3)2O)6, *m/z* 445.120025) was used for internal recalibration in real time. MS/MS analysis was done in data dependent mode (DTA) using Xcalibur software (Thermo Scientific, Waltham, MA, US) with target ions previously selected for the MS/MS dynamically excluded for 30 sec. To ensure the stability and repeatability of the LC-MS systems, ten runs of pooled samples were done on the system before the sample run sequence. Samples were run in an order that alternated the SHAM 7'MCAo/SHAMpMCAo and pMCAo groups to reduce any systematic error associated with instrumental drift.

3.4.3. Untargeted metabolomics data processing

All LC-MS files were analyzed using the MS label free differential analysis software SIEVE v1.3 (ThermoFisher, Cambridge, MA, US). SIEVE was run on all the LC-MS full-scan chromatograms using the *small molecule* setting. The chromatograms were time-aligned, referencing the SHAM7'MCAo/SHAMpMCAo samples acquired in the middle of the sequence. The framing parameters were set at 0.01 Da for the *m/z* window and 0.35 min for the retention time (RT) window; 500,000 was used as the intensity threshold. SIEVE software was used to determine significant differences in the frame profiles of SHAM7'MCAo, 7'MCAo, SHAM7'MCAo/pMCAo, pMCAo, 7'MCAo/pMCAo plasma samples by applying the following filtering criteria: frame

intensity coefficient of variation (CV%) <20%, and unpaired t-test for unequal variance (Welch's test) p≤0.01.

3.4.4. Stastical Analysis

Metabolomic data were analyzed by multivariate techniques. The analysis was performed with Simca-P 13 software (Umetrics AB, Umea, Sweden). The data was mean-centered and Pareto-scaled prior to multivariate statistical analysis. The dataset was examined using Partial-Least Square-Discriminant Analysis (PLS-DA). In this pattern recognition technique, a regression model is formed between the expression value of features and class membership (*e.g.* sham and/or 7'MCAo plasma samples). The loadings plot was examined to identify which feature (variable) was significant in classifying the data. Differential variables (features) responsible for the clustering were then selected based on a threshold of variable importance in the projection (VIP) value (VIP>1). This threshold is based on the fact that the sum of squares of all VIP values is equal to the number of terms in the model, hence the average VIP is equal to 1.

3.4.5. Identification of plasma metabolites

For metabolite identification, the frame m/z values were used for batch searches on the KEGG database (http://www.genome.jp/kegg/) and Human Metabolome Database (HMDB, http://www.hmdb.ca/). Accurate mass data and isotopic distribution for the precursor and product ion were compared to spectral data of the reference compounds in the databases. Identifications were reported only for metabolites with accurate mass match <5 ppm.

The resulting metabolite identifications based upon spectral similarities with public spectral libriers, as performed in this study, are defined as putative (Sumner *et al* 2007, Dunn 2012).The final unambiguous identity of a metabolite can be achieved only referencing to

authentic chemical standards, a strategy that has not been performed at this stage of my study.

3.4.6. Mapping metabolic pathways

For biological interpretation of the metabolite dataset by our untargeted strategy, we mapped the identified metabolites to the KEGG pathway database (Kyoto Encyclopedia of Genes and Genomes; (www.genome.jp/kegg/), using MetaboAnalyst 2.0, a comprehensive online tool suite for metabolomic data analysis and interpretation (www.metaboanalyst.ca). Metabolite sets were analyzed to identify biologically meaningful patterns that were significantly enriched in our metabolomic data. The OverRepresentation Analysis (ORA) algorithm was applied and the hypergeometric test was used to see whether a particular metabolite set was represented more than expected by chance in the given compounds list. Then the Pathway Analysis Module was used to combine the enrichment analysis results with the pathway topology analysis (centrality measures to estimate node importance) to identify the most important pathways involved.

CHAPTER 4

RESULTS

4.1. PROFILING THE BRAIN PROTEOME BY 2-DE AND LC-MS/MS

The expression profiles of brain proteins derived from animals subjected to different ischemia regimes were examined to evaluate the effects of brain IPC on a subsequent more severe ischemic event, and to highlight putative IPC mediators. To achieve this goal technical replicates of pooled cortex proteins were separated by two-dimensional gel electrophoresis (2-DE) and protein expression was analysed in 5 different experimental conditions, namely, IPC stimulus (7'MCAo), severe ischemia (pMCAo), the combination of the two (7'MCAo/pMCAo), and 2 groups of sham-operated controls (figure 4.1).

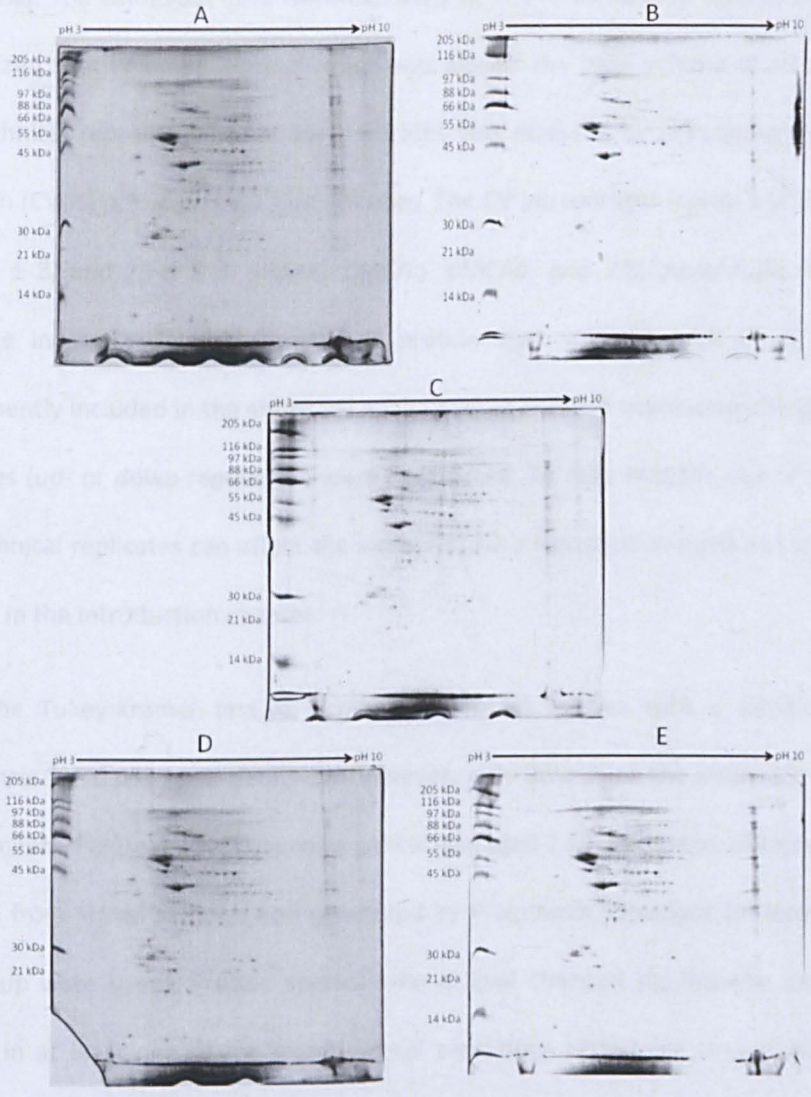

Figure 4.1. Representetive gel images of the five experimental conditions: (A) 7'MCAo, (B) pMCAo, (C) 7'MCAo/pMCAo, (D) SHAM 7'MCAo, (E) SHAM 7'MCAo/pMCAo.

Analysis of gel images and statistical comparisons of the two sham groups (sham7'MCAo and sham7'MCAo/pMCAo), indicated that they were not significantly different (data not shown). Therefore, the two groups were merged for all subsequent image analyses and statistical comparisons to obtain a larger sham group, named SHAM. This had the advantage of increasing the statistical power of the study, allowing for better detection of differences among the experimental groups. Overall, gel image analysis by Progenesis SameSpot software detected about 800 spots/gel. Further, 89 protein spots matched in all the experimental conditions and showed changes in intensity in at least one of them (one-way ANOVA $p<0.05$, FDR < 5%). The SameSpot data were exported to PG240 for further statistical analysis on the normalized spot volumes. Normalization was against the total volume of all spots in the gel. The technical reproducibility of the replicates was assessed by calculating the coefficient of variation (CV %) of the protein spot volumes. The CV percentages (mean ± SD) were 25 ± 5, 22 ± 9, 18 ± 8, and 23 ± 8 in SHAM, 7'MCAo, pMCAo, and 7'MCAo/pMCAo, respectively. To minimize incorrect data interpretation, protein spot volumes with CV ≥ 35% were not subsequently included in the statistical analysis; only relevant expression changes greater than 1.5 times (up- or down-regulation) were considered. To note that the use of pooled samples and technical replicates can affect the strenght of my statistical analysis as I already stated at page 53 in the Introduction chapter.

Using the Tukey-Kramer test, a number of protein species with a significant change in abundance ($p <0.05$) were detected. However, only 28 out of the initial 89 met the above requirements. Figure 4.2 reproduces a typical averaged 2-DE gel image, obtained using 100 μg proteins from SHAM samples and generated by Progenesis SameSpot (at least four replicate gels/group were used). Protein species whose level changed significantly (one-way ANOVA $p<0.05$) in at least one of the experimental conditions tested are circled. Numbered spots indicate protein species with a change in expression ≥ 1.5-fold vs. SHAM (Tukey-Kramer $p<0.05$).

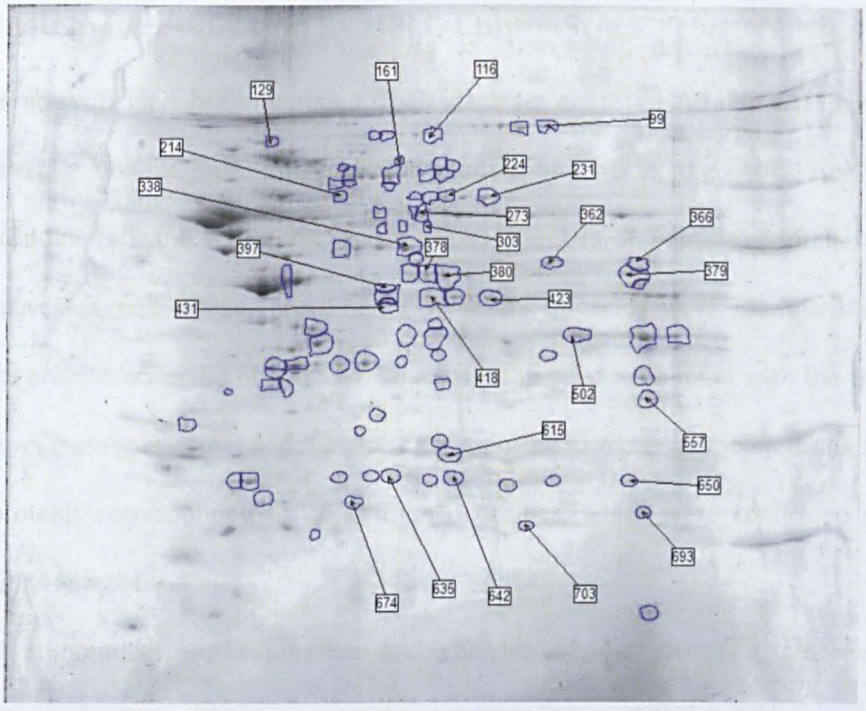

Figure 4.2. Image of a Colloidal Coomassie blue stained 2-DE gel of pooled brain cortices from SHAM samples (100 µg proteins). The average 2-DE map generated by image analysis of 10 replicates is shown. The 2-DE map shows 89 differentially expressed protein spots (circled spots, ANOVA $p<0.05$) and 28 protein spots with expression levels of 1.5-fold or greater (numbered spots).

4.1.1. Protein identification by HPLC-Chip-MS/MS

All numbered spots have been identified. Their identities are listed in Table 4.1, together with their respective UniProt_SwissProt accession number and name, theoretical and observed isoelectric point (pI) and molecular weight (MW), number of peptide identified for each protein, coverage percentage, and Phenyx score. All proteins were identified with high confidence and the observed pI and MW values were in good agreement with the theoretical ones. Phenyx mass spectrometric parameters are reported in material and methods, page 89.

The 28 proteins corresponded to 26 different identities, which were confirmed using the search engine Mascot.

Table 4.2 summarizes the expression fold changes of the identified proteins in the experimental ischemia models as compared to SHAM. Up-regulation is shown in bold (fold change ≥ 1.5), whereas down-regulation is shown in bold-italic (fold change ≥ -1.5).

The most relevant expression changes were induced by pMCAo, where 22 out of 28 proteins (79%) resulted increased compared to SHAM. In the preconditioned group (7'MCAo/pMCAo) a number of proteins overexpressed after pMCAo returned to SHAM levels, but the abundance of 12 proteins was changed compared to SHAM. 7 of these proteins remained up-regulated as in pMCAo, whereas 5 proteins (namely, succinate dehydrogenase (DHSA), dihydrolipoyl dehydrogenase (DLDH), fascin, one of the two isoforms of glutamine synthetase (GLNA), one of the two isoforms of fructose-biphosphate aldolase C (ALDOC), that were unchanged in pMCAo, were found to be down-regulated only in this experimental condition, suggesting their possible role in brain preconditioning. The IPC stimulus alone (7'MCAo) affected only a limited number of proteins as compared to SHAM. The expression of 2 proteins (namely, L-lactate dehydrogenase (LDHA), and glutathione *S*-transferase M1 (GSTM1), was down-regulated by IPC. Remarkably, only the heat shock protein 70 (HSP70) was increased in this group when compared to SHAM. However, its expression remained unchanged after pMCAo, both in preconditioned and non-preconditioned brains.

Further statistical comparisons (Tukey-Kramer test) on the normalized spot volumes of the identified proteins are shown in the Figure 4.3, which highlights the differences between paired experimental groups. From this figure the preconditioning effect (7'MCAo/pMCAo) in preventing the robust protein over-expression observed after severe ischemia (pMCAo) is even more evident, since the trend observed for almost the totality of the proteins was a decreased expression in preconditioned brain cortices.

Table 4.1. Proteins differentially expressed in mouse brain cortex ischemia models. Identification was by LC-MS/MS and use of the Phenyx search engine. The table reports the access numbers and entry names associated with the UniProt-Sprot database.

[a]Theor.: Theoretical, data-based annotation; Exp.: experimental, from two-dimensional gels

[b]#Unique pept.: number of unique peptide matches found for a given protein.

[c]Cov%: all amino acids from valid peptide matches as a percentage of the total number of amino acids in protein.

[d]Score: the protein score is calculated from the individual normalized Z-score of validated peptides. Peptide Z-score refers to the distribution of calculated scores compared with that of random peptide sequence in order to find the mean and variance (www.phenyx-ms.com).

Spot #	Protein name	Uniprot-Sprot Acc number	Uniprot-Sprot entry name	pI, theor./exp.[a]	MW (kDa), theor./exp.[a]	# Unique pept.[b]	Cov%[c]	Score[d]
99	Aconitate hydratase	Q99KI0	ACON_MOUSE	7.6/8	85/86	16	16	102.9
116	Vesicle-fusing ATPase	P46460	NSF_MOUSE	6.67/6.5	82/83	3	4	25.1
129	Heat shock 70	P20029	HSP70_MOUSE	5.0/5.0	70.46/70	44	38	215.1
161	Succinate dehydrogenase	Q8K2B3	DHSA_MOUSE	6.4/7.0	68/70	20	19	95.9
214	Protein disulfide-isomerase A3 precursor	P27773	PDIA3_MOUSE	5.78/6.0	54.2/57	4	7	28.6
224	Dihydrolipoyl dehydrogenase	O08749	DLDH_MOUSE	6.5/8.0	50.2/50	30	33	133.4
231	Pyruvate kinase	P52480	KPYM_MOUSE	6.9/7.0	57.9/60	77	55	293.7
273	Fascin	Q61553	FSCN1_MOUSE	6.6/6.0	54.5/55	43	47	181.5
303	Septin-11	Q8C1B7	SEP11_MOUSE	6.5/6.0	48.9/50	28	45	145.2
338	Alpha-enolase	P17182	ENOA_MOUSE	6.63/6.0	47/45	29	37	174.6
362	Creatine kinase	P30275	KCRU_MOUSE	8.5/8.0	47/50	34	34	116.5
366	Betaine--homocysteine S-methyltransferase 1	O35490	BHMT2_MOUSE	8.3/8.0	45/50	22	47	126
378	Glutamine synthetase	P15105	GLNA_MOUSE	6.85/6.5	42/40	9	20	72.4
379	Phosphoglycerate kinase 1	P09411	PGK1_MOUSE	8.3/8.0	44.5/40	46	47	181.5
380	Glutamine synthetase	P15105	GLNA_MOUSE	6.85/6.5	42/40	12	22	97
397	Septin-5	Q9Z2Q6	SEPT5_MOUSE	6.3/6.0	42.7/40	7	12	30.95
418	Fructose-bisphosphate aldolase C	P05063	ALDOC_MOUSE	7.0/6.5	39.4/45	13	35	127.3
423	Fructose-bisphosphate aldolase C	P05063	ALDOC_MOUSE	7.2/6.5	46/45	25	30	129.3
431	NADH dehydrogenase	Q99LC3	NDUAA_MOUSE	6.1/7.0	36.9/40	7	21	49.7
502	L-lactate dehydrogenase A	P06151	LDHA_MOUSE	8.0/7.5	36.5/35	9	22	74
557	Vacuolar ATP synthase subunit E 1	P50518	VATE1_MOUSE	8.7/8.5	26.1/25	41	47	108
615	Phosphoglycerate mutase 1	Q9DBJ1	PGAM1_MOUSE	7.0/6.5	28.8/28	22	43	124.8
635	Peroxiredoxin-6	O08709	PRDX6_MOUSE	5.9/5.5	24.8/25	8	34	66.1
642	Triosephosphate isomerase	P17751	TPIS_MOUSE	7.58/7.5	26.7/25	7	28	57.6
650	Glutathione S-transferase Mu 1	P10649	GSTM1_MOUSE	8.5/8.0	25.8/25	69	58	155.1
674	Ras-related protein Rab-11A	P62492	RB11A_MOUSE	5.8/6.0	24.5/20	9	20	39.6
693	Glutathione S-transferase P 1	P19157	GSTP1_MOUSE	8.35/7.5	23.6/25	6	23	37.3
703	Superoxide dismutase	P09671	SODM_MOUSE	8.9/9.0	24.6/25	17	37	96.1

Table 4.2. Fold changes of proteins in the mouse brain cortex after preconditioning alone (7'MCAo) or severe ischemia with (7'MCAo/pMCAo) or without preconditioning (pMCAo) as compared to SHAM. Up- or downregulation is shown in **bold** (fold change ≥ 1.5), or in ***bold-italic*** (fold change ≥ -1.5).

SPOT No.	PROTEINS IDENTIFIED	EXPRESSION FOLD CHANGE Vs SHAM		
		7'MCAo	pMCAo	7'MCAo/pMCAo
99	Aconitate hydratase	-1.23	**4.5**	**3.0**
116	Vesicle-fusing ATPase	1.2	**2.8**	1.4
129	Heat shock protein 70	**1.5**	1.3	-1.3
161	Succinate dehydrogenase	1.1	-1.0	***-2.9***
214	Protein disulfide-isomerase A3 precursor	-1.4	**1.6**	1.2
224	Dihydrolipoyl dehydrogenase	-1.0	-1.5*	***-3.6***
231	Pyruvate kinase	-1.2	**2.2**	1.2
273	Fascin	-1.0	-1.2	***-2.8***
303	Septin-11	-1.0	**1.8**	-1.1
338	Alpha-enolase	-1.1	**2.2**	1.2
362	Creatine kinase	-1.7*	**3.3**	**2.4**
366	Betaine--homocysteine S-methyltransferase 1	1.3	**1.9**	-1.0
378	Glutamine synthetase	-1.1	1.2	***-2.0***
379	Phosphoglycerate kinase 1	1.4	**2.4**	-1.5*
380	Glutamine synthetase	-1.3	**2.2**	-1.2
397	Septin-5	1.1	**1.7**	-1.4
418	Fructose-bisphosphate aldolase C	1.1	1.2	***-1.8***
423	Fructose-bisphosphate aldolase C	-1.4	**1.9**	1.3
431	NADH dehydrogenase	1.3	**1.7**	***-1.5***
502	L-lactate dehydrogenase A	***-2.5***	**2.2**	**1.9**
557	Vacuolar ATP synthase subunit E 1	1.0	**2.6**	**1.8**
615	Phosphoglycerate mutase 1	-1.1	**1.7**	-1.2
635	Peroxiredoxin-6	-1.2	**2.1**	1.1
642	Triosephosphate isomerase	-1.3	**1.7**	-1.2
650	Glutathione S-transferase Mu 1	***-2.4***	**3.3**	**2.2**
674	Ras-related protein Rab-11A	-1.2	**1.5**	-1.0
693	Glutathione S-transferase P 1	-1.5*	**3.9**	**2.5**
703	Superoxide Dismutase	-1.1	**1.8**	**1.9**

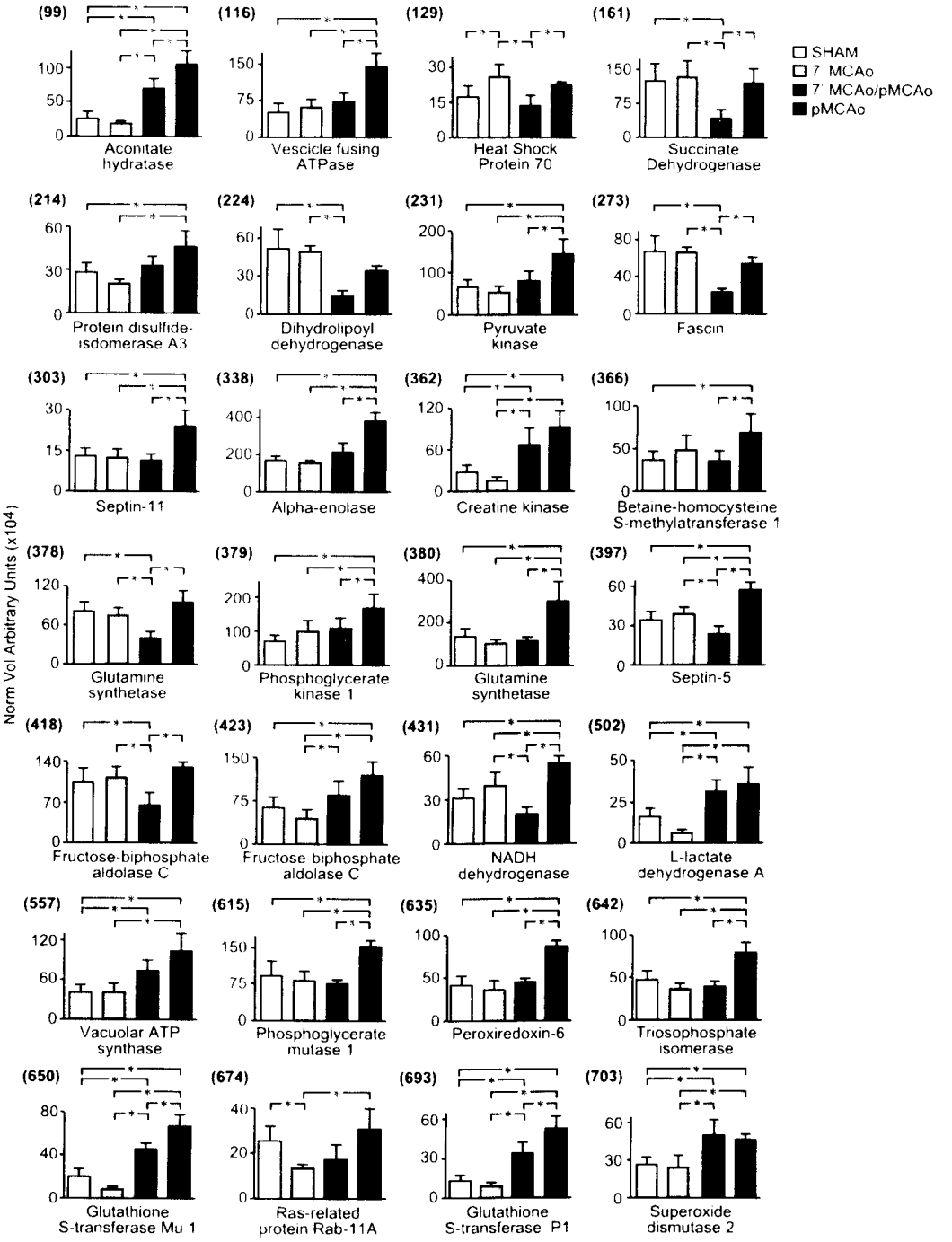

Figure 4.3. Histograms of normalized spot volumes of the identified proteins and paired statistical comparisons (Tukey-Kramer HSD $p < 0.05$). Each bar represents the normalized spot volume (mean ± SD). The vertical axis shows arbitrary normalized volume unit. Spot numbers are given in parenthesis and are from the Progenesis SameSpot analysis. Asterisks mark significant expression changes.

4.1.2. Pathway analysis

MetaCore software was used to identify pathways and processes significantly perturbed in our experimental conditions. Individual protein expression changes were compared using the 'Compare Experiments Workflow' tool to analyse their distribution in MetaCore's ontologies. The histograms of Figure 4.4A indicate that glycolysis and the tricarboxylic acid cycle are among the top 10 most significant pathways affected. As shown in Figure 4.4B, the top 10 most significant process networks include the response to unfolded proteins, immune response, response to hypoxia and oxidative stress. The list of proteins significantly involved in the perturbed pathway maps and process networks is reported in Table 4.3.

I used the MetaCore's network algorithm "shortest paths" (two steps) to map the shortest path for protein-protein interactions among the dysregulated proteins. The pathway analysis generated the global network of Figure 4.5, which shows direct and indirect interactions among all the dysregulated proteins; however, alpha-enolase was not linked to any network protein.

The presence of androgen receptor (AR) among the most highly connected proteins (hubs) defined by the network statistics is noteworthy. AR was directly linked to 9 dysregulated brain proteins, including HSP70 (involved in protein folding and stress response), the anti-oxidant proteins superoxide dismutase-2 (SOD2) and GSTP1, ALDOC (glycolysis), aconitate hydratase (ACON, tricarboxylic acid cycle), DLDH, (tricarboxylic acid cycle), GLNA (glutamate and GABA synthesis), betaine homocysteine s-methyltransferase (BHMT, amino acids synthesis), and protein disulphide-isomerase A3 (PDIA3, rearrangements of S-S bonds). Two further hubs, namely hypoxia inducible factor 1 (HIF-1) and nuclear factor-kappa B (NF-κB), attracted our attention since they were directly connected to many of the remaining proteins. Seven proteins, phosphoglycerate mutase 1 (PGM1), fascin, HSP70, pyruvate kinase (KPYM), LDHA, ALDOC, and phosphoglycerate kinase (PGK1) were directly linked to hypoxia inducible factor 1

(HIF1), and 10 proteins (fascin, ACON, GLNA, HSP70, Septin 11, ALDOC, PGK1, SOD2, GSTM1, and GSTP1) to nuclear factor κB (NF-κB).

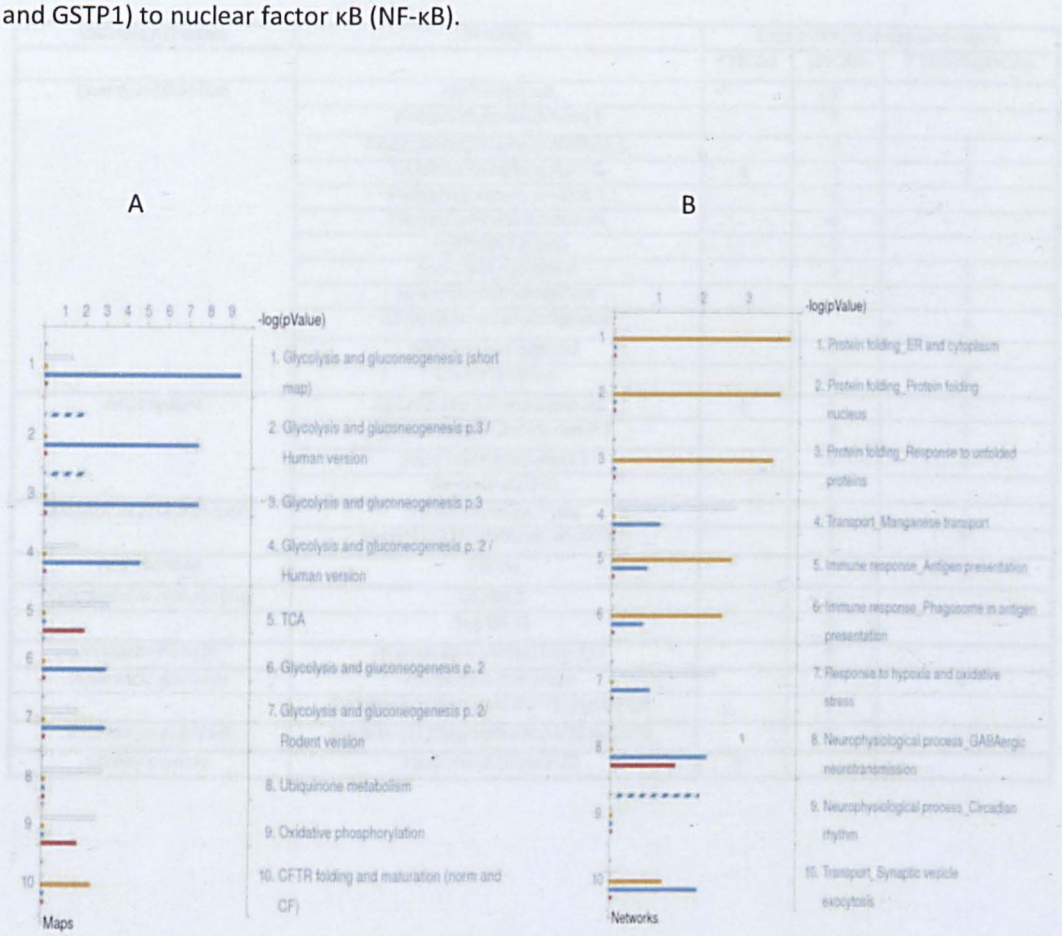

Figure 4.4. MetaCore analysis using the 'Compare Experiments workflow' application. The bars represent the ten most significant biological pathway maps (Panel A) and biological process networks (Panel B) in which the differentially expressed proteins are involved. The results are ranked by the -log(p-value). Yellow, blue, and red bars refer to 7'MCAo, pMCAo, and 7'MCAo/pMCAo, respectively. White and hatched bars indicate similar or common pathway maps and biological processes, respectively .

Table 4.3. Biological processes involving the dysregulated proteins, together with the direction of their expression change, as indicated by the GeneGo (MetaCore) and GO software tools.

Biological Process	Proteins	Expression change directions		
		7'MCAo	pMCAo	7'MCAO/pMCAo
Energy metabolism	Alpha-enolase		↑	
	Phosphoglycerate kinase 1		↑	
	Fructose-bisphosphate aldolase C		↑	↓
	L-lactate dehydrogenase A	↓	↑	↑
	Phosphoglycerate mutase 1		↑	
	Triosephosphate isomerase		↑	
	Pyruvate kinase		↑	
	Aconitate hydratase		↑	↑
	Succinate dehydrogenase			↓
	Dihydrolipoyl dehydrogenase			↓
	NADH dehydrogenase		↑	
	Creatine kinase		↑	↑
Antioxydant	Glutathione S-transferase Mu 1	↓	↑	↑
	Glutathione S-transferase P 1		↑	↑
	Superoxide dismutase 2		↑	↑
	Peroxiredoxin 6		↑	
Synaptic vesicle transport	Vesicle fusing ATPase		↑	
	Vacuolar ATP synthase subunit E 1		↑	↑
Actin binding	Fascin			↑
Cytoskeleton remodelling	Septin 5		↑	
	Septin 11		↑	
Membrane traffic	Ras-related protein Rab-11a		↑	
Aminoacid synthesis	Glutamine sinthetase		↑	↓
	Betaine homocysteine S-metiltansferase		↑	
Rearrangment of S-S	Protein disulfide-isomerase A3 precursor		↑	
Stress response	Heat shock protein 70	↑		

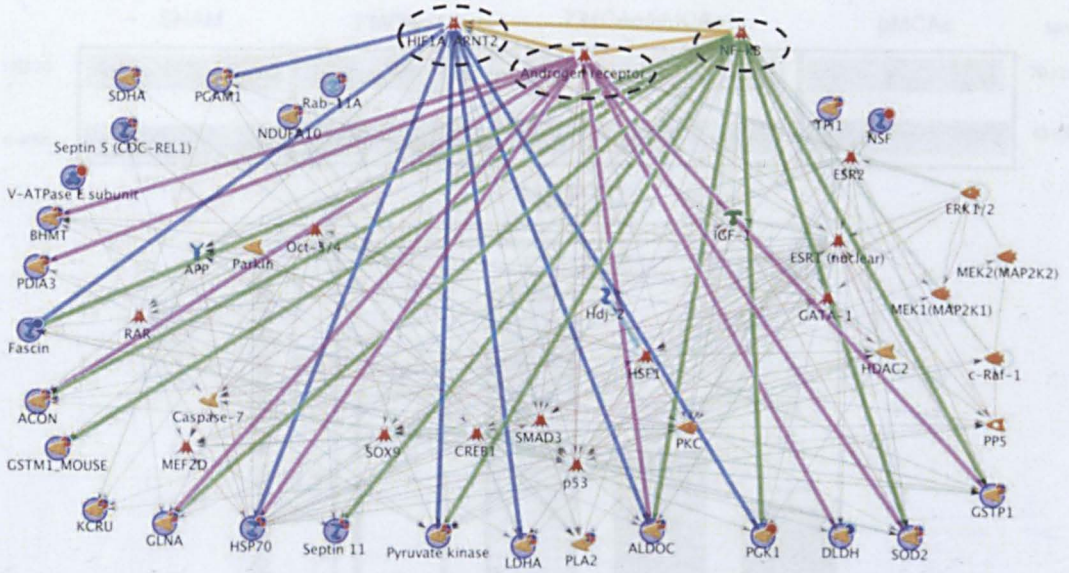

Figure 4.5. Global network associated with the proteins differentially expressed in transient and permanent ischemia models. MetaCore's network algorithm "shortest paths" (two steps) was used to map the shortest path for protein-protein interactions. Individual proteins are represented as nodes of different shapes, according to their functional class. Circled nodes denote proteins identified in this study; small full red and blue circles indicate up- and down-regulation, respectively. Lines between nodes indicate direct protein-protein interaction, the arrowheads indicate the direction of the interaction. Broken line circles highlight network hubs highly connected with the dysregulated proteins, as indicated by network statistics. Yellow lines highlight the direct interaction between these hubs. Blue, purple, and green lines highlight, respectively, direct interactions between HIF1, AR, and NF-κB and the dysregulated proteins. In the figure Peroxiredoxin 6 is referred as PLA2.

4.1.3. Western blot validation

Immunoblotting experiments were used to confirm key proteomic data and were performed on technical replicates of pooled samples. Specifically, the expression profile of HSP70 was validated by Western blotting, as this was the only protein found upregulated after 7'MCAo, and SOD2 was analysed as an example of a protein whose expression was highly increased both after severe ischemia and after 7'MCAo/pMCAo. In addition, on the basis of the pathway analysis results, AR was checked by Western blotting to verify its expression in our experimental models, since it appeared to be a major hub in the affected network. The Western blot analysis of HSP70 and SOD2 confirmed the 2-DE data (Figure 4.6 A and B respectively). AR expression paralleled HSP70 expression, though the difference reached statistical significance only for the comparison 7'MCAo vs. pMCAo (Figure 4.6 C).

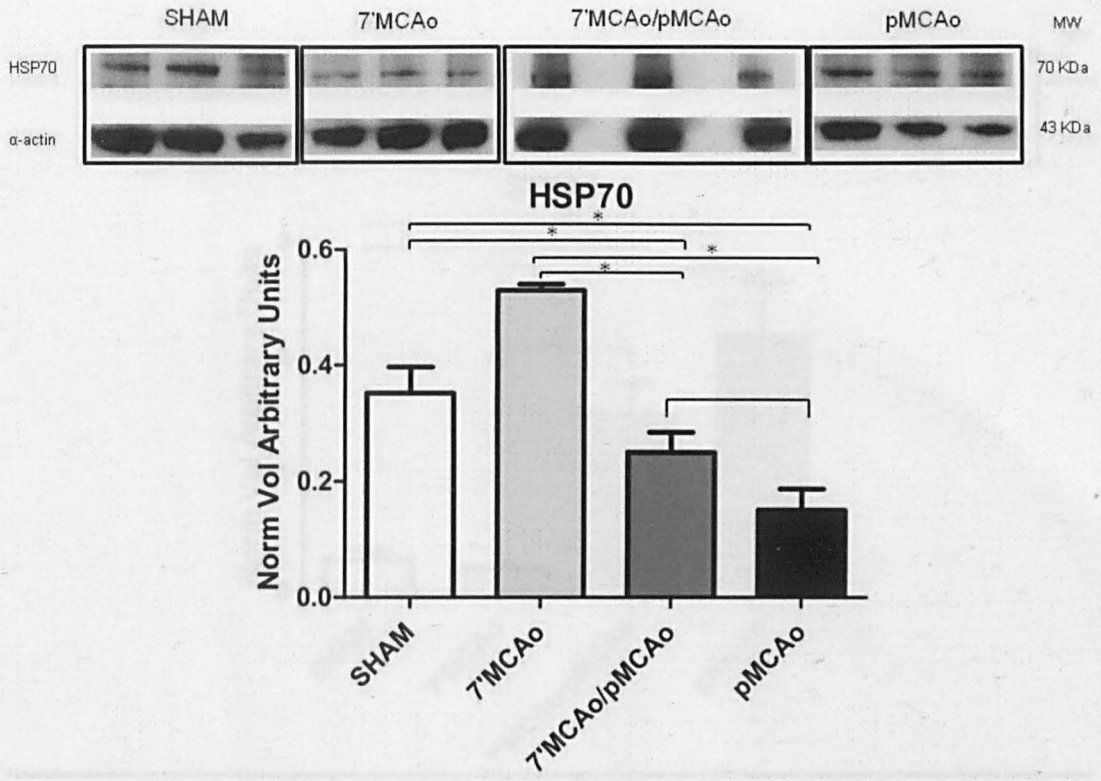

Figure 4.6 A. HSP70 expression analyzed by Western blot. Protein bands in the autoradiograms were quantified by scanning densitometry. Expression data were normalized relative to α-actin. Each bar represents the normalized volume density (mean ± SD, n=3). The vertical axis shows arbitrary density unit. Asterisks mark significant expression changes (Tukey-Kramer HSD $p < 0.05$).

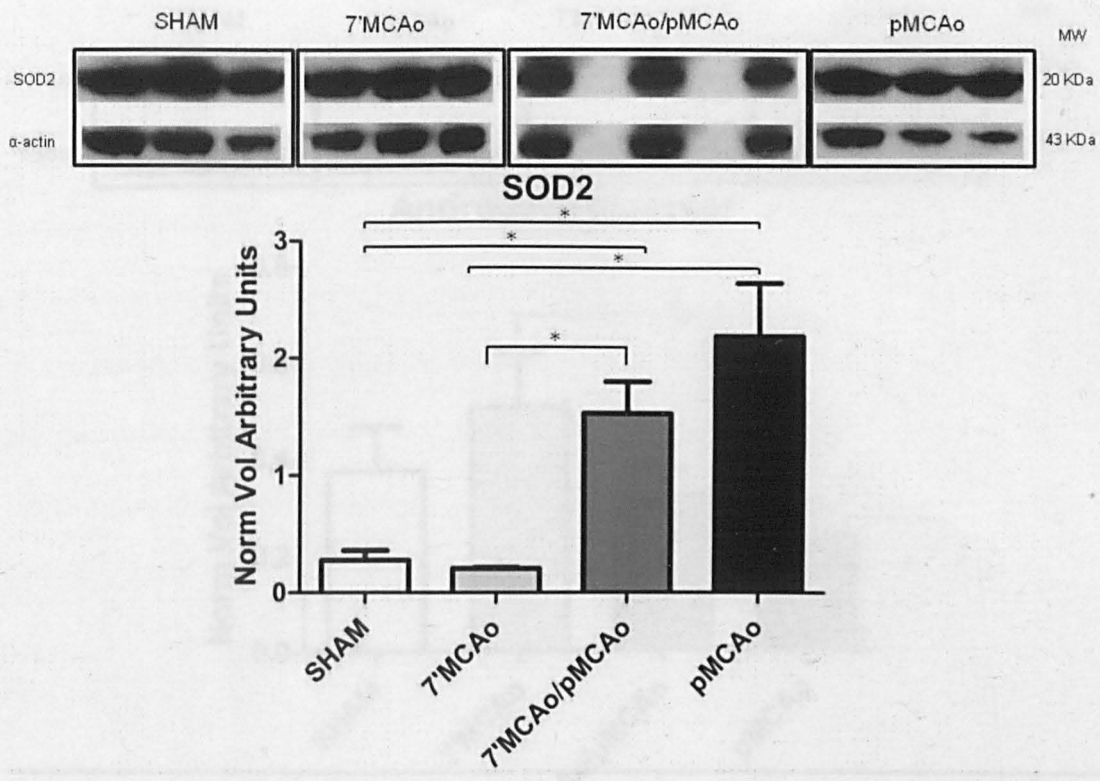

Figure 4.6 B. SOD2 expression analyzed by Western blot. Protein bands in the autoradiograms were quantified by scanning densitometry. Expression data were normalized relative to α-actin. Each bar represents the normalized volume density (mean ± SD, n=3). The vertical axis shows arbitrary density unit. Asterisks mark significant expression changes (Tukey-Kramer HSD $p < 0.05$).

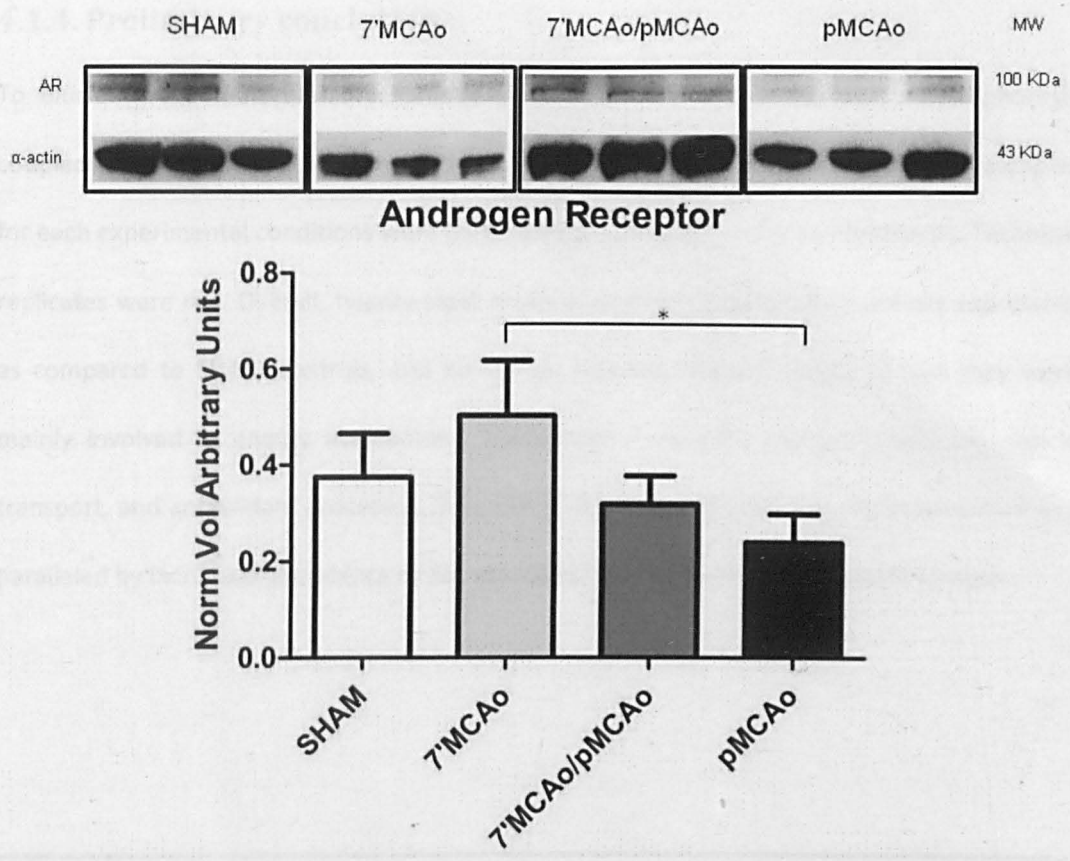

Figure 4.6 C. AR expression analyzed by Western blot. Protein bands in the autoradiograms were quantified by scanning densitometry. Expression data were normalized relative to α-actin. Each bar represents the normalized volume density (mean ± SD, n=3). The vertical axis shows arbitrary density unit. Asterisks mark significant expression changes (Tukey-Kramer HSD $p < 0.05$).

4.1.4. Preliminary conclusions

To elucidate the molecular mechanisms involved in IPC two-dimensional electrophoresis coupled to liquid chromatography-tandem mass spectrometry on brain cortex pool samples for each experimental conditions were performed to overcome resource constraints. Technical replicates were run. Overall, twenty-eight proteins were detected as differentially expressed, as compared to SHAM controls, and identified. Pathway analysis indicated that they were mainly involved in energy metabolism, mitochondrial electron transport, synaptic vesicle transport, and antioxidant processes. Differential expression of HSP70 in the brain cortex was paralleled by increased abundance of AR, as validated by western blot on pooled samples.

4.2. 1-DE-LC-MS/MS PLASMA PROTEOME ANALYSIS

During the development of this thesis, a linear ion trap Orbitrap instrument (LTQ Orbitrap XL) became available to the laboratory. This instrument combines the fast duty cycle of linear ion traps for MS/MS along with the high resolution and high mass accuracy capabilities of the Orbitrap. Thus, it is well suited for quantitative proteomics using a label-free strategy.

This prompted an investigation of changes in the plasma samples by a one-dimensional (1D) gel approach following protein pre-fractionation (Figure 4.7 shown the 1D gels used to excise gel bands for tryptic digestions), which was integrated into a typical LC-MS/MS workflow for protein identification, using the LTQ Orbitrap XL mass spectrometer. A simple and convenient label-free approach (spectral counting) was then used to estimate the relative abundance of proteins in 5 different experimental conditions (Matherials and Methods, Figure 3.3, page 86), namely, IPC stimulus (7'MCAo), severe ischemia (pMCAo), the combination of the two (7'MCAo/pMCAo), and 2 groups of sham-operated controls sham7'MCAo and sham7'MCAo/pMCAo. For convenience, sham7'MCAo will be referred to as sham 1OP (sham animals with one surgical operation) and sham7'MCAo/pMCAo will be referred to as sham 2OP (sham animals with two surgical operations). Analysis was performed on pooled samples for each experimental condition to overcome resource constrains.

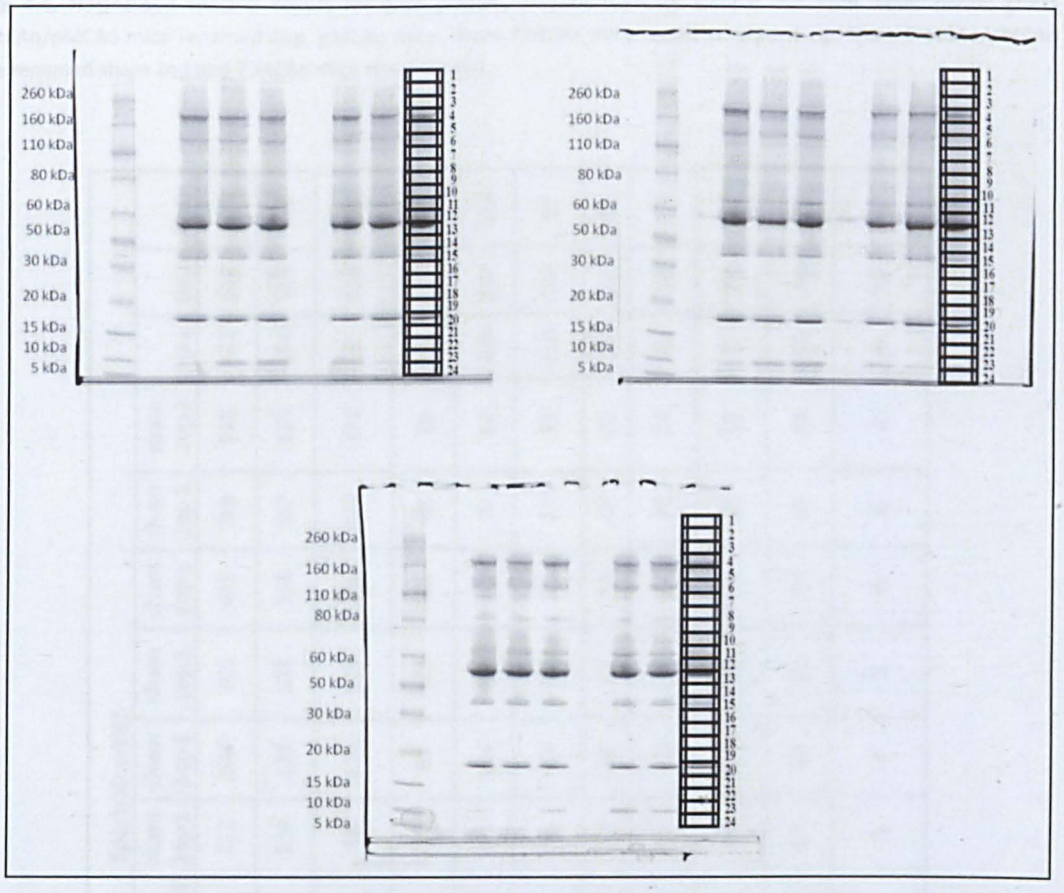

Figure 4.7. One-dimensional gels used to excise gel bands for tryptic digestions; in each gel samples were loaded in the following order (from left to right) : 7'MCAo, pMCAo, 7'MCAo/pMCAo, SHAM 7'MCAo, SHAM 7'MCAo/pMCAo and a SHAM merge obtained mixing an equal amount of protein from the two SHAM groups. In the last lane was reported an example of the mask that was used to cut the bands for tryptic digestions.

4.2.1. Differential protein expression

Proteomic analysis identified 143 proteins in mouse plasma that differed between the experimental groups. The quantitative data trend (normalized spectral counts for each protein in each replicate sample for each experimental group Table 4.4) was explored by PLS-DA to evaluate differences in the levels of protein expression in the different experimental groups.

Table 4.4. Normalized spectral counts for each protein, in each replicate sample, for each experimental group (7'MCAo/pMCAo mice renamed 2op, pMCAo mice, Sham 7'MCAo mice renamed sham 1 op, Sham 7'MCAo/pMCAo mice renamed sham 2op and 7'MCAo mice renamed tia).

		Spectral counts														
		2op 1	2op 2	2op 3	pmcao 1	pmcao 2	pmcao 3	sham 1op 1	sham 1op 2	sham 1op 3	sham 2op 1	sham 2op 2	sham 2op 3	tia 1	tia 2	tia 3
2	Complement C3	432	370	477	331	351	468	373	644	601	425	410	528	472	638	470
6	Serotransferrin	205	210	194	170	164	159	170	133	173	183	207	175	154	153	133
8	Alpha-2-macroglobulin	145	145	144	104	95	115	92	130	120	150	133	171	87	116	83
10	Complement factor H	107	82	82	90	84	84	90	83	115	65	61	76	99	128	81
11	Fibrinogen gamma chain	58	72	69	60	63	59	106	107	92	69	93	82	119	147	117
14	Fibrinogen beta	70	41	45	59	46	51	98	83	58	51	55	53	116	133	93
32	Gelsolin	21	27	20	19	23	23	45	31	27	29	42	25	27	34	28
34	Epidermal growth factor receptor	32	41	24	31	21	25	42	36	27	31	26	24	21	28	18
42	Prothrombin	19	15	15	17	27	18	20	21	23	20	15	18	12	19	17
45	Clusterin	22	20	18	14	17	18	19	19	31	13	15	19	13	24	21
80	Insulin-like growth factor-binding protein complex acid labile subunit	3	3	4	4	3	4	3	3	3	4	6	4	6	10	6

As shown in Figure 4.8, the scores demonstrated an acceptable separation between set 1 (7'MCAo and sham 1OP) and set 2 (pMCAo, 7'MCAo/pMCAo and sham 2OP) (Figure 4.8 panel A), using two principal components ($R^2(X) = 0.332$, $R^2(Y) = 0.205$, $Q^2 = 0.0456$); a good separation within each set was also obtained as shown in Figure 4.8 panel B and Figure 4.8 panel C (for set 1: $R^2(X) = 0.385$, $R^2(Y) = 0.846$, $Q^2 = 0.61$; for set 2: $R^2(X) = 0.267$, $R^2(Y) = 0.419$, $Q^2 = 0.148$).

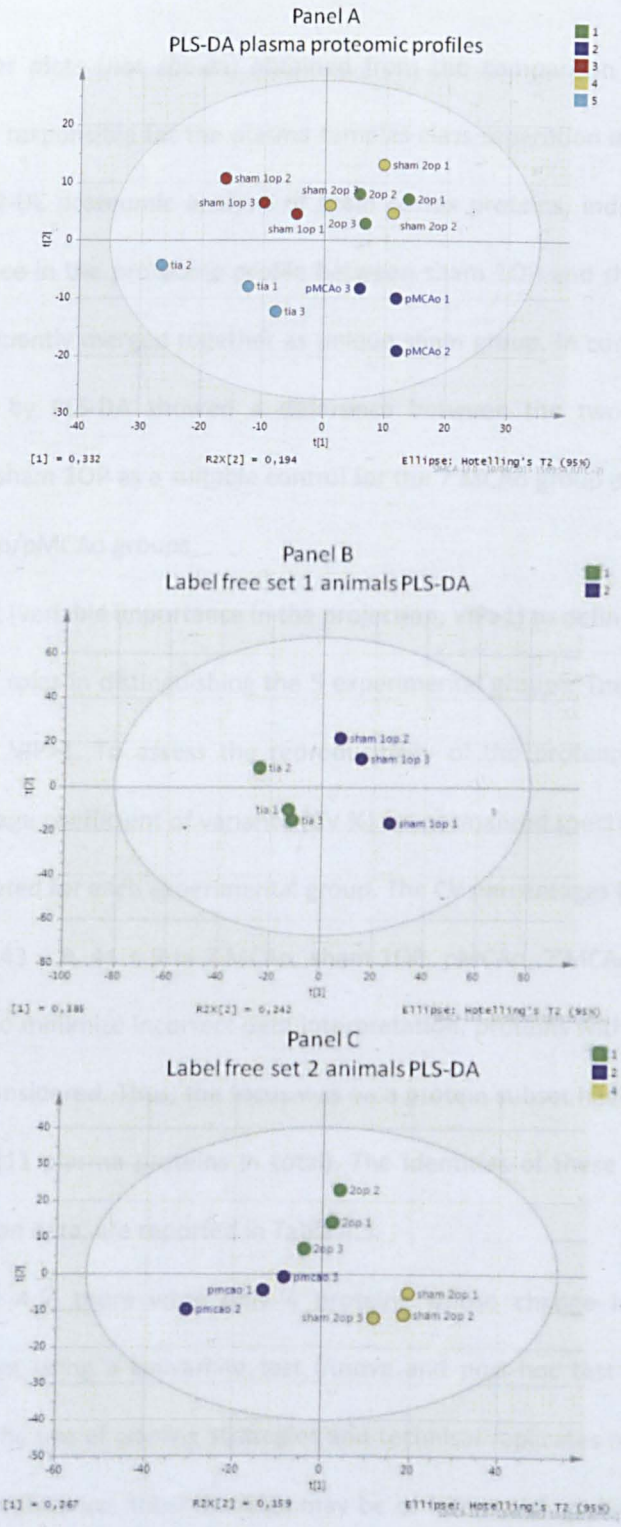

Figure 4.8. Panel A: PLS-DA score of plasma proteomic profiles from 7'MCAo mice (pale blue spots renamed tia), Sham 7'MCAo mice (red spots renamed sham 1 op), pMCAo mice (blue spots), 7'MCAo/pMCAo mice (green spots renamed 2op) and Sham 7'MCAo/pMCAo mice (yellow spots renamed sham 2op); **panel B**: PLS-DA score of plasma proteomic profiles from 7'MCAo mice (green spots renamed tia), Sham 7'MCAo mice (blue spots renamed sham 1 op); **panel C**: PLS-DA score of plasma proteomic profiles from pMCAo mice (blue spots), 7'MCAo/pMCAo mice (green spots renamed 2op) and Sham 7'MCAo/pMCAo mice (yellow spots renamed sham 2op).

The loading scatter plots (*not shown*) obtained from the comparison of the two datasets identified proteins responsible for the plasma samples class separation in all groups. It will be recalled that the 2-DE proteomic analysis of brain cortex proteins, indicated no statistically significant difference in the proteome profile between sham 1OP and sham 2OP, and hence, these were consequently merged together as unique sham group. In contrast, analysis of the plasma proteome by PLS-DA showed a difference between the two Sham groups. This prompted the use sham 1OP as a suitable control for the 7'MCAo group and sham 2OP for the pMCAo and 7'MCAo/pMCAo groups.

A threshold was set (variable importance in the projection, VIP>1) to define those proteins that played significantly roles in distinguishing the 5 experimental groups. There were 41 proteins out of 143 with a VIP>1. To assess the reproducibility of the protein quantitation in the replicates, the average coefficient of variance (CV %) for normalized spectral counts in the VIP-proteins was calculated for each experimental group. The CV percentages (mean ± SD) were 48 ± 8, 45± 9, 44 ± 6, 43 ± 8, 44 ± 9 in 7'MCAo, sham 1OP, pMCAo, 7'MCAo/pMCAo and sham 2OP, respectively. To minimize incorrect data interpretation, proteins with CVs of ≥ 35% were not subsequently considered. Thus, the focus was on a protein subset having VIP values of > 1 and CVs of ≤ 35% (11 plasma proteins in total). The identities of these proteins, and their differential expression data, are reported in Table 4.5.

As shown in Table 4.5, there were only 4 proteins whose change in abundance were statistically significant using a Univariate test (Anova and post-hoc test Tukey-Kramer HSD $p<0.05$). Althought the use of pooling strategies and technical replicates makes the statistical results with limited relevance, these findings may be of interest as global viwe of the most relevenat changes that occur during IPC. The expression of Insulin-like Growth Factor-binding protein complex Acid Labile Subunit (IGFALS) was more than doubled in 7'MCAo compared to sham 1OP, whereas it was almost halved in 7'MCAo when compared to pMCAo and 7'MCAo/pMCAo. The abundance of Epidermal Growth Factor Receptor (EGFR) was decreased

1.6-fold in 7'MCAo when compared to sham 1OP. The fibrinogen gamma and beta chains were downregulated by almost 2-fold in 7'MCAo when compared to pMCAo and/or 7'MCAo/pMCAo.

Table 4.5. Protein expression fold change in mouse plasma after preconditioning alone (7'MCAo) or severe ischemia with (7'MCAo/pMCAo) or without preconditioning (pMCAo) as compared to SHAM. Up- or downregulated proteins are shown in **bold** (fold change ≥ 1.5), or in ***bold-italic*** (fold change ≥ -1.5), respectively (Tukey-Kramer HSD $p < 0.05$).

#	Identified Proteins	Access number	Entry name	Expression fold changes					
				7'MCAo Vs sham 1OP	pMCAo Vs sham 2 OP	7'MCAo/pMCAo Vs sham 2OP	7'MCAo/pMCAo Vs pMCAo	pMCAo Vs 7'MCAo	7'MCAo/pMCAo Vs 7'MCAo
2	Complement C3	P01027	CO3_MOUSE	-1	-1.1	-1	1.1	-1.3	-1.2
6	Serotransferrin	Q92111	TRFE_MOUSE	-1	-1.1	1	1.2	1.1	1.3
8	Alpha-2-macroglobulin	Q61838	A2M_MOUSE	-1.2	-1.4	-1	1.4	1.11	***1.5***
10	Complement factor H	P06909	CFAH_MOUSE	1	1.2	1.3	1	-1.18	-1.1
11	Fibrinogen gamma chain	Q8VCM7	FIBG_MOUSE	1.2	-1.3	-1.2	1	***-2***	***-1.9***
14	Fibrinogen beta chain	Q8K0E8	FIBB_MOUSE	1.4	-1	-1	-1	***-2.1***	***-2.1***
32	Gelsolin	P13020	GELS_MOUSE	-1.1	-1.4	-1.4	1	-1.3	-1.3
34	Epidermal growth factor receptor	Q01279	EGFR_MOUSE	***-1.5***	-1	1.1	1.2	1.1	1.4
42	Prothrombin	P19221	THRB_MOUSE	-1.3	1.1	-1.1	-1.3	1.3	1
45	Clusterin	Q06890	CLUS_MOUSE	-1.2	1	1.2	1.2	-1.1	1
80	Insulin-like growth factor-binding protein complex acid labile subunit	P70389	LGFALS_MOUSE	***2.4***	-1.3	-1.4	-1	***-2***	***-2.2***

To understand the biological relevance of the differentially expressed plasma proteins, the 11 proteins identified above (i.e. with VIP values of > 1 and CVs of ≤ 35%; Table 4.5) and their expression data were visualized using the pre-existing pathway maps application of MetaCore (Matherials and Methods, page 100). Pathway reconstruction identified *Immune response-complement system* and *blood coagulation* (Figure 4.9 and Table 4.6), as the main pathways differently modulated in the mouse plasma from different experimental groups.

With this subset of 11 plasma proteins, biological network were built using the "shortest paths" (two steps) Metacore's network algorithm to evaluate protein-protein interaction

network. All the 11 plasma proteins of the subset used were brought together in the network (Figure 4.10).

The network statistics indicates Epidermal Growth Factor Receptor (EGFR), Clusterin and Insulin-like Growth Factor 1 (IGF-1) as the major hubs of this network, with respectively 15, 11 and 11 connections. Interestingly EGFR was directly connected with the Androgen Receptor (AR) and Heat Shock 70kDa Protein 5 (GRP78), member of the HSP70 family, proteins already highlighted by proteomic profiling of the brain cortex samples. Moreover, a further plasma protein, Clusterin, was directly linked to AR and to GRP78. Furthermore, the third hub, IGF1 was directly linked to the plasma protein IGFALS and again to Clusterin and to AR, suggesting again that AR might be an important player in the preconditioning stimulus (7'MCAo group).

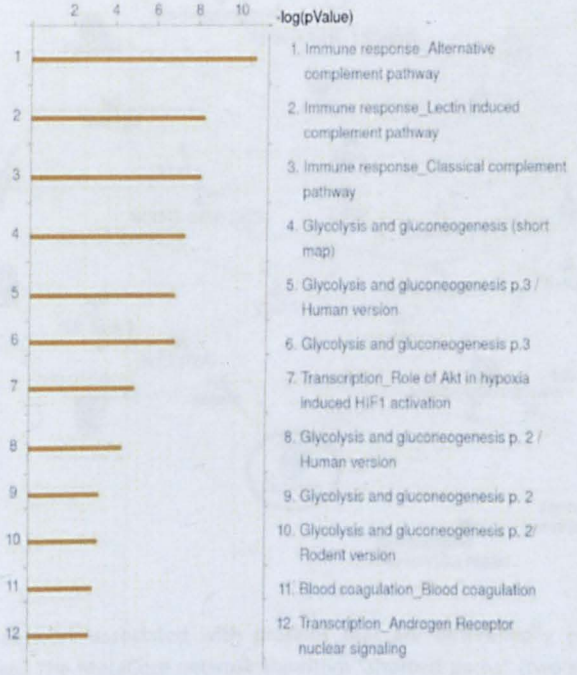

Figure 4.9. Functional Ontology Enrichment generated by the MetaCore software. The bars represent the most significant biological pathway maps overrepresented in the list of plasma proteins perturbed in the experimental models. Results are ranked by the -log(pValue).

Table 4.6. Mapping differently modulated proteins to pathways using the Metacore software package.

Pathway		Proteins
Immune response	Alternative complement pathway	Complement C3, Clusterin, Complement factor H
	Lectin induced complement pathway	Complement C3, Clusterin
	Classical complement pathway	Complement C3, Clusterin
Blood Coagulation		Alpha-2-macroglobulin
		Prothrombin
		Fibrinogen gamma chain
		Fibrinogen beta chain

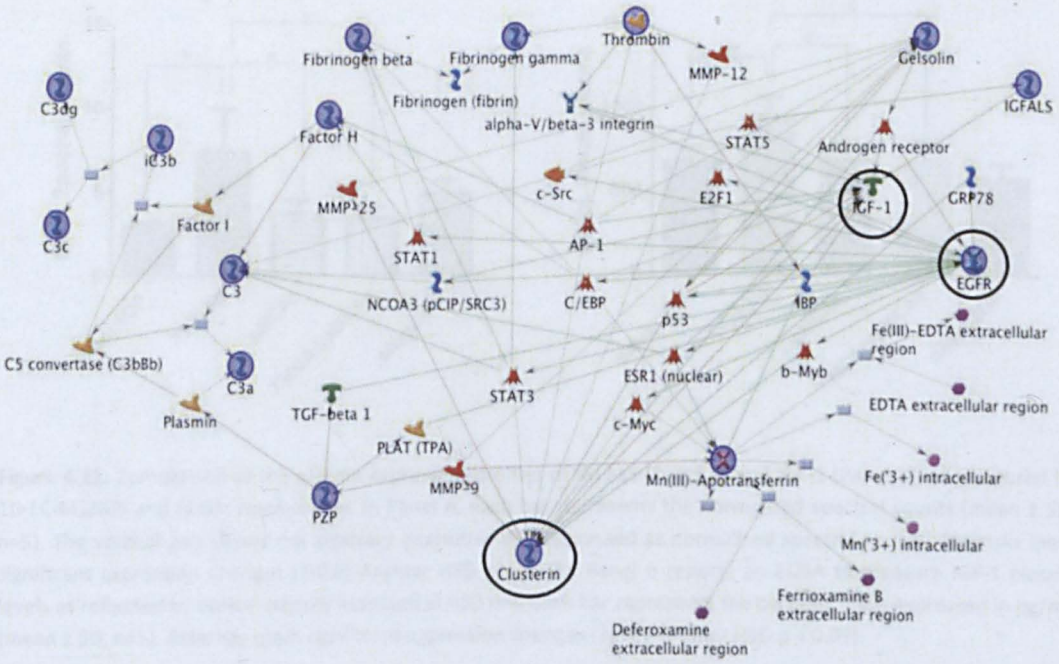

Figure 4.10. The global network associated with proteins that are differentially expressed in transient and permanent ischemia models. The MetaCore network algorithm "shortest paths" (two steps) was used to map the shortest path for protein-protein interactions. Individual proteins are represented as nodes of different shapes, according to their functional class. Circled nodes denote proteins identified in this study. Lines between nodes indicate direct protein-protein interactions, the arrowheads indicate the direction of the interaction. Black circles highlight network hubs highly connected with the dysregulated proteins, as indicated by network statistics.

4.2.3. IGF-1 plasma expression.

Since IGFALS was directly connected to IGF1 protein by network analysis, and IGF1 represented a major hub in the network, it was decided to validate the IGF1 expression trend in plasma biological replicates by a standardized and commercially available ELISA method (Matherials and Methods, page 100).

As shown in Figure 4.11, the expression trends of plasma IGFALS measured by label-free MS (panel A) paralleled those of IGF1 measured by ELISA (panel B). Indeed, an increased expression of both proteins was observed in the 7'MCAo group when compared to the proper SHAM group and also to pMCAo and 7'MCAo/pMCAo.

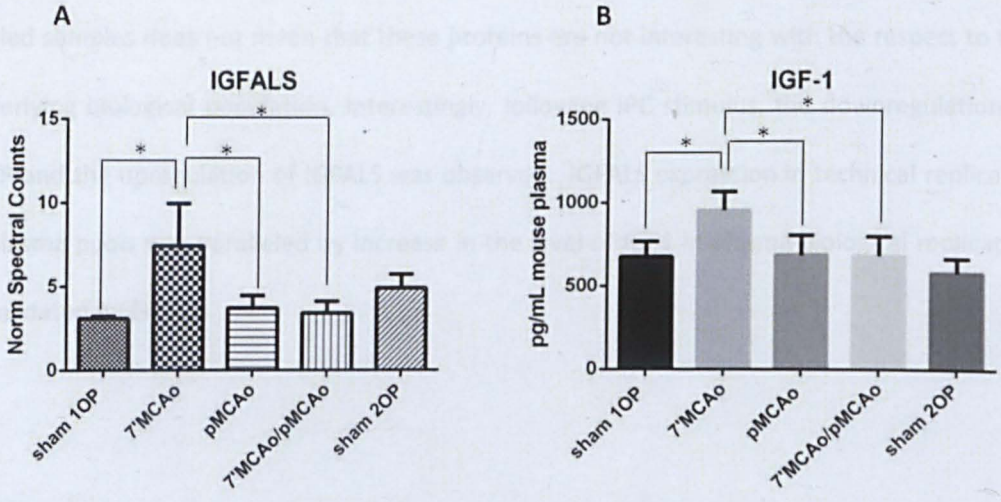

Figure 4.11. Comparison of the plasma expression profiles of IGFALS (Panel A) and IGF-1 (Panel B), as measured by 1D LC-MS/MS and ELISA, respectively. In Panel A, each bar represents the normalized spectral counts (mean ± SD, n=5). The vertical axis shows the arbitrary quantities unit expressed as normalized spectral counts. Asterisks mark significant expression changes (Tukey-Kramer HSD $p < 0.05$). Panel B reports an ELISA to measure IGF-1 plasma levels as reflected by optical density assessed at 450 nm. Each bar represents the concentration expressed in pg/mL (mean ± SD, n=5). Asterisks mark significant expression changes (Tukey-Kramer HSD $p < 0.05$).

4.2.4. Preliminary conclusions

The application of a 1D gel approach for plasma protein pre-fractionation integrated into a typical LC-MS/MS workflow successfully highlighted a small subset of plasma proteins (11 proteins), involved in inflammation and blood coagulation pathways, whose abundance significantly changed in different settings of the ischemic mouse models analyzed.

It has to keep in mind that the above results are based on pooled samples and technical replicates and no information on biological variation is available, limiting the statistical confidence. However the assumption of biological averaging is usually met in animal models where the source of bias (subject-to-subject variation) are small and can be neglected (Karp *et al.* 2009). Nevertheless the identification of up- and down-regulated proteins expression from pooled samples does not mean that these proteins are not interesting with the respect to the underlying biological population. Interestingly, following IPC stimulus, the downregulation of EGFR and the upregulation of IGFALS was observed. IGFALS expression in technical replicates of plasma pools was paralleled by increase in the level of IGF1 in plasma biological replicates, as validated by ELISA.

4.3 CORRELATION BETWEEN BRAIN CORTEX AND PLASMA PROTEOMIC RESULTS

As mentioned in the aims of this thesis (page 77), there was particular interest in evaluating to what extent the changes in protein expression observed in the brain of the IT mouse model correlate with those in their plasma, in order to discover a panel of candidate protein mediators for stroke progression and prognosis.

To achieve this goal it is necessary to integrate the proteomic results obtained from the different methodological approaches and scrutinize them using bioinformatic tools such as MetaCore (Matherials and Methods, page 100).

The protein sets that were used in this analysis are those reported in the 2-DE-LC-MS/MS brain results (Table 4.2 page 112) and in the 1D-LC-MS/MS plasma results (Table 4.5 page 128).

The two proteomics dataset were merged into a unique list of proteins (together with their expression data in each experimental group), which was subsequently used for network analysis to find the shortest path of interaction between the differentially expressed brain and plasma proteins (nodes). The MetaCore algorithm employed was 'Shortest paths', with a 2 steps maximum length for a path to be included and with a "Through" list of nodes, meaning that every path pass through all the nodes. All plasma and brain proteins were brought together in the network either by direct and indirect connections (Figure 4.12).

Interestingly, the 3 main hubs of this network were: Androgen Receptor (AR), Epidermal Growth Factor Receptor (EGFR) and the Insulin-like Growth Factor 1 (IGF-1), with respectively 102, 45 and 21 connections (Figure 4.13). These three protein hubs were in turn directly connected among each other. More precisely, AR exerted an activation effect on IGF-1 and it had an inhibitory effect on EGFR.

The reduction of the maximum length for the path (1 step instead of the previous 2 steps) highlights the important role of AR in controlling the expression of 8 brain proteins (GRP78: Heat shock protein 78; GSTP1: Glutathione *S*-transferase P1; ACON: Aconitate hydratase;

BHMT: Betaine homocysteine *S*-methyltransferase; V-ATPase E subunit: Vesicle fusing ATPase E subunit; NSG peroxidase: Peroxiredoxin-6; DLDH: Dihydrolipoyl dehydrogenase; PDIA3: Protein disulfide isomerase A3; and 4 plasma proteins (EGFR: Epidermal Growth Factor Receptor; Gelsolin; IGF-1: Insulin-like Growth Factor 1; Clusterin) (Figure 4.14).

An important detail from the previous network is reported in Figure 4.15 where the type of connections between the proteins changed following the preconditioning stimulus (7'MCAo group) are shown, suggesting again the important role of AR in this model setting.

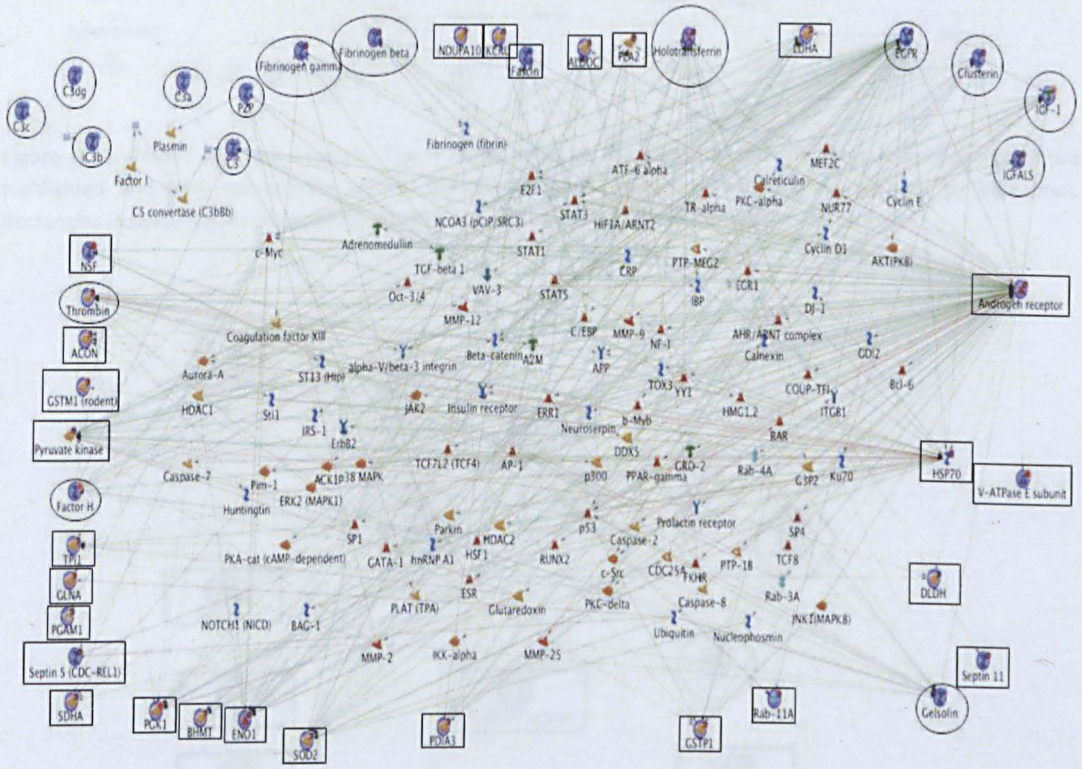

Figure 4.12. Global network associated with the proteins that were detected as differentially expressed in transient and permanent ischemia models. The MetaCore network algorithm "shortest paths" (two steps) was used to map the shortest path for protein-protein interactions. Circled nodes denote proteins identified in this study, small full red and blue circles indicate up- and down-regulation, respectively. Individual proteins are represented as nodes of different shapes, according to their functional class. Lines between nodes indicate direct protein-protein interactions, the arrowheads indicate the direction of the interaction. Rectangles indicate the identified brain proteins and circles indicate the identified plasma proteins.

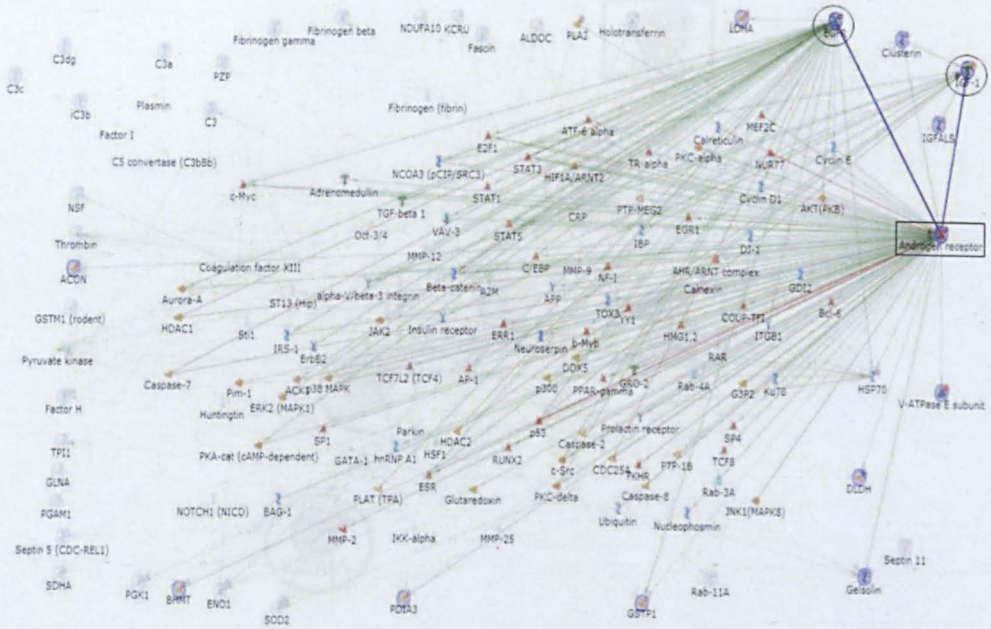

Figure 4.13. Traced network analysis. The 3 major hubs of the network and the directly linked objects are highlighted and their connections traced. Direct connections between hubs are represented by blue lines. Rectangles indicate the identified brain proteins and circles indicate the identified plasma proteins.

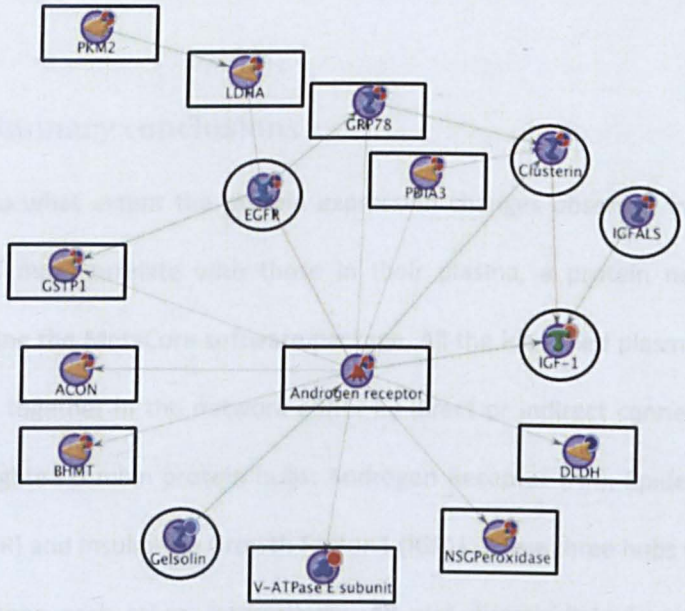

Figure 4.14. Global network associated with the proteins that were detected as differentially expressed in transient and permanent ischemia models. The MetaCore network algorithm "shortest paths" (one step) was used to map the shortest path for protein-protein interactions. Circled nodes denote proteins identified in this study, small full red and blue circles indicate up- and down-regulation, respectively. Individual proteins are represented as nodes of different shapes, according to their functional class. Lines between nodes indicate direct protein-protein interactions, while the arrowheads indicate the direction of the interaction. Rectangles indicate the identified brain proteins and circles indicate the identified plasma proteins.

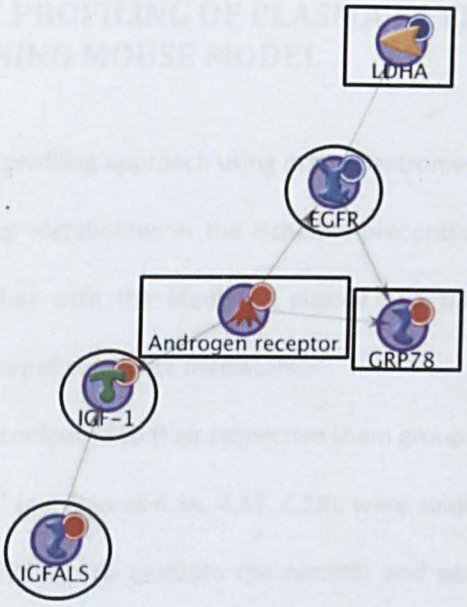

Figure 4.15. The network associated with the proteins that were differentially expressed in the 7'MCAo group. The MetaCore network algorithm "shortest paths" (one step) was used to map the shortest path for protein-protein interactions. Circled nodes denote proteins identified in this study, small full red and blue circles indicate up- and down-regulation, respectively. Individual proteins are represented as nodes of different shapes, according to their functional class. Lines between nodes indicate direct protein-protein interaction, while the arrowheads indicate the direction of the interaction. Rectangles indicate the identified brain proteins and circles indicate the identified plasma proteins.

4.3.1. Preliminary conclusions

To evaluate to what extent the protein expression changes observed in the brain of the IT mouse model may correlate with those in their plasma, a protein network analysis was performed using the MetaCore software package. All the identified plasma and brain proteins were brought together in the network either by direct or indirect connections. The network analysis highlighted 3 main protein hubs: Androgen Receptor (AR), Epidermal Growth Factor Receptor (EGFR) and Insulin-like Growth Factor 1 (IGF1). These three hubs were in turn directly connected among each other. Interestingly, AR was directly linked to the majority of the identified brain and plasma proteins.

4.4. METABOLOMIC PROFILING OF PLASMA IN THE ISCHEMIC PRECONDITIONING MOUSE MODEL

An unbiased metabolomic profiling approach using mass spectrometry was adopted to explore perturbations in circulating metabolites in the ischemic preconditioning mouse model. The rationale was that, together with the identified plasma and brain proteins, these might represent an innovative array of candidate mediators.

Experimental groups were compared to their respective sham group. Mass-spectral data of the single charged ions, $[M+H]^+$ (e.g Figures 4.16, 4.17, 4.18), were subject to peak alignment and data pre-processing by SIEVE v2. To evaluate the number and percentage of features that varied significantly between the different sample sets, filtering criteria were applied and significant differences were considered only for features with intensity coefficients of variation (CV%) of <20% and unpaired t-test for unequal variance (Welch's test) of $p \leq 0.01$. For convenience, sham7'MCAo is denoted as sham 1OP (i.e. sham animals with one surgical operation) and sham7'MCAo/pMCAo is denoted as sham 2OP (i.e. sham animals with two surgical operations). Althought the use of pooling strategies and technical replicates makes the statistical results with limited relevance, these findings may be of interest as global view of the most relevant changes that occurs during IPC.

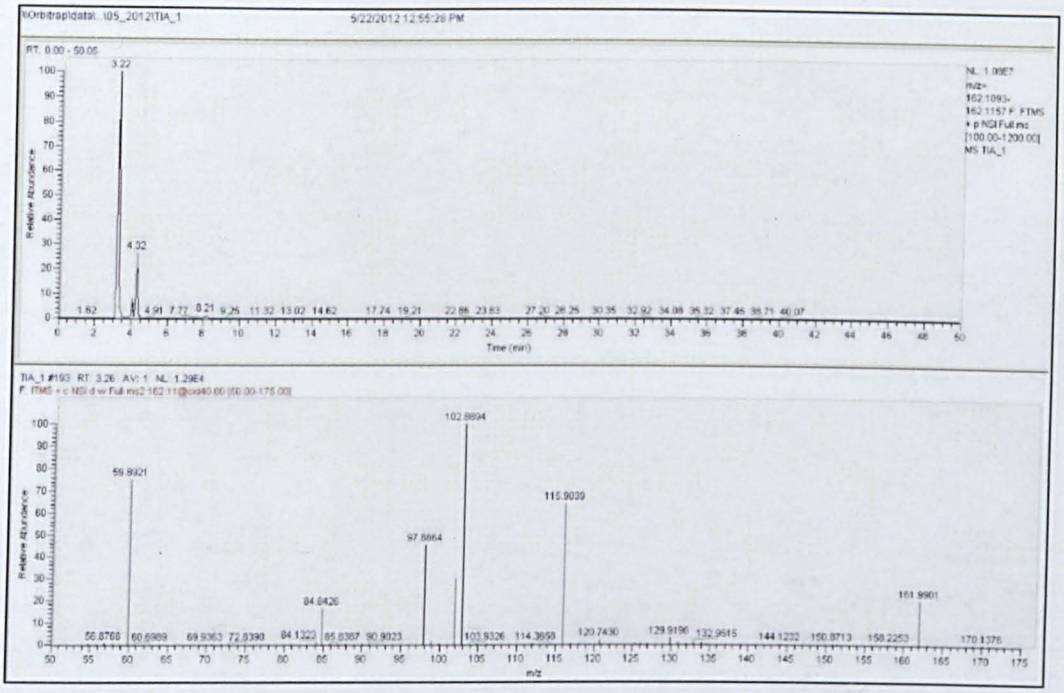

Figure 4.16. Carnitine $[M+H]^+$ m/z 162.1124 ; mass spectra acquired using LTQ Orbitrap XL™ (Thermo Scientific, Waltham, MA, US)in data depending mode. In the upper panel the MS spectrum is reported; in the lower panel the MS/MS spectrum is reported.

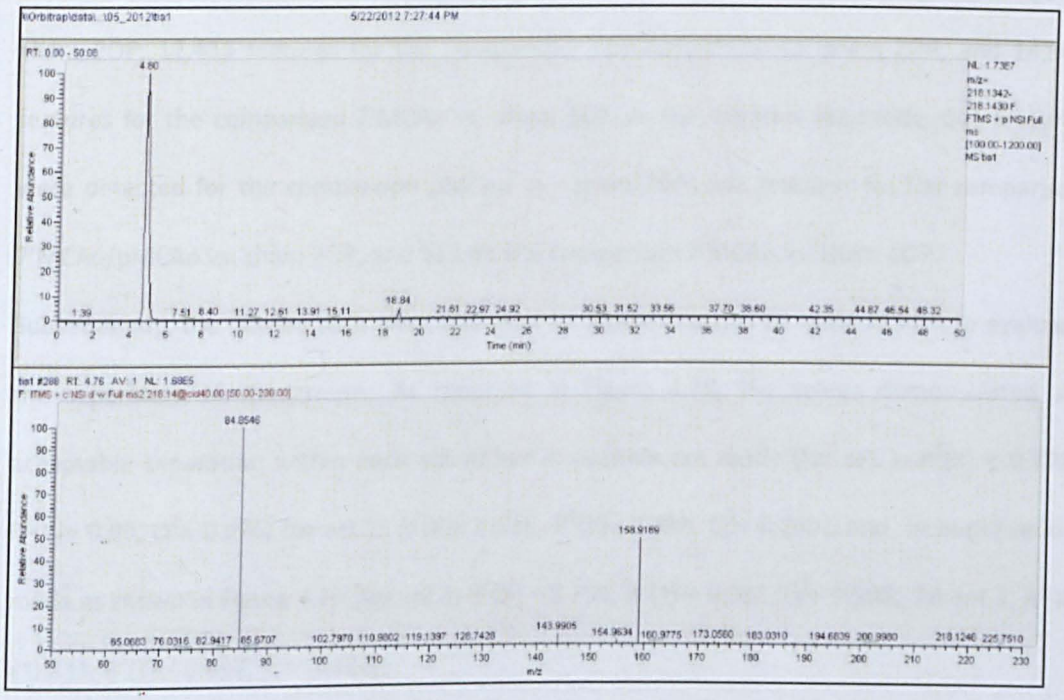

Figure 4.17. Propionylcarnitine $[M+H]^+$ m/z 218.1386; mass spectra acquired using LTQ Orbitrap XL™ (Thermo Scientific, Waltham, MA, US)in data depending mode. In the upper panel the MS spectrum is reported; in the lower panel the MS/MS spectrum is reported.

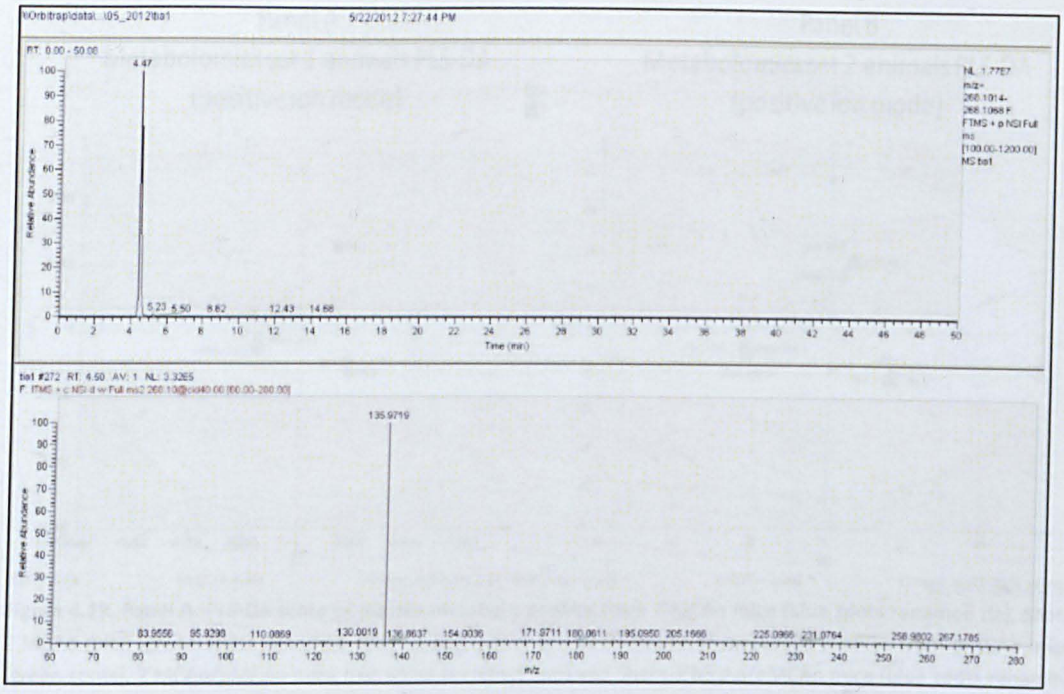

Figure 4.18. Adenosine $[M+H]^+$ m/z 268.1041; mass spectra acquired using LTQ Orbitrap XL™ (Thermo Scientific, Waltham, MA, US)in data depending mode. In the upper panel the MS spectrum is reported; in the lower panel the MS/MS spectrum is reported.

Overall, in the positive ion mode 12,436 features were detected for the comparison pMCAo vs. sham 2OP; 12,433 features for the comparison 7'MCAo/pMCAo vs. sham 2OP, and 14,940 features for the comparison 7'MCAo vs. sham 1OP. In the negative ion mode, 645 features were detected for the comparison pMCAo vs. sham 2OP; 642 features for the comparison 7'MCAo/pMCAo vs. sham 2OP, and 513 for the comparison 7'MCAo vs. sham 1OP.

Subsequently, the filtered data were analyzed for global changes by using PLS-DA to evaluate the separation of the groups. As reported in Figure 4.19, the scores demonstrated an acceptable separation within each set either in positive ion mode (for set 1: $R^2(X) = 0.778$, $R^2(Y) = 0.99$, $Q^2 = 0.976$; for set 2: $R^2(X) = 0.536$, $R^2(Y) = 0.498$, $Q^2 = 0.289$); and in negative ion mode as shown in Figure 4.20 (for set 1: $R^2(X) = 0.798$, $R^2(Y) = 0.981$, $Q^2 = 0.968$; for set 2: $R^2(X) = 0.833$, $R^2(Y) = 0.492$, $Q^2 = 0.432$).

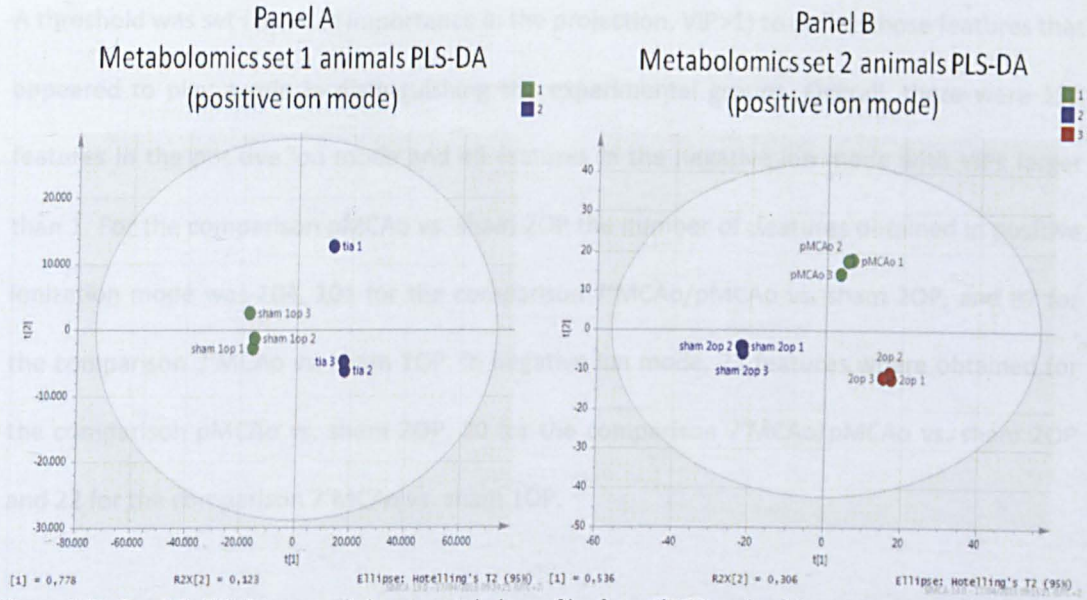

Figure 4.19. Panel A: PLS-DA score of plasma metabolic profiles from 7'MCAo mice (blue spots renamed tia), Sham 7'MCAo mice (green spots renamed sham 1 op); **panel B**: PLS-DA score of metabolic profiles from pMCAo mice (green spots), 7'MCAo/pMCAo mice (red spots renamed 2op) and Sham 7'MCAo/pMCAo mice (blue spots renamed sham 2op). Data acquired in positive ion mode.

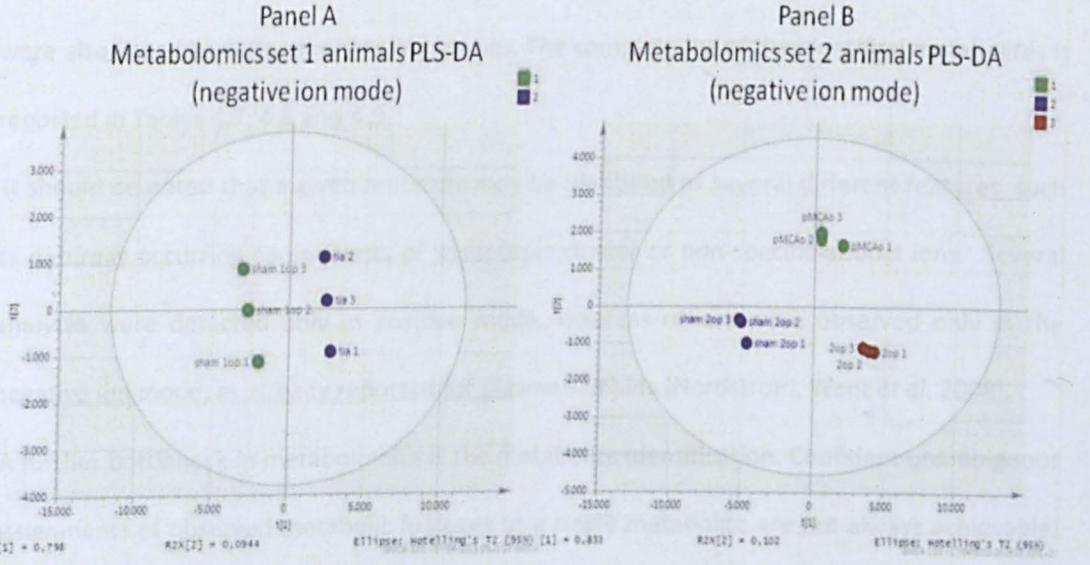

Figure 4.20. Panel A: PLS-DA score of plasma metabolic profiles from 7'MCAo mice (blue spots renamed tia), Sham 7'MCAo mice (green spots renamed sham 1 op); **panel B**: PLS-DA score of metabolic profiles from pMCAo mice (green spots), 7'MCAo/pMCAo mice (red spots renamed 2op) and Sham 7'MCAo/pMCAo mice (blue spots renamed sham 2op). Data acquired in negative ion mode.

A threshold was set (variable importance in the projection, VIP>1) to define those features that appeared to play a role in distinguishing the experimental groups. Overall, there were 191 features in the positive ion mode and 45 features in the negative ion mode with VIPs larger than 1. For the comparison pMCAo vs. sham 2OP the number of features obtained in positive ionization mode was 104, 101 for the comparison 7'MCAo/pMCAo vs. sham 2OP, and 87 for the comparison 7'MCAo vs. sham 1OP. In negative ion mode, 23 features where obtained for the comparison pMCAo vs. sham 2OP, 20 for the comparison 7'MCAo/pMCAo vs. sham 2OP and 22 for the comparison 7'MCAo vs. sham 1OP.

4.4.1. Identification of metabolites

By searching the KEGG and HMDB databases, 50% of the overall features in positive ion mode with VIPs > 1 were identified. 38% of the overall features in negative ion mode with VIPs > 1 were also linked to defined molecular species. The complete list of the identified metabolites is reported in Tables 4.7, 4.8 and 4.9.

It should be noted that a given molecule may be identified as several different features, such as naturally occurring components of its isotopic cluster or non-specific adduct ions. Several analytes were detected only in positive mode, whereas others were observed only in the negative ion mode, as already reported for plasma samples (Nordstrom, Want *et al.* 2008).

A further bottleneck in metabolomics is the metabolite identification. Confident unambiguous assignments of observed metabolic features to a single metabolite are not always achievable. The Chemical Analysis Working Group of the Metabolomics Standards Initiative (MSI; http://msi-workgroups.sourceforge.net) has defined four different levels of metabolite identification confidence and methods on how to report metabolite identities (Sumner *et al.* 2007; Dunn *et al.* 2012).

In my study the confidence of identity was mainly based upon mass spectral similarities with public spectral libraries (as reported in Matherial and Methods page 104), without reference to

authentic chemical standards. Therefore the resulting identifications herein reported are defined as putative (Sumner *et al.* 2007; Dunn *et al* 2012).

The 7'MCAo group was the only group with metabolites whose level was more than 10 times higher than the Sham counterpart instead in the other groups (pMCAo and 7'MCAo/pMCAo), the changes were all quite modest (Tables 4.7, 4.8 and 4.9).

Table 4.7. Metabolites whose abundance is significantly changed (VIP>1) in the pMCAo vs. Sham7'MCAo/pMCAo (sham 2OP) group. In each case, the following parameters are reported: the measured mass, mass error (delta ppm), type of adduct, expected mass value and the intensity ratio expressed as fold change value and calculated against the sham counterpart.

Metabolite	Measured Mass	Delta ppm	Adduct	MW	pMCAo Vs sham 2OP fold changes
2-Aminooctanoic acid	159.1257	1.3	+1H	160.1330	-1.2
3a,12a-dihydroxy-7-oxo-5b-cholan-24-oic acid	406.2717	0.6	+1H	407.2790	-41.3
3-Amino-3-(4-hydroxyphenyl)propanoic acid	181.0739	0.1	+1H	182.0812	1.6
3-Hydroxy-7-oxocholan-24-oic acid	390.2769	0.3	+1H	391.2841	-1.3
4-Hydroxy-4-(3-pyridinyl)butanoic acid	181.0740	0.1	+1H	182.0813	1.6
4-Oxo-4-(3-pyridinyl)butanoic acid	179.0581	0.6	+1H	180.0654	-1.4
4-Oxopentanoic acid	116.0477	2.9	-1H	117.0562	-1.3
Indoleacrylic acid	187.0635	0.8	+1H	188.0708	1.3
Indolelactic acid	205.0740	0.3	+1H	206.0812	-1.3
indoxyl	133.0526	1.1	+1H	134.0599	1
isocitric acid	192.0272	0.9	-1H	225.0615	1.3
L-(-)-methionine	149.0509	0.9	+1H	150.0582	1.2
L-(-)-Phenylalanine	165.0790	0.3	+1H	166.0863	1.7
L-(+)-Carnitine	161.1052	0.01	+1H	162.1125	1.8
L-(+)-Leucine	131.0946	0.6	+1H	132.1018	2
L-Valine	117.0788	1.3	+1H	118.0861	1.7
LysoPC(18:3(9Z,12Z,15Z))	517.3166	0.5	+1H	518.3239	4.2
LysoPC(20:3(8Z,11Z,14Z))	545.3472	1.6	+1H	546.3544	6.2
LysoPC(20:4(8Z,11Z,14Z,17Z))	543.3317	0.5	+1H	544.3390	2.7
LysoPC(20:5(5Z,8Z,11Z,14Z,17Z))	541.3163	0.9	+1H	542.3236	11.6
LysoPC(22:6(4Z,7Z,10Z,13Z,16Z,19Z))	567.3320	0.8	+1H	568.3393	2.5
LysoPE(18:2(9Z,12Z)/0:0)	477.2854	0.2	-1H	500.2782	2.4
LysoPE(20:4(8Z,11Z,14Z,17Z)/0:0)	501.2855	0.1	-1H	524.2784	2.3
Proline betaine	143.0943	2.2	+1H	144.1016	-1.7
propionylcarnitine	217.1313	0.3	+1H	218.1386	-1
tryptophan	204.0898	0.3	+1H	205.0971	1.3

Table 4.8. Metabolites whose abundance is significantly changed (VIP>1) in the 7'MCAo/pMCAo (2op) group vs. Sham7'MCAo/pMCAo (sham 2OP) group. In each case, the following parameters are reported: the measured mass, mass error (delta ppm), type of adduct, expected mass value and the intensity ratio expressed as fold change value and calculated against the sham counterpart.

Metabolite	Measured Mass	Delta ppm	Adduct	MW	2op Vs sham 2OP fold changes
2-Aminooctanoic acid	159.1257	1.3	+1H	160.1330	1.4
3-Amino-3-(4-hydroxyphenyl)propanoic acid	181.0739	0.1	+1H	182.0812	1.2
3-Hydroxy-7-oxocholan-24-oic acid	390.2769	0.3	+1H	391.2841	-1.4
4-Hydroxy-4-(3-pyridinyl)butanoic acid	181.0740	0.1	+1H	182.0813	1.2
4-Oxo-4-(3-pyridinyl)butanoic acid	179.0581	0.6	+1H	180.0654	2.5
4-Oxopentanoic acid	116.0477	2.9	-1H	117.0562	-1
Indoleacrylic acid	187.0635	0.8	+1H	188.0708	1.2
Indolelactic acid	205.0739	0.2	+1H	206.0812	1.8
indoxyl	133.0526	1.1	+1H	134.0599	-1.3
isocitric acid	192.0272	0.9	-1H	225.0615	1.3
L-(-)-methionine	149.0509	0.9	+1H	150.0582	1.1
L-(-)-Phenylalanine	165.0789	0.4	+1H	166.0862	1.5
L-(+)-Carnitine	161.1052	0.01	+1H	162.1125	2
L-(+)-Leucine	131.0946	0.6	+1H	132.1018	1.5
L-Valine	117.0788	1.3	+1H	118.0861	1.4
LysoPC(18:3(9Z,12Z,15Z))	517.3166	0.5	+1H	518.3239	4.8
LysoPC(20:3(8Z,11Z,14Z))	545.3472	1.6	+1H	546.3544	5
LysoPC(20:4(8Z,11Z,14Z,17Z))	543.3317	0.5	+1H	544.3390	2.6
LysoPC(20:5(5Z,8Z,11Z,14Z,17Z))	541.3163	0.9	+1H	542.3236	6.7
LysoPC(22:6(4Z,7Z,10Z,13Z,16Z,19Z))	567.3320	0.8	+1H	568.3393	2.4
LysoPE(18:2(9Z,12Z)/0:0)	477.2854	0.2	-1H	500.2782	4
LysoPE(20:4(8Z,11Z,14Z,17Z)/0:0)	501.2855	0.1	-1H	524.2784	4
Proline betaine	143.0943	2.2	+1H	144.1016	-2.6
propionylcarnitine	217.1313	0.3	+1H	218.1386	-1.4
tryptophan	204.0898	0.3	+1H	205.0971	1.2

Table 4.9. Metabolites whose abundance is significantly changed (VIP>1) in the 7'MCAo (TIA) group vs. Sham7'MCAo (sham 1OP) group. In each case, the following parameters are reported: the measured mass, mass error (delta ppm), type of adduct, expected mass value and the intensity ratio expressed as fold change value and calculated against the sham counterpart.

Metabolite	Measured Mass	Delta ppm	Adduct	MW	TIA Vs sham 1OP fold changes
(2R)-1-[(Hydroxy{[(1s,3R)-2,3,4,5,6-pentahydroxycyclohexyl]oxy}phosphoryl)oxy]-3-(palmitoyloxy)-2-propanyl (5Z,8Z,11Z)-5,8,11-icosatrienoate	860.5410	0.6	-1H	883.5339	1.4
(2R)-2-Hydroxy-3-[(5Z,8Z,11Z,14Z,17Z)-5,8,11,14,17-icosapentaenoyloxy]propyl 2-(trimethylammonio)ethyl phosphate	541.3161	1.3	+1H	542.3234	1.4
(2R)-2-Hydroxy-3-[(9Z)-9-octadecenoyloxy]propyl 2-(trimethylammonio)ethyl phosphate	521.3476	0.8	+1H	522.3549	1
(2R)-3-[(9Z)-9-Hexadecenoyloxy]-2-hydroxypropyl 2-(trimethylammonio)ethyl phosphate	493.3162	1.2	+1H	494.3235	-1.1
(4Z)-2-Amino-3-hydroxy-4-octadecen-1-yl dihydrogen phosphate	379.2484	0.9	+1H	380.2557	2.1
2,2-Dimethylsuccinic Acid	146.0578	0.9	+1H	147.0650	-28
2-Methylbutyrylglycine	159.0894	1.0	+1H	160.0966	4
3-Methyl-2-oxopentanoic acid	130.0632	1.6	-1H	131.0715	1.3
Adenosine	267.0969	0.2	+1H	268.1042	39.3
Adipic acid	146.0581	0.4	-1H	147.0665	9.1
butyrylcarnitine	231.1472	0.5	+1H	232.1544	19.2
D-Panthotenic Acid	219.1108	0.4	+1H	220.1180	1.8
Glucose	180.0636	1.1	-1H	145.0507	-11.3
Hippuric acid	179.0583	1.5	+1H	180.0655	2
homocitric acid	206.0425	0.9	-1H	171.0276	1.9
Hypoxanthine	136.0387	2.0	-1H	137.0457	2.6
indol-3-ylacetaldehyde	159.0683	1.9	+1H	160.0756	61.2
indoleacrylic acid	187.0634	0.4	+1H	188.0707	1.4
Indolelactic acid	205.0740	0.3	+1H	206.0812	3.3
L-(-)-methionine	149.0510	0.1	+1H	150.0583	1.3
L-(-)-Phenylalanine	165.0790	0.1	+1H	166.0862	1.4
L-(+)-Carnitine	161.1052	0.01	+1H	162.1125	1.4
L-Hexanoylcarnitine	259.1785	0.8	+1H	260.1858	58.1
LysoPC(18:2(9Z,12Z))	519.3324	0.02	+1H	520.3397	1.1
LysoPC(20:4(8Z,11Z,14Z,17Z))	543.3320	0.02	+1H	544.3392	1.5
LysoPE(18:2(9Z,12Z)/0:0)	477.2853	0.5	-1H	500.2783	2.4
LysoPE(18:2(9Z,12Z)/0:0)	477.2852	0.7	+1H	478.2925	2.4
N-Acetyl-L-phenylalanine	207.0898	1.1	+1H	208.0970	12.3
N-Acetylneuraminic acid	309.1064	1.3	+1H	310.1137	-1.1
N-caproylglycine	173.1051	0.3	+1H	174.1124	15.3
Niacinamide	122.0478	1.4	+1H	123.0551	-1.1
Phenylpyruvic acid	164.0471	0.6	+1H	165.0544	1.5
propionylcarnitine	217.1314	0.01	+1H	218.1387	4.9
Serotonin	176.0950	0.01	+1H	177.1022	54.9
threonic acid	136.0374	1.4	-1H	137.0457	2.1
tryptophan	204.0900	0.7	+1H	205.0973	1.5
tyrosine	181.0739	0.1	+1H	182.0812	1.6

4.4.2. Biological pathways and metabolic networks

To further interpret the biological significance of the overall metabolomics data, the software tool MetaboAnalyst was used to link the identified metabolites to metabolic pathways (Figure 4.21 and Figure 4.22). Panel A gives the summary plot for the metabolite set enrichment, panel B shows the difference in the abundance of the metabolites, mapped into enrichment categories, and panel C shows all metabolic pathways arranged according to the scores from enrichment analysis (*y* axis) and topology analysis (*x* axis).

The analysis of the differences between the two datasets indicated that the *protein biosynthesis* and *oxidation of branched fatty acids* were the most over-represented metabolic pathways for all the groups (Panel A, Figure 4.21 and Figure.4.22).

The 7'MCAo group showed plasma changes mainly in amino acids involved in protein biosynthesis and, more specifically, phenylalanine and tyrosine metabolism (Figure 4.21, panel A). For example, there was an overall increase, albeit modest, in the concentrations of methionine, phenylalanine, tyrosine and tryptophan compared to the sham control (Figure 4.22, panel B). Mice from the 7'MCAo group also had higher levels of carnitine and propionylcarnitine, which are involved in the oxidation of branched fatty acids, compared to the sham animals. Interestingly two metabolites (serotonin and indole-3-acetaldehyde), which contributes to the tryptophan metabolism, showed striking increases in their concentrations in the 7'MCAo compared to the sham.

Similarly, both pMCAo and 7'MCAO/pMCAo groups had a modest increase in the plasma levels of amino acids involved in protein biosynthesis (e.g. leucine, valine, methionine, phenylalanine, and tryptophan) when compared to their respective sham controls. In contrast to the 7'MCAo group, the pMCAo and 7'MCAO/pMCAo groups showed a slightly reduced plasma concentration of propionylcarnitine when compared to their controls (panel A and panel B Figure 4.22).

Metabolic pathway analysis arranged according to enrichment analysis (Panel C Figure 4.21) showed that tryptophan and phenylalanine metabolism are more likely to be perturbed as a consequence of preconditoning stimulus (7'MCAo group); whereas valine, leucine and isoleucine biosynthesis might have a major impact in the pMCAo and in 7'MCAo/pMCAo groups (Panel C Figure 4.22). Tables 4.10 and 4.11 report the lists of metabolites with the enriched and network pathways in which they are involved for the two experimental sets.

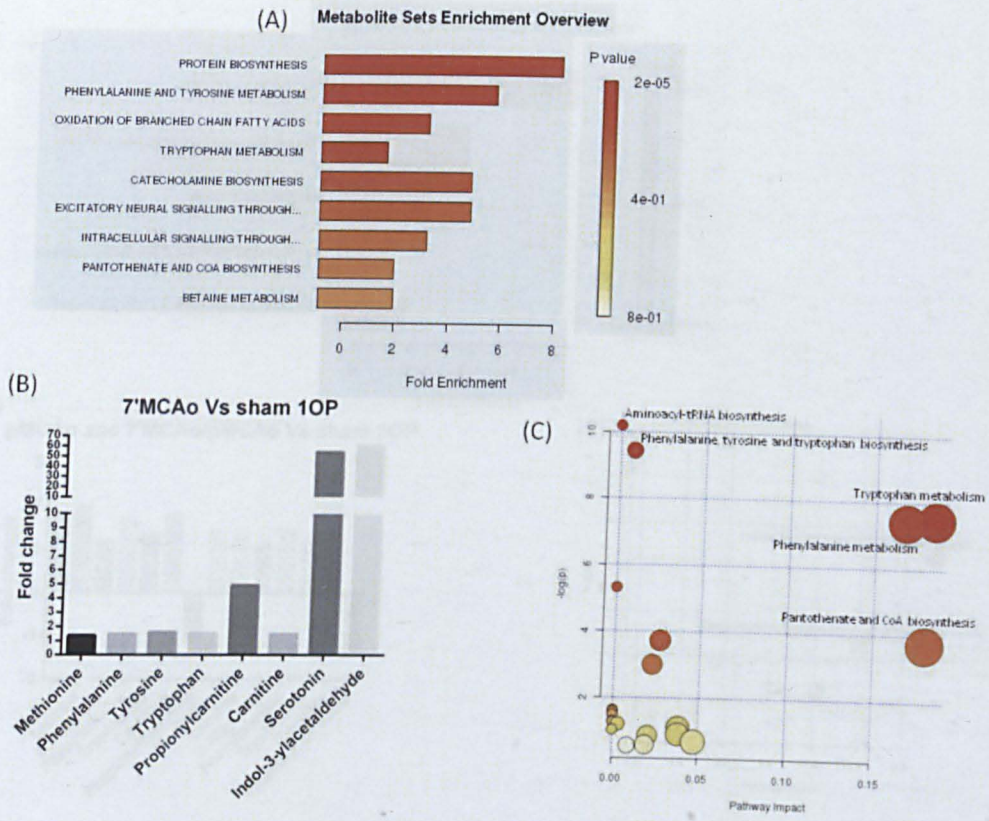

Figure 4.21. Metabolic pathway analyses related to the metabolites that specifically differ in the comparison 7'MCAo vs. SHAM 7'MCAo (sham 1OP) utilizing the MetaboAnalyst functional interpretation tools.
Panel A, graphic summary of metabolite set enrichment analysis; the horizontal bars summarize the main metabolite sets identified in this analysis; the bars are coloured according to the p-values and the bar length is based on the fold enrichment. **Panel B** shows the difference in abundance expressed as Fold change of the metabolite subset mapped into the enrichment categories. **Panel C** shows all metabolic pathways arranged according to enrichment analysis (*y* axis) and topology analysis (*x* axis) scores.

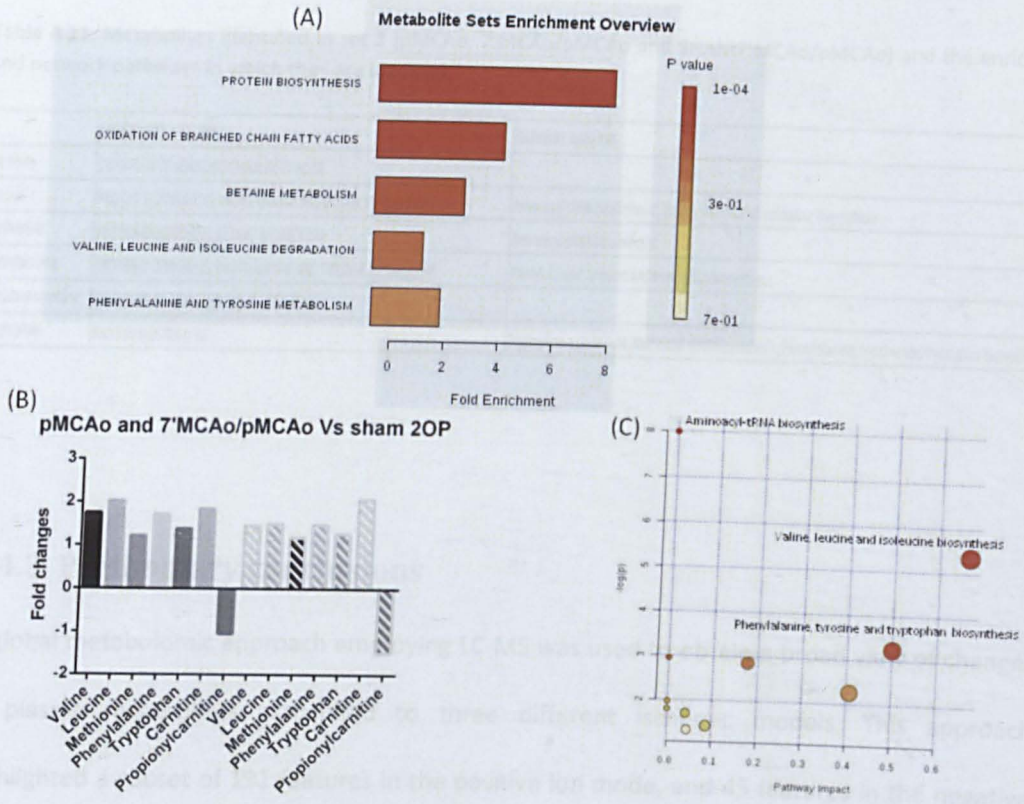

Figure 4.22. Metabolic pathway analyses related to the metabolites that specifically differ in the comparison pMCAo and 7'MCAo/pMCAo Vs sham 7'MCAo/pMCAo (sham 2OP) utilizing the MetaboAnalyst functional interpretation tools. **Panel A**, graphic summary of metabolite set enrichment analysis; the horizontal bars summarize the main metabolite sets identified in this analysis; the bars are coloured according to the p-values and the bar length is based on the fold enrichment. **Panel B** shows the difference in abundance expressed as Fold change of the metabolite subset mapped into the enrichment categories; full bars represent pMCAo metabolites; striped bars represent the 7'MCAo/pMCAo metabolites. **Panel C** shows all metabolic pathways arranged according to enrichment analysis (*y* axis) and topology analysis (*x* axis) scores.

Table 4.10. Metabolites identified in set 1 (7'MCAo and SHAM7'MCAo) and the enriched and network pathways in which they are involved.

	ENRICHMENT ANALYSIS	PATHWAY ANALYSIS
Carnitine	OXIDATION OF BRANCHED CHAIN FATTY ACIDS	
Indol-3-ylacetaldehyde	TRYPTOPHAN METABOLISM	Tryptophan metabolism
Indoleacrilic acid	TRYPTOPHAN METABOLISM	Tryptophan metabolism;
Indolelactic acid	TRYPTOPHAN METABOLISM	Tryptophan metabolism
Methionine	PROTEIN BIOSYNTHESIS; BETAINE METABOLISM	Aminoacyl-tRNA biosinthesis
N-Acetyl-L-phenylalanine	PHENYLALANINE AND TYROSINE METABOLISM	Phenylalanine metabolism; Phenylalanine, tyrosine and tryptophan metabolism
Pantothenic Acid	PANTOTHENATE AND COA BIOSYNTHESIS	Pantothenate and COA biosynthesis
Phenylalanine	PROTEIN BIOSYNTHESIS, PHENYLALANINE AND TYROSINE METABOLISM	Phenylalanine metabolism; Aminoacyl-tRNA biosinthesis; Phenylalanine, tyrosine and tryptophan metabolism
Phenylpyruvic acid	PHENYLALANINE AND TYROSINE METABOLISM	Phenylalanine metabolism; Phenylalanine, tyrosine and tryptophan metabolism
Propionylcarnitine	OXIDATION OF BRANCHED CHAIN FATTY ACIDS	
Serotonin	TRYPTOPHAN METABOLISM; EXCITATORY NEURAL SIGNALLING	Tryptophan metabolism; Phenylalanine, tyrosine and tryptophan metabolism

Table 4.11. Metabolites identified in set 2 (pMCAo, 7'MCAo/pMCAo and SHAM7'MCAo/pMCAo) and the enriched and network pathways in which they are involved.

	ENRICHMENT ANALYSIS	PATHWAY ANALYSIS
Carnitine	OXIDATION OF BRANCHED CHAIN FATTY ACIDS	
Leucine	PROTEIN BIOSYNTHESIS; VALINE, LEUCINE AND ISOLEUCINE DEGRADATION	Aminoacyl-tRNA biosinthesis; Valine, leucine and isoleucine biosynthesis
Methionine	PROTEIN BIOSYNTHESIS; BETAINE METABOLISM	Aminoacyl-tRNA biosinthesis
Phenylalanine	PROTEIN BIOSYNTHESIS; PHENYLALANINE AND TYROSINE METABOLISM	Phenylalanine, tyrosine and tryptophan biosynthesis
Propionylcarnitine	OXIDATION OF BRANCHED CHAIN FATTY ACIDS	
Tryptophan	PROTEIN BIOSYNTHESIS	Tryptophan metabolism; Aminoacyl-tRNA biosinthesis; Phenylalanine, tyrosine and tryptophan biosynthesis

4.4.3. Preliminary conclusions

A global metabolomic approach employing LC-MS was used to obtain a broad view of changes in plasma metabolites associated to three different ischemic models. This approach highlighted a subset of 191 features in the positive ion mode, and 45 features in the negative ion mode. Metabolite identification was successful for 50% and 38% of the features in positive and negative ion modes, respectively. The IPC stimulus group was the only in which the levels of certain metabolites was altered more than 10-fold relative to the Sham counterpart.

As already stated, althought the use of pooling strategies and technical replicates affect the strenght of the statistical analysis, these findings may be of interest as global view of the most relevant metabolomics changes that occur during IPC.

The profiling data was then used to detect altered biochemical processes using bioinformatics-based pathway mapping. The processes mainly affected by the different ischemic stimuli were *'proteins biosynthesis'*, *'phenylalanine and tyrosine metabo*lism', *'oxidation of branched fatty acid'* and *'tryptophan metabolism'*.

CHAPTER 5

DISCUSSION AND CONCLUSIONS

5.1. DISCUSSION

The molecular mechanisms underlying cerebral preconditioning are not well-understood, although it is generally accepted that this phenomenon requires a subthreshold dose of an otherwise harmful stimulus to induce protection against subsequent injurious challenge (Dirnagl, Becker *et al.* 2009). The use of experimental animal models may help understanding the molecular mechanisms of neuroprotection and lead to the identification of potential therapeutic targets. Gesuete *et al.* (Gesuete, Orsini *et al.* 2011) have previously shown that 7 min of ischemia (7'MCAo) is an ischemic pre-conditioning stimulus (IPC) capable of reducing the ischemic volume (as assessed 7 days after injury) induced by a subsequent severe ischemia. The 7'MCAo-induced protective mechanisms were effective 3 days after the IPC stimulus and lasted for 2 days (Gesuete, Orsini *et al.* 2011). I have used this mouse model of different ischemia sets to study the molecular mechanisms involved in the neuroprotection induced by IPC. In particular I performed a differential expression profiling of proteins and metabolites in brain and plasma of mice exposed to: (i) an IPC stimulus alone (7'MCAo), (ii) severe ischemia alone (pMCAo) and (iii) the IPC stimulus followed by severe ischemia (7'MCAo/pMCAo), in comparison to their sham operated counterparts.

I used mass spectrometry-based proteomics and metabolomics approaches to obtain a global overview of proteins and metabolites profile changes induced by IPC, with the ultimate aim of identifying possible mediators and their corresponding biological processes that may have a key role in the IPC induced protective mechanisms.

I am aware that there are some limitations in the overall strategy of my study. Firstly, the different time points used for samples collection (4 days for 7'MCAo and 11 days for pMCAo and 7'MCAo/pMCAo) might have affected proteomics and metabolomics profiles. Secondly, the use of pooling samples strategy and only technical replicates to overcome resources constraints weakened the strength of the statistical anaylses. Nevertheless I think this explorative study provides the following three main findings:

1. Brain and plasma proteomics highlighted a neuroprotective profile in ischemic tolerance, characterized by a hitherto unrecognized cross-talk mechanism between AR and HSP70, IGF-1, EGFR.

The protein profile changes were initially assessed in mouse brain cortices. Fewer proteins were affected after IPC stimulus alone (7'MCAo) than after severe stroke or the combination of two. A peculiarity four days after the IPC stimulus alone was a specific increase in the expression of HSP70. In line with this, HSP70 upregulation at transcriptional and protein expression levels 24h after an IPC stimulus consisting of 10 min transient MCAo in rats has been previously shown (Dhodda, Sailor *et al.* 2004). HSP70 and other heat shock proteins may play a role in the protection of the nervous system, particularly when induced before severe ischemia (Obrenovitch 2008; Ottens, Bustamante *et al.* 2010). I observed the increase in HSP70 four days after the IPC stimulus, whereas its expression was no longer affected seven days after severe ischemia, in either preconditioned or not preconditioned brains.

The pathway analysis of brain dysregulated proteins showed evidence of a direct interaction between HSP70 and AR. I showed that AR protein expression parallels that of HSP70, suggesting a role of this receptor in the preconditioning.

Androgen receptor is a nuclear receptor expressed in many tissue including both male and female brains (Dart *et al.* 2013); AR is activated by steroidal androgens (eg. testosterone, 5-α-dihydrotestosterone) exerting a transcriptional activity and can also be activated by non-steroid mechanism inducing the activation of MAPK pathway (Heinlein and Chang 2002); AR is involved in cell growth (Cai *et al.* 2011), in the remielization of axon in neurons (Hussain *et al.* 2013) and in the neurological effects associated to androgens also in brain ischemia (Uchida *et al.* 2009, Cheng *et al.* 2009). Male sex is an acknowledged risk factor for human stroke and the outcome from brain ischemic injury is sex-linked also in animals (Appelros *et al.* 2009; Cheng and Hurn 2010). However, the roles of steroidal androgens in brain ischemia is not clear and in

some cases contradictory (Cheng *et al* 2007; Uchida 2009). In fact, AR was also associated with a neuroprotective profile in castrated male mouse ischemic models (Ayala *et al.* 2011) although the signalling mechanism remains unclear.

As reported by others (Meehan and Sadar 2003), AR is associated in the cytoplasm with a complex of HSP90 and HSP70 that undergoes dissociation from AR in cells exposed to androgen. Moreover, Lu *et al.* (Lu, Tan *et al.* 2010), demonstrated that AR could regulate the expression level of HSP70-1 in prostate cancer cells, suggesting a feedback mechanism that regulate the homeostasis of HSP70 family (Lu, Tan *et al.* 2010).

My findings support the notion that HSP70 participates in the induction of ischemic tolerance and that its increased expression might be the result of synergistic effects of several mechanisms, including AR mediated androgen neuroprotection.

Besides upregulating HSP70 and AR, the IPC stimulus alone caused the downregulation of GSTM1 and LDHA. Glutathione *S*-transferases are detoxifying enzymes that catalyze the conjugation of reduced glutathione to reactive molecules from xenobiotics or products of oxidative stress, including reactive oxygen species (ROS). Thus, one would expect GSTM1 expression to increase, even after a mild ischemic insult. Instead, GSTM1 was dowregulated after four days of reperfusion, an adaptive response that might compromise the brain's capacity to deal with oxidative stress. However, mitochondrial ROS generation plays an important role in preconditioning so it is plausible to hypothesize that GSTM1 is downregulated to maintain a favorable mitochondrial redox status (Correia, Carvalho *et al.* 2010).

LDHA is the enzyme that converts pyruvate into lactate and back to pyruvate which is a substrate for the mitochondrial TCA cycle. Lactate has been proposed as a major energy source in the brain, since its oxidation can produce a significant amount of ATP (Schurr 2006). The decreasing LDHA expression observed in this study might be an indicator of metabolic

downregulation, suggested to play a role in IPC (Stenzel-Poore, Stevens *et al.* 2003; Stenzel-Poore, Stevens *et al.* 2007; Yenari, Kitagawa *et al.* 2008).

The involvement of metabolic downregulation is even more evident from protein expression after severe injury in preconditioned and non-preconditioned brains. Ischemia alone caused a strong upregulation of nearly all the proteins, and those with the largest expression changes (-fold change greater than 2) mainly coordinate energy metabolism, mitochondrial electron transport, synaptic vesicle transport and antioxidant processes. The response to ischemic injury after preconditioning revealed a striking difference. Preconditioning (7'MCAo/pMCAo) caused clear downregulation of energy metabolism (glycolysis, TCA cycle and mitochondrial electron transport) compared to pMCAo alone. These changes are unlikely to be long-lasting effects of IPC alone (7'MCAo) since when pMCAo was performed 5 days after 7'MCAo, the IPC stimulus was no longer protective (Gesuete, Orsini *et al.* 2011).

Downregulation of the energy metabolism at both transcriptional and protein levels is a clear outcome in animals preconditioned with brief ischemia before exposure to injurious ischemia (Stenzel-Poore, Stevens *et al.* 2003; Dhodda, Sailor *et al.* 2004). In line with this, preconditioned brains displayed strong downregulation of DHDL (Table 3, expression 3.6 times lower than in SHAM), one of the subunits of the pyruvate dehydrogenase complex that serves as the critical link between glycolysis (anaerobic energy metabolism) and TCA cycle (aerobic metabolism) by catalyzing the oxidative decarboxylation of pyruvate to form acetyl-CoA (Martin, Rosenthal *et al.* 2005). Reduced cerebral glucose metabolism and oxygen consumption after cerebral ischemia might depend on the low activity of pyruvate dehydrogenase complex (Fukuchi, Katayama *et al.* 1998).

Besides the decrease in expression of DHDL after preconditioning, I observed downregulation of succinate dehydrogenase (DHSA), and NADH dehydrogenase, both of which are involved in the generation of ROS by the mitochondrial electron transport chain. In line with these findings, respiratory chain inhibition may induce tolerance to focal cerebral ischemia

(Wiegand, Liao *et al.* 1999). The downregulation of these proteins could be indicative of an IPC-induced process aimed at mitochondrial preservation during ischemia. When ischemia is followed by reperfusion, the increase in oxygen supply results in a burst of mitochondrial ROS production (Dirnagl and Meisel 2008). These highly reactive molecules may damage nucleic acids, proteins and lipids. Mitochondrial biomolecules are especially susceptible to oxidative stress because of their proximity to ROS production. Thus, mitochondria are at the same time ROS generators and targets of oxidative stress (Dirnagl and Meisel 2008). To cope with the danger induced by ROS, protective mechanisms must be called into play and in fact antioxidant proteins such as GSTM1, GSTP1, and SOD2 remained upregulated in preconditioned brains.

Previously it has been shown that astrocytes are involved in IPC, both *in vivo* and *in vitro* (Gesuete, Orsini *et al.* 2011). This is further supported by the present findings indicating downregulation of one of the GLNA isoforms. GLNA is a glial-specific enzyme that converts the glutamate released during synaptic transmission to glutamine, which is then transported back to neurons, where it is converted to glutamate to close the glutamine-glutamate cycle in the brain (Zwingmann and Leibfritz 2003). The literature on GLNA expression in the brain after ischemia or hypoxia is scanty and contradictory (Hoshi, Nakahara *et al.* 2006; Lee, Lingwood **et** *al.* 2010) In the general metabolic down-regulation scenario uncovered in the present study, the reduction in GLNA expression after ischemic tolerance induction might reflect a lower energy demand, since glutamine has been reported to be an energy substrate in cultured neurons during glucose deprivation (Peng, Gu *et al.* 2007).

Another feature of preconditioning is the decrease in expression of fascin, a key regulator of cytoskeleton dynamics that organizes actin filaments and is abundant in the brain. Using an *in vitro* model, Meller *et al.* (Meller, Thompson *et al.* 2008) showed that two actin-binding proteins (MARCKS and fascin) are degraded by the ubiquitin–proteasome system soon after preconditioning ischemia and suggested that the loss of these actin-binding proteins promoted actin filament reorganization and could be involved in the acquisition of rapid (protein

synthesis-independent) ischemic tolerance (Meller, Thompson *et al.* 2008). The data in the present study suggest that regulation of proteins involved in cytoskeleton remodeling occurs also after IPC-induced delayed ischemic tolerance, as fascin downregulation was observed seven days after ischemia. However, the mechanism underlying these results could be different, possibly linked to protein synthesis modifications.

The proteomic approach used here was also successful in identifying circulating protein changes in the plasma of the different ischemic sets. When the ischemic preconditioning group was compared to its proper control, I observed an increased level of IGFALS, a glycoprotein that forms a ternary complex with IGF-1, IGF-2 and Insulin-like Growth Factor Binding Protein species (e.g. IGFBP-3) (Boisclair, Rhoads *et al.* 2001). Even though there is no direct correlation between IGFALS and neuro-protection, the latter has been associated with IGF-1 and IGFBP3 in the treatment of acute ischemic stroke (Kooijman, Sarre *et al.* 2009; De Smedt, Brouns *et al.* 2011). As reported by Boisclair *et al.* (Boisclair, Rhoads *et al.* 2001), IGFALS is a critical component that contributes to the development of a large reservoir of serum IGFs to facilitate their endocrine actions, to prolong their half-lives and to minimize their local effects. The increased abundance of plasma IGFALS, observed 4 days after the IPC stimulus, but no longer present at seven days after severe ischemia, suggests its involvement in the induction of tolerance. The increase in plasma IGF-1 parallels that of IGFALS, pointing toward a contribution of both proteins in the induction of the neuroprotective profile in ischemic preconditioning. This is in accordance with the notion that IGF-1, an endogenous survival factor for neurons, glia and endothelial cells, probably exerts its neuroprotective role in stroke by its anti-apoptotic, anti-inflammatory and regenerative properties (De Smedt, Brouns *et al.* 2011).

The IPC stimulus alone also induces lower levels of Epidermal Growth Factor Receptor (EGFR), a tyrosine kinase receptor that binds ligands of the Epidermal Growth Factor family. These ligands induce receptor activation by autophosphorylation. The activated receptor initiates a signal transduction cascade leading mainly to cell growth. The levels of EGFR may be

modulated at the genomic level by aldosterone, a steroid hormone produced by adrenal cortex considered a risk factor for stroke, due to its role in the pathogenesis of vascular disease (Dorrance, Osborn *et al.* 2001). The remodelling of the cerebral vasculature induced by EGFR activation, contributes to the pathogenesis of cerebral ischemia and the administration of spironolactone, an aldosterone antagonist, reduces the expression of mRNA for EGFR and the size of the ischemic damage (Dorrance, Osborn *et al.* 2001). Thus, the decreased level of plasma EGFR observed after the pre-conditioning stimulus alone could reflect an adaptive mechanism leading to a reduction in the remodelling of the cerebral vasculature and in the infarct size.

Changes in the levels of plasma fibrinogen gamma and fibrinogen beta, two polypeptide chains of fibrinogen, were observed in the severe stroke and ischemic-tolerant groups, when compared to the IPC stimulus alone. Fibrinogen is an hexameric plasma glycoprotein that is converted by thrombin in cross-linked fibrin taking part in the blood clot formation. Mediators of the acute-phase inflammatory response like glucocorticoids or IL-6, stimulate an increase of fibrinogen mRNA and protein levels; increased fibrinogen levels replenish fibrinogen lost due to bleeding or clotting, and contribute to wound healing (Fish and Neerman-Arbez 2012). Therefore the changes observed for the two fibrinogen chains could be related to the different time points at which the plasma samples were collected (4 days for 7'MCAo and 7 days for pMCAo and 7'MCAo/pMCAo) rather than to the different ischemic sets. As a matter of fact, no significant changes of these proteins were found when each ischemic set was compared to its proper sham. My explanation could be supported by Shenhar-Tsarfaty's work (Shenhar-Tsarfaty, Ben Assayag *et al.* 2008), which reported an increase in the human fibrinogen levels in the first few days after ischemia reflecting the acute-phase related to the inflamation. Since the final infarct size depends on the occlusion time of the MCA, and some processes involved in reperfusion, e.g. blood coagulation, could increase the size of infarct, the involvement of

blood coagulation processes in some models of brain ischemia is still debated (Braeuninger, Kleinschnitz *et al.* 2012).

Nevertheless, blood coagulation processes undoubtedly have a role in my differential ischemic sets, since plasma Alpha-2-macroglobulin (α2M) was increased in ischemic-tolerant mice when compared to the preconditioning stimulus group. α2M is a glycoprotein involved in blood coagulation, exhibiting a procoagulant activity by inhibiting plasmin and hence blocking the dissolution of the fibrin polymers (Schaller and Gerber 2011). At the same time, α2M can have an anticoagulant activity in antithrombin-deficient subjects inhibiting thrombin and the conversion of fibrinogen to fibrin (Mitchell, Piovella *et al.* 1991; Tripodi, Chantarangkul *et al.* 2000). Although no clear correlation exists between α2M and brain ischemia, its expression has been associated with genes related to the STAT3 pathway in the traumatic brain injury (TBI) (Oliva, Kang *et al.* 2012) a model known to share many aspects with brain ischemia. Moreover, STAT3 activation has been related to the neuroprotective role of IL-6 in the ischemic stroke (Jung, Kim *et al.* 2011) and it has been reported that STAT3 in Middle Cerebral Artery Occlusion (MCAo) mice models works as mediator of neuronal function after injury controlling metabolic, synaptic, structural and transcriptional pathway (Di Domenico, Casalena *et al.* 2012). On the basis of the above considerations, it is reasonable to assume that an activation of α2M by STAT3 might also occur in brain ischemia, and the levels changes observed could be associated with the protection induced by preconditioning against the severe stroke.

The key finding arising from the integration of the results of the brain and plasma proteomic study is the evidence of a neuro-protective profile characterizing the ischemic preconditioning group. As a matter of fact, in the brain of mice exposed to IPC only, HSP70 and AR could contribute to a neuroprotective profile, whereas in their plasma the neuro-protection could be related to the activity of the Insulin-like Growth Factor-1. This scenario represents a novel finding in the ischemic settings, since cross-talk among these proteins has previously been

suggested only in cancer-related studies, where IGF-1 may influence the expression of AR (Cohen, Peehl *et al.* 1991; Iwamura, Sluss *et al.* 1993; Pietrzkowski, Mulholland *et al.* 1993; Tong da, Wu *et al.* 2012). Similarly, the cross-talk between AR and EGFR has been suggested in prostatic and bladder cancer, where EGFR, in association with other tyrosine kinase receptors, e.g. ErbB2, could directly or indirectly induce a modulation in the expression and functions of AR (Cai, Portnoy *et al.* 2009; Izumi, Zheng *et al.* 2012).

On the basis of these data and the protein network findings, it is tempting to speculate that in the preconditioning stimulus alone group, crosstalk between IGF-1, AR and EGFR might occur and contribute to the restoration of an ischemic tolerant profile. Notably, combination of the brain and plasma proteomics findings through network analysis indicates that the AR was directly connected to proteins involved in energy metabolism (Aconitate hydratase, Dihydrolipoyl dehydrogenase), antioxidant processes (Glutathione *S*-transferase P1, Peroxiredoxin-6), stress response (Heat shock protein 78), amino acid biosynthesis (Betaine homocysteine *S*-methyltransferase), synaptic vesicle transport (Vesicle fusing ATPase E subunit), rearrangement of disulfide bonds (Protein disulfide isomerase A3) and cell growth (Epidermal growth factor receptor, Insulin like growth factor 1). Considering that some of these biological processes are upregulated in mice with severe stroke where AR is downregulated, it is reasonable to hypothesize that an inverse correlation between AR expression and those biological processes might occur.

2. Untargeted metabolomics analysis reveals fatty acids oxidation and branched-chain amino acid metabolism as the main biological processes modulated in ischemic tolerance (IT).

An unbiased metabolomic profiling approach using mass spectrometry was used to identify perturbations in circulating metabolites that could be involved in ischemic preconditioning and

might reflect amplifications of the changes that occurred in the transcriptome and the proteome (Kell 2005).

It is readily acknowledged that the metabolomics study that was performed is preliminary and that further validation of the changes in the concentration of metabolites found in the IT mice model is warranted.

Moreover, these metabolomics findings are purely observational and do not allow the identification of causal relationships to determine whether changes in circulating molecules are likely to be the consequence of the observed ischemic phenotypes. Moreover it is not known to what extent changes in plasma metabolites might interfere with brain metabolism and vice-versa.

Nevertheless, my preliminary data have shown that the IPC stimulus alone lead to the highest number of metabolites changes, when compared to severe stroke or preconditioned settings. Many biochemical alterations were in line with those already reported in the literature on cerebral ischemia, supporting the feasibility and robustness of this explorative untargeted LC-MS strategy. For example, there were changes in the plasma levels of carnitine and its esters, which play pivotal roles in transporting fatty acids into the mitochondria, where they are oxidized to produce energy (Virmani and Binienda 2004). Their role in brain neuropathology has been extensively investigated, providing evidence of neuro-protective, neuro-modulatory, and neurotrophic properties that may counteract various neurological disease processes (Virmani and Binienda 2004). Indeed, the supplementation of carnitine and its esters have shown beneficial effects in some neurological dysfunctions and in hypoxia-ischemia (Wainwright, Kohli *et al.* 2006; Jones, McDonald *et al.* 2010). In line with these observations, the levels of plasma carnitine esters particularly elevated in IPC animals, but generally reduced in severe-stroke and ischemic-tolerant mice, might corroborate the neuro-protective phenotype of the IPC mice. Changes in energy homeostasis pathways to sustain ischemic stress by IPC stimulus may be also supported by the elevation of plasma adipic acid, a dicarboxylic

acid derived from omega-oxidation of fatty acids. A plausible acceleration in fatty acid metabolism would inhibit an intracellular accumulation of detrimental fatty acids as proposed for myocardial ischemic preconditioning (Matsuki, Nozawa *et al.* 2009).

Evidence of a neuro-protective metabotype of the IPC setting can be inferred also from the high levels of plasma adenosine. Adenosine is a well known neuromodulator (Cunha 2001) that plays a key role in the induction of brain tolerance thought the activation of A1 receptors, which induces mitochondrial K^{+}_{ATP} channels opening, mitochondrial membrane depolarization and ROS reduction (Rudolphi, Schubert *et al.* 1992; Fellows, Boutelle *et al.* 1993; Heurteaux, Lauritzen *et al.* 1995; Perez-Pinzon and Born 1999). The surge in plasma adenosine likely mirrors an increased production in brain after TIA, where its accumulation may reflect an acute adaptation to the transient ischemic stress with a negative feedback modulation on hemodynamic causes and metabolic consequences of TIA, as suggested by Laghi Pasini *et al.* (Laghi Pasini, Guideri *et al.* 2000).

There is a convincing body of evidence for the role of branched-chain amino acids (BCAA) in brain functions. BCAA are integral to the glutamate/glutamine cycle, which is critical for the efficient uptake of glutamate during excitatory neuronal signaling (Hutson, Lieth *et al.* 2001; Fernstrom 2005). In the present study, mice exposed to severe stroke showed increased plasma levels of BCAA such as valine and leucine, suggesting a metabolic imbalance with a plausible detrimental effect on neurological functions due to their impaired catabolism (Kasinski, Doering *et al.* 2004). These results are in apparent contrast with the recent findings by Kimberly *et al.* (Kimberly, Wang *et al.* 2013) reporting a reduction in plasma concentration of BCAA associated with stroke severity. The conflicting data might be explained by the different animal models of acute ischemic stroke used and also by the different plasma sampling time following ischemia. Alternatively the increases in BCAA level we observed may reflect a slow-down in metabolic pathways leading to BCAA incorporation into structural

proteins, since BCAA are also known to have role in protein metabolism and in catabolic energy metabolism.

Notably, the BCAA leucine is an important regulator of the mammalian target of rapamycin (mTOR) and strongly inhibits autophagy by mTOR modulation (Pignataro, Capone *et al.* 2011 ; Ishizuka, Kakiya *et al.* 2008). Autophagy has been implicated in mediating neuroprotection in response to IPC (Papadakis, Hadley *et al.* 2013; Sheng, Zhang *et al.* 2010). Therefore it is likely that the systemic elevated level of leucine found in severe ischemia-exposed mice could participate in the mTOR activation, which might in turn result in the inhibition of autophagy and consequent cerebral damage.

3. The integration of -omics data points toward androgen receptor as a core molecule connecting protein and metabolite profiles to sustain brain ischemic tolerance.

Results from the literature demonstrate that androgens can regulate multiple molecular pathways involved in neurodegeneration exerting both neuroprotective and neurotoxic effects in an age- and dose-dependent way, likely involving AR signalling (Cheng and Hurn 2010, Uchida, Palmateer *et al.* 2009). However, recent findings show that AR deficiency is associated with greater ischemia-induced cellular apoptosis, providing evidence of a novel neuroprotective role of AR in promoting sex-independent angiogenesis (Yoshida, Aihara *et al.* 2013).

So far, in the present study, the AR-related implicated mechanisms could be solely inferred by network analysis.

As indicated by my proteomics findings, AR is likely to participate with many brain and plasma proteins (*e.g.* HSP70, IGF-1, EGFR) to improve brain defence and to reduce the abnormal response to an ischemic stress. Such an IPC-induced neuro-protection is likely to be achieved by reducing energy metabolism and mitochondrial respiratory chain activity.

I observed that AR is involved also in the instauration of a neuro-protective metabotype, being correlated with carnitine/carnitine esters and adenosine, whose systemic levels increased in the ischemic preconditioning set.

It has been reported that in prostatic cancer cells (Lin, Lu *et al.* 2010), AR activation increases the expression of carnitine palmitoyltransferases 1 (CPT1). CPT1 with carnitine palmitoyltransferases 2 compose the carnitine shuttle responsible for the mitochondrial import and export of long-chain acylcarnitines (Violante, Ijlst *et al.* 2013). The AR-induced increased expression of CPT might therefore increase the mitochondrial uptake of fatty acids, leading to their oxidation. As reported for myocardial ischemic preconditioning (Matsuki, Nozawa *et al.* 2009), this would lead to an accelerated oxidation of fatty acids and would inhibit an intracellular accumulation of detrimental fatty acids metabolites. IPC could induce an ischemic tolerant state with enhanced capacity for mitochondrial respiration and ATP synthesis.

Enhanced plasma levels of adenosine fits perfectly into this scenario of a homeostatic bioenergetic network, due to its direct biochemical interactions with energy homeostasis, nucleic acid metabolism, methylation status and adenosine receptor signialling pathways (Shen, Lusardi *et al.* 2011). The interaction between adenosine and AR could be mediated by adenosine kinase (ADK), which controls cellular levels of adenosine (Shen, Lusardi *et al.* 2011). Recently, it has been proposed that ADK activates protein kinase A and positively regulates the expression of the AR (Sarwar, Sandberg *et al.* 2013). The protective role of ADK in brain ischemia was previously demonstrated through the maintenance of energy homeostasis by promoting catabolic pathways for ATP production and limiting processes that consume ATP (Manwani and McCullough 2013).

5.2. CONCLUDING REMARKS

Mass spectrometry-based proteomics and metabolomics strategies once again offer promise for the discovery of potential biomarkers in cerebral ischemic preconditioning, despite some limitations intrinsic to the technologies, *e.g.* partial proteome/metabolome coverage.

My study provides the first application of both approaches in cerebral ischemic sets, highlighting the cross-talk between the metabolome and proteome, through the identification of biological entities relevant to ischemic preconditioning. Althought some weakness and limitations in the experimental design of my work (e.g. the use of technical replicates of pooled samples, the different time points for sample collection), overall, my study recapitulates some of the findings in the literature and provides evidence of an anticipated role of AR as point of convergence for a proteomic and metabolomic neuro-protective profile.

I had no chance to measure androgen or estrogen hormones, that could have supported the data on AR, so the use of additional methods and approaches for validating the AR role and related pathways in preconditioning is warrented.

CHAPTER 6

References

- Ackermann, B. L., M. J. Berna, J. A. Eckstein, L. W. Ott and A. K. Chaudhary (2008). "Current applications of liquid chromatography/mass spectrometry in pharmaceutical discovery after a decade of innovation." Annu Rev Anal Chem (Palo Alto Calif) **1**: 357-396.
- Adams, H. P., Jr. (1993). "Trials of trials in acute ischemic stroke. The Humana Lecture." Stroke **24**(9): 1410-1415.
- Aebersold, R. and M. Mann (2003). "Mass spectrometry-based proteomics." Nature **422**(6928): 198-207.
- Albers, G. W., L. R. Caplan, J. D. Easton, P. B. Fayad, J. P. Mohr, J. L. Saver and D. G. Sherman (2002). "Transient ischemic attack--proposal for a new definition." N Engl J Med **347**(21): 1713-1716.
- Appelros, P., B. Stegmayr, A.Terént (2009). "Sex differences in stroke epidemiology: a systematic review." Stroke **40**(4):1082-90.
- Arthur, P. G., S. C. Lim, B. P. Meloni, S. E. Munns, A. Chan and N. W. Knuckey (2004). "The protective effect of hypoxic preconditioning on cortical neuronal cultures is associated with increases in the activity of several antioxidant enzymes." Brain Res **1017**(1-2): 146-154.
- Ayala, P., M. Uchida, K. Akiyoshi, J. Cheng, J. Hashimoto, T. Jia, O.K. Ronnekleiv, S.J. Murphy, K.M. Wiren, P.D. Hurn (2011). "Androgen receptor overexpression is neuroprotective in experimental stroke." Transl Stroke Res **2**(3):346-57.
- Baldwin, M. A. (2004). "Protein identification by mass spectrometry: issues to be considered." Mol Cell Proteomics **3**(1): 1-9.
- Barabasi, A. L. and Z. N. Oltvai (2004). "Network biology: understanding the cell's functional organization." Nat Rev Genet **5**(2): 101-113.
- Baranova, O., L. F. Miranda, P. Pichiule, I. Dragatsis, R. S. Johnson and J. C. Chavez (2007). "Neuron-specific inactivation of the hypoxia inducible factor 1 alpha increases brain injury in a mouse model of transient focal cerebral ischemia." J Neurosci **27**(23): 6320-6332.
- Barone, F. C., R. F. White, P. A. Spera, J. Ellison, R. W. Currie, X. Wang and G. Z. Feuerstein (1998). "Ischemic preconditioning and brain tolerance: temporal histological and functional outcomes, protein synthesis requirement, and interleukin-1 receptor antagonist and early gene expression." Stroke **29**(9): 1937-1950; discussion 1950-1931.
- Becker, K. J., D. L. Kindrick, M. P. Lester, C. Shea and Z. C. Ye (2005). "Sensitization to brain antigens after stroke is augmented by lipopolysaccharide." J Cereb Blood Flow Metab **25**(12): 1634-1644.
- Bergeron, M., J. M. Gidday, A. Y. Yu, G. L. Semenza, D. M. Ferriero and F. R. Sharp (2000). "Role of hypoxia-inducible factor-1 in hypoxia-induced ischemic tolerance in neonatal rat brain." Ann Neurol **48**(3): 285-296.
- Bernaudin, M., A. S. Nedelec, D. Divoux, E. T. MacKenzie, E. Petit and P. Schumann-Bard (2002). "Normobaric hypoxia induces tolerance to focal permanent cerebral ischemia in association with an increased expression of hypoxia-inducible factor-1 and its target genes, erythropoietin and VEGF, in the adult mouse brain." J Cereb Blood Flow Metab **22**(4): 393-403.
- Bernaudin, M., Y. Tang, M. Reilly, E. Petit and F. R. Sharp (2002). "Brain genomic response following hypoxia and re-oxygenation in the neonatal rat. Identification of genes that might contribute to hypoxia-induced ischemic tolerance." J Biol Chem **277**(42): 39728-39738.
- Boisclair, Y. R., R. P. Rhoads, I. Ueki, J. Wang and G. T. Ooi (2001). "The acid-labile subunit (ALS) of the 150 kDa IGF-binding protein complex: an important but forgotten component of the circulating IGF system." J Endocrinol **170**(1): 63-70.
- Bond, A., D. Lodge, C. A. Hicks, M. A. Ward and M. J. O'Neill (1999). "NMDA receptor antagonism, but not AMPA receptor antagonism attenuates induced ischaemic tolerance in the gerbil hippocampus." Eur J Pharmacol **380**(2-3): 91-99.
- Braeuninger, S., C. Kleinschnitz, B. Nieswandt and G. Stoll (2012). "Focal cerebral ischemia." Methods Mol Biol **788**: 29-42.
- Bristow, A. W., K. S. Webb, A. T. Lubben and J. Halket (2004). "Reproducible product-ion tandem mass spectra on various liquid chromatography/mass spectrometry instruments for the development of spectral libraries." Rapid Commun Mass Spectrom **18**(13): 1447-1454.

- Buchholz, A., J. Hurlebaus, C. Wandrey and R. Takors (2002). "Metabolomics: quantification of intracellular metabolite dynamics." Biomol Eng **19**(1): 5-15.
- Cai, J., Y. Hong, C. Weng, C. Tan, J. Imperato-McGinley, Y.S. Zhu (2011). "Androgen stimulates endothelial cell proliferation via an androgen receptor/VEGF/cyclin A-mediated mechanism." Am J Physiol Heart Circ Physiol **300**(4):1210-21.
- Cappadona, S., P. R. Baker, P. R. Cutillas, A. J. Heck and B. van Breukelen (2012). "Current challenges in software solutions for mass spectrometry-based quantitative proteomics." Amino Acids **43**(3): 1087-1108.
- Carpi, D., M. Korkalainen, L. Airoldi, R. Fanelli, H. Hakansson, V. Muhonen, J. Tuukkanen, M. Viluksela and R. Pastorelli (2009). "Dioxin-sensitive proteins in differentiating osteoblasts: effects on bone formation in vitro." Toxicol Sci **108**(2): 330-343.
- Chelius, D. and P. V. Bondarenko (2002). "Quantitative profiling of proteins in complex mixtures using liquid chromatography and mass spectrometry." J Proteome Res **1**(4): 317-323.
- Cheng, J. and P. D. Hurn (2010). "Sex shapes experimental ischemic brain injury." Steroids **75**(11): 754-759.
- Cheng, J., W. Hu, T.J. Toung, Z. Zhang, S.M. Parker, C.E. Roselli, P.D. Hurn (2009). "Age-dependent effects of testosterone in experimental stroke." J Cereb Blood Flow Metab **29**(3):486-94.
- Cheng, J., N.J. Alkayed, P.D. Hurn (2007). "Deleterious effects of dihydrotestosterone on cerebral ischemic injury." J Cereb Blood Flow Metab **27**(9):1553-62.
- Choy, M., V. Ganesan, D. L. Thomas, J. S. Thornton, E. Proctor, M. D. King, L. van der Weerd, D. G. Gadian and M. F. Lythgoe (2006). "The chronic vascular and haemodynamic response after permanent bilateral common carotid occlusion in newborn and adult rats." J Cereb Blood Flow Metab **26**(8): 1066-1075.
- Cohen, P., D. M. Peehl, G. Lamson and R. G. Rosenfeld (1991). "Insulin-like growth factors (IGFs), IGF receptors, and IGF-binding proteins in primary cultures of prostate epithelial cells." J Clin Endocrinol Metab **73**(2): 401-407.
- Correia, S. C., C. Carvalho, S. Cardoso, R. X. Santos, M. S. Santos, C. R. Oliveira, G. Perry, X. Zhu, M. A. Smith and P. I. Moreira (2010). "Mitochondrial preconditioning: a potential neuroprotective strategy." Front Aging Neurosci **2**.
- Cunha, R. A. (2001). "Adenosine as a neuromodulator and as a homeostatic regulator in the nervous system: different roles, different sources and different receptors." Neurochem Int **38**(2): 107-125.
- Dart, D.A., J. Waxman, E.O. Aboagye, C.L. Bevan (2013). "Visualising androgen receptor activity in male and female mice." PLoS One **8**(8):e71694.
- Dave, K. R., C. Lange-Asschenfeldt, A. P. Raval, R. Prado, R. Busto, I. Saul and M. A. Perez-Pinzon (2005). "Ischemic preconditioning ameliorates excitotoxicity by shifting glutamate/gamma-aminobutyric acid release and biosynthesis." J Neurosci Res **82**(5): 665-673.
- Dave, K. R., I. Saul, R. Busto, M. D. Ginsberg, T. J. Sick and M. A. Perez-Pinzon (2001). "Ischemic preconditioning preserves mitochondrial function after global cerebral ischemia in rat hippocampus." J Cereb Blood Flow Metab **21**(12): 1401-1410.
- De Simoni, M. G., C. Storini, M. Barba, L. Catapano, A. M. Arabia, E. Rossi and L. Bergamaschini (2003). "Neuroprotection by complement (C1) inhibitor in mouse transient brain ischemia." J Cereb Blood Flow Metab **23**(2): 232-239.
- De Smedt, A., R. Brouns, M. Uyttenboogaart, S. De Raedt, M. Moens, N. Wilczak, G. J. Luijckx and J. De Keyser (2011). "Insulin-like growth factor I serum levels influence ischemic stroke outcome." Stroke **42**(8): 2180-2185.
- de Vries, H. E., J. Kuiper, A. G. de Boer, T. J. Van Berkel and D. D. Breimer (1997). "The blood-brain barrier in neuroinflammatory diseases." Pharmacol Rev **49**(2): 143-155.
- del Zoppo, G., I. Ginis, J. M. Hallenbeck, C. Iadecola, X. Wang and G. Z. Feuerstein (2000). "Inflammation and stroke: putative role for cytokines, adhesion molecules and iNOS in brain response to ischemia." Brain Pathol **10**(1): 95-112.

- Dharap, A. and R. Vemuganti (2010). "Ischemic pre-conditioning alters cerebral microRNAs that are upstream to neuroprotective signaling pathways." J Neurochem **113**(6): 1685-1691.
- Dhodda, V. K., K. A. Sailor, K. K. Bowen and R. Vemuganti (2004). "Putative endogenous mediators of preconditioning-induced ischemic tolerance in rat brain identified by genomic and proteomic analysis." J Neurochem **89**(1): 73-89.
- Di Domenico, F., G. Casalena, J. Jia, R. Sultana, E. Barone, J. Cai, W. M. Pierce, C. Cini, C. Mancuso, M. Perluigi, C. M. Davis, N. J. Alkayed and D. A. Butterfield (2012). "Sex differences in brain proteomes of neuron-specific STAT3-null mice after cerebral ischemia/reperfusion." J Neurochem **121**(4): 680-692.
- Dirnagl, U., K. Becker and A. Meisel (2009). "Preconditioning and tolerance against cerebral ischaemia: from experimental strategies to clinical use." Lancet Neurol **8**(4): 398-412.
- Dirnagl, U., C. Iadecola and M. A. Moskowitz (1999). "Pathobiology of ischaemic stroke: an integrated view." Trends Neurosci **22**(9): 391-397.
- Dirnagl, U. and A. Meisel (2008). "Endogenous neuroprotection: mitochondria as gateways to cerebral preconditioning?" Neuropharmacology **55**(3): 334-344.
- Dirnagl, U., R. P. Simon and J. M. Hallenbeck (2003). "Ischemic tolerance and endogenous neuroprotection." Trends Neurosci **26**(5): 248-254.
- Diz, A.P., M. Truebano, D.O. Skibinski (2009). "The consequences of sample pooling in proteomics: an empirical study." Electrophoresis **30**(17):2967-75.
- Domon, B. and R. Aebersold (2006). "Mass spectrometry and protein analysis." Science **312**(5771): 212-217.
- Dorrance, A. M., H. L. Osborn, R. Grekin and R. C. Webb (2001). "Spironolactone reduces cerebral infarct size and EGF-receptor mRNA in stroke-prone rats." Am J Physiol Regul Integr Comp Physiol **281**(3): R944-950.
- Doyle, K. P., R. P. Simon and M. P. Stenzel-Poore (2008). "Mechanisms of ischemic brain damage." Neuropharmacology **55**(3): 310-318.
- Dunn, W. B., N. J. Bailey and H. E. Johnson (2005). "Measuring the metabolome: current analytical technologies." Analyst **130**(5): 606-625.
- Dunn, W.B., I.D. Wilson, A.W. Nicholls, D. Broadhurst (2012). "The importance of experimental design and QC samples in large-scale and MS-driven untargeted metabolomic studies of humans." Bioanalysis **4**(18):2249-64.
- Elias, J. E. and S. P. Gygi (2007). "Target-decoy search strategy for increased confidence in large-scale protein identifications by mass spectrometry." Nat Methods **4**(3): 207-214.
- Fabricius, M., S. Fuhr, R. Bhatia, M. Boutelle, P. Hashemi, A. J. Strong and M. Lauritzen (2006). "Cortical spreading depression and peri-infarct depolarization in acutely injured human cerebral cortex." Brain **129**(Pt 3): 778-790.
- Farkas, E., P. G. Luiten and F. Bari (2007). "Permanent, bilateral common carotid artery occlusion in the rat: a model for chronic cerebral hypoperfusion-related neurodegenerative diseases." Brain Res Rev **54**(1): 162-180.
- Fellows, L. K., M. G. Boutelle and M. Fillenz (1993). "ATP-sensitive potassium channels and local energy demands in the rat hippocampus: an in vivo study." J Neurochem **61**(3): 949-954.
- Fenn, J. B., M. Mann, C. K. Meng, S. F. Wong and C. M. Whitehouse (1989). "Electrospray ionization for mass spectrometry of large biomolecules." Science **246**(4926): 64-71.
- Fernstrom, J. D. (2005). "Branched-chain amino acids and brain function." J Nutr **135**(6 Suppl): 1539S-1546S.
- Fish, R. J. and M. Neerman-Arbez (2012). "Fibrinogen gene regulation." Thromb Haemost **108**(3): 419-426.
- Fitzgibbon, M., Q. Li and M. McIntosh (2008). "Modes of inference for evaluating the confidence of peptide identifications." J Proteome Res **7**(1): 35-39.
- Fridman, E. and E. Pichersky (2005). "Metabolomics, genomics, proteomics, and the identification of enzymes and their substrates and products." Curr Opin Plant Biol **8**(3): 242-248.

- Fu, Y., J. L. Sun, J. F. Ma, X. Geng, J. Sun, J. R. Liu, Y. J. Song and S. D. Chen (2008). "The neuroprotection of prodromal transient ischaemic attack on cerebral infarction." Eur J Neurol **15**(8): 797-801.
- Fukuchi, T., Y. Katayama, T. Kamiya, A. McKee, F. Kashiwagi and A. Terashi (1998). "The effect of duration of cerebral ischemia on brain pyruvate dehydrogenase activity, energy metabolites, and blood flow during reperfusion in gerbil brain." Brain Res **792**(1): 59-65.
- Fukuda, R., H. Zhang, J. W. Kim, L. Shimoda, C. V. Dang and G. L. Semenza (2007). "HIF-1 regulates cytochrome oxidase subunits to optimize efficiency of respiration in hypoxic cells." Cell **129**(1): 111-122.
- Garnier, P., C. Demougeot, N. Bertrand, A. Prigent-Tessier, C. Marie and A. Beley (2001). "Stress response to hypoxia in gerbil brain: HO-1 and Mn SOD expression and glial activation." Brain Res **893**(1-2): 301-309.
- Gesuete, R., F. Orsini, E. R. Zanier, D. Albani, M. A. Deli, G. Bazzoni and M. G. De Simoni (2011). "Glial cells drive preconditioning-induced blood-brain barrier protection." Stroke **42**(5): 1445-1453.
- Gesuete, R., A. E. Packard, K. B. Vartanian, V. K. Conrad, S. L. Stevens, F. R. Bahjat, T. Yang and M. P. Stenzel-Poore (2012). "Poly-ICLC preconditioning protects the blood-brain barrier against ischemic injury in vitro through type I interferon signaling." J Neurochem **123 Suppl 2**: 75-85.
- Gevaert, K. and J. Vandekerckhove (2000). "Protein identification methods in proteomics." Electrophoresis **21**(6): 1145-1154.
- Gidday, J. M. (2006). "Cerebral preconditioning and ischaemic tolerance." Nat Rev Neurosci **7**(6): 437-448.
- Glantz, L., A. Avramovich, V. Trembovler, V. Gurvitz, R. Kohen, L. A. Eidelman and E. Shohami (2005). "Ischemic preconditioning increases antioxidants in the brain and peripheral organs after cerebral ischemia." Exp Neurol **192**(1): 117-124.
- Gong, C., Z. Qin, A. L. Betz, X. H. Liu and G. Y. Yang (1998). "Cellular localization of tumor necrosis factor alpha following focal cerebral ischemia in mice." Brain Res **801**(1-2): 1-8.
- Gorg, A., C. Obermaier, G. Boguth, A. Harder, B. Scheibe, R. Wildgruber and W. Weiss (2000). "The current state of two-dimensional electrophoresis with immobilized pH gradients." Electrophoresis **21**(6): 1037-1053.
- Grabb, M. C. and D. W. Choi (1999). "Ischemic tolerance in murine cortical cell culture: critical role for NMDA receptors." J Neurosci **19**(5): 1657-1662.
- Green, D. R. and J. C. Reed (1998). "Mitochondria and apoptosis." Science **281**(5381): 1309-1312.
- Greenberg, D. A. and K. Jin (2005). "From angiogenesis to neuropathology." Nature **438**(7070): 954-959.
- Guerrera, I. C. and O. Kleiner (2005). "Application of mass spectrometry in proteomics." Biosci Rep **25**(1-2): 71-93.
- Guerrero, C., C. Tagwerker, P. Kaiser and L. Huang (2006). "An integrated mass spectrometry-based proteomic approach: quantitative analysis of tandem affinity-purified in vivo cross-linked protein complexes (QTAX) to decipher the 26 S proteasome-interacting network." Mol Cell Proteomics **5**(2): 366-378.
- Gygi, S. P., B. Rist, S. A. Gerber, F. Turecek, M. H. Gelb and R. Aebersold (1999). "Quantitative analysis of complex protein mixtures using isotope-coded affinity tags." Nat Biotechnol **17**(10): 994-999.
- Hansen, K. C., G. Schmitt-Ulms, R. J. Chalkley, J. Hirsch, M. A. Baldwin and A. L. Burlingame (2003). "Mass spectrometric analysis of protein mixtures at low levels using cleavable 13C-isotope-coded affinity tag and multidimensional chromatography." Mol Cell Proteomics **2**(5): 299-314.
- Hashiguchi, A., S. Yano, M. Morioka, J. Hamada, Y. Ushio, Y. Takeuchi and K. Fukunaga (2004). "Up-regulation of endothelial nitric oxide synthase via phosphatidylinositol 3-kinase pathway contributes to ischemic tolerance in the CA1 subfield of gerbil hippocampus." J Cereb Blood Flow Metab **24**(3): 271-279.

- Hawkins, B. T. and T. P. Davis (2005). "The blood-brain barrier/neurovascular unit in health and disease." Pharmacol Rev **57**(2): 173-185.
- Hay, R. T. (2005). "SUMO: a history of modification." Mol Cell **18**(1): 1-12.
- Hayashi, T., A. Saito, S. Okuno, M. Ferrand-Drake and P. H. Chan (2003). "Induction of GRP78 by ischemic preconditioning reduces endoplasmic reticulum stress and prevents delayed neuronal cell death." J Cereb Blood Flow Metab **23**(8): 949-961.
- Healthcare, G., Ed. (1998). 2DE electrophoresis, Principles & Methods.
- Heijne, W. H., A. S. Kienhuis, B. van Ommen, R. H. Stierum and J. P. Groten (2005). "Systems toxicology: applications of toxicogenomics, transcriptomics, proteomics and metabolomics in toxicology." Expert Rev Proteomics **2**(5): 767-780.
- Heil, M. and W. Schaper (2005). "Arteriogenic growth factors, chemokines and proteases as a prerequisite for arteriogenesis." Drug News Perspect **18**(5): 317-322.
- Heinlein, C.A., C.Chang (2002). "The roles of androgen receptors and androgen-binding proteins in nongenomic androgen actions." Mol Endocrinol **16**(10):2181-7.
- Helton, R., J. Cui, J. R. Scheel, J. A. Ellison, C. Ames, C. Gibson, B. Blouw, L. Ouyang, I. Dragatsis, S. Zeitlin, R. S. Johnson, S. A. Lipton and C. Barlow (2005). "Brain-specific knock-out of hypoxia-inducible factor-1alpha reduces rather than increases hypoxic-ischemic damage." J Neurosci **25**(16): 4099-4107.
- Heurteaux, C., I. Lauritzen, C. Widmann and M. Lazdunski (1995). "Essential role of adenosine, adenosine A1 receptors, and ATP-sensitive K+ channels in cerebral ischemic preconditioning." Proc Natl Acad Sci U S A **92**(10): 4666-4670.
- Hoehenwarter, W. and S. Wienkoop (2010). "Spectral counting robust on high mass accuracy mass spectrometers." Rapid Commun Mass Spectrom **24**(24): 3609-3614.
- Hoshi, A., T. Nakahara, H. Kayama and T. Yamamoto (2006). "Ischemic tolerance in chemical preconditioning: possible role of astrocytic glutamine synthetase buffering glutamate-mediated neurotoxicity." J Neurosci Res **84**(1): 130-141.
- http://www.thermo.com/eThermo/CMA/PDFs/Various/File_26638.pdf.
- https://portal.genego.com/help/MetaCore_Advanced_Training_Manual_5.0.pdf.
- Hu, Q., R. J. Noll, H. Li, A. Makarov, M. Hardman and R. Graham Cooks (2005). "The Orbitrap: a new mass spectrometer." J Mass Spectrom **40**(4): 430-443.
- Hua, F., J. Ma, T. Ha, J. Kelley, D. L. Williams, R. L. Kao, J. H. Kalbfleisch, I. W. Browder and C. Li (2008). "Preconditioning with a TLR2 specific ligand increases resistance to cerebral ischemia/reperfusion injury." J Neuroimmunol **199**(1-2): 75-82.
- Huang da, W., B. T. Sherman and R. A. Lempicki (2009). "Systematic and integrative analysis of large gene lists using DAVID bioinformatics resources." Nat Protoc **4**(1): 44-57.
- Huang, J., U. M. Upadhyay and R. J. Tamargo (2006). "Inflammation in stroke and focal cerebral ischemia." Surg Neurol **66**(3): 232-245.
- Hussain, R., A.M. Ghoumari, B. Bielecki, J. Steibel, N. Boehm, P. Liere, W.B. Macklin, N. Kumar, R. Habert, S. Mhaouty-Kodja, F. Tronche, R. Sitruk-Ware, M. Schumacher, M.S. Ghandour (2013). "The neural androgen receptor: a therapeutic target for myelin repair in chronic demyelination." Brain **136**:132-46.
- Hutson, S. M., E. Lieth and K. F. LaNoue (2001). "Function of leucine in excitatory neurotransmitter metabolism in the central nervous system." J Nutr **131**(3): 846S-850S.
- Ishihama, Y., Y. Oda, T. Tabata, T. Sato, T. Nagasu, J. Rappsilber and M. Mann (2005). "Exponentially modified protein abundance index (emPAI) for estimation of absolute protein amount in proteomics by the number of sequenced peptides per protein." Mol Cell Proteomics **4**(9): 1265-1272.
- Ishizuka, Y., N. Kakiya, H. Nawa and N. Takei (2008). "Leucine induces phosphorylation and activation of p70S6K in cortical neurons via the system L amino acid transporter." J Neurochem **106**(2): 934-942.

- Iwamura, M., P. M. Sluss, J. B. Casamento and A. T. Cockett (1993). "Insulin-like growth factor I: action and receptor characterization in human prostate cancer cell lines." Prostate **22**(3): 243-252.
- Izumi, K., Y. Zheng, Y. Li, J. Zaengle and H. Miyamoto (2012). "Epidermal growth factor induces bladder cancer cell proliferation through activation of the androgen receptor." Int J Oncol **41**(5): 1587-1592.
- Janoff, A. (1964). "Alterations in lysosomes (intracellular enzymes) during shock; effects of preconditioning (tolerance) and protective drugs." Int Anesthesiol Clin **2**: 251-269.
- Jansen, R., G. Lachatre and P. Marquet (2005). "LC-MS/MS systematic toxicological analysis: comparison of MS/MS spectra obtained with different instruments and settings." Clin Biochem **38**(4): 362-372.
- Jones, L. L., D. A. McDonald and P. R. Borum (2010). "Acylcarnitines: role in brain." Prog Lipid Res **49**(1): 61-75.
- Jung, J. E., G. S. Kim and P. H. Chan (2011). "Neuroprotection by interleukin-6 is mediated by signal transducer and activator of transcription 3 and antioxidative signaling in ischemic stroke." Stroke **42**(12): 3574-3579.
- Kariko, K., D. Weissman and F. A. Welsh (2004). "Inhibition of toll-like receptor and cytokine signaling--a unifying theme in ischemic tolerance." J Cereb Blood Flow Metab **24**(11): 1288-1304.
- Karp, N.A., K.S.Lilley (2009) "Investigating sample pooling strategies for DIGE experiments to address biological variability." Proteomics **9**(2):388-97.
- Kasinski, A., C. B. Doering and D. J. Danner (2004). "Leucine toxicity in a neuronal cell model with inhibited branched chain amino acid catabolism." Brain Res Mol Brain Res **122**(2): 180-187.
- Kell, D. B. (2005). "Metabolomics, machine learning and modelling: towards an understanding of the language of cells." Biochem Soc Trans **33**(Pt 3): 520-524.
- Keller, A., S. Purvine, A. I. Nesvizhskii, S. Stolyar, D. R. Goodlett and E. Kolker (2002). "Experimental protein mixture for validating tandem mass spectral analysis." OMICS **6**(2): 207-212.
- Kendziorski, C., R.A. Irizarry, K.S. Chen, J.D. Haag, M.N.Gould (2005). "On the utility of pooling biological samples in microarray experiments." Proc Natl Acad Sci U S A **102**(12):4252-7.
- Kerr, J. F., A. H. Wyllie and A. R. Currie (1972). "Apoptosis: a basic biological phenomenon with wide-ranging implications in tissue kinetics." Br J Cancer **26**(4): 239-257.
- Keun, H. C. (2006). "Metabonomic modeling of drug toxicity." Pharmacol Ther **109**(1-2): 92-106.
- Kilic, U., E. Kilic, C. M. Matter, C. L. Bassetti and D. M. Hermann (2008). "TLR-4 deficiency protects against focal cerebral ischemia and axotomy-induced neurodegeneration." Neurobiol Dis **31**(1): 33-40.
- Kimberly, W. T., Y. Wang, L. Pham, K. L. Furie and R. E. Gerszten (2013). "Metabolite profiling identifies a branched chain amino acid signature in acute cardioembolic stroke." Stroke **44**(5): 1389-1395.
- Kind, T. and O. Fiehn (2006). "Metabolomic database annotations via query of elemental compositions: mass accuracy is insufficient even at less than 1 ppm." BMC Bioinformatics **7**: 234.
- Kirino, T. (2002). "Ischemic tolerance." J Cereb Blood Flow Metab **22**(11): 1283-1296.
- Kirino, T., Y. Tsujita and A. Tamura (1991). "Induced tolerance to ischemia in gerbil hippocampal neurons." J Cereb Blood Flow Metab **11**(2): 299-307.
- Kitagawa, K., M. Matsumoto, K. Kuwabara, M. Tagaya, T. Ohtsuki, R. Hata, H. Ueda, N. Handa, K. Kimura and T. Kamada (1991). "'Ischemic tolerance' phenomenon detected in various brain regions." Brain Res **561**(2): 203-211.
- Kitagawa, K., M. Matsumoto, M. Tagaya, R. Hata, H. Ueda, M. Niinobe, N. Handa, R. Fukunaga, K. Kimura, K. Mikoshiba and et al. (1990). "'Ischemic tolerance' phenomenon found in the brain." Brain Res **528**(1): 21-24.
- Klose, J. (1975). "Protein mapping by combined isoelectric focusing and electrophoresis of mouse tissues. A novel approach to testing for induced point mutations in mammals." Humangenetik **26**(3): 231-243.

- Kooijman, R., S. Sarre, Y. Michotte and J. De Keyser (2009). "Insulin-like growth factor I: a potential neuroprotective compound for the treatment of acute ischemic stroke?" Stroke **40**(4): e83-88.
- Kuhner, S. and A. C. Gavin (2007). Towards quantitative analysis of proteome dynamics. Nat Biotechnol. United States. **25:** 298-300.
- Laghi Pasini, F., F. Guideri, E. Picano, G. Parenti, C. Petersen, A. Varga and T. Di Perri (2000). "Increase in plasma adenosine during brain ischemia in man: a study during transient ischemic attacks, and stroke." Brain Res Bull **51**(4): 327-330.
- Latour, L. L., D. W. Kang, M. A. Ezzeddine, J. A. Chalela and S. Warach (2004). "Early blood-brain barrier disruption in human focal brain ischemia." Ann Neurol **56**(4): 468-477.
- Lee, A., B. E. Lingwood, S. T. Bjorkman, S. M. Miller, P. Poronnik, N. L. Barnett, P. Colditz and D. V. Pow (2010). "Rapid loss of glutamine synthetase from astrocytes in response to hypoxia: implications for excitotoxicity." J Chem Neuroanat **39**(3): 211-220.
- Lee, Y. J., P. Castri, J. Bembry, D. Maric, S. Auh and J. M. Hallenbeck (2009). "SUMOylation participates in induction of ischemic tolerance." J Neurochem **109**(1): 257-267.
- Lee, Y. J., S. Miyake, H. Wakita, D. C. McMullen, Y. Azuma, S. Auh and J. M. Hallenbeck (2007). "Protein SUMOylation is massively increased in hibernation torpor and is critical for the cytoprotection provided by ischemic preconditioning and hypothermia in SHSY5Y cells." J Cereb Blood Flow Metab **27**(5): 950-962.
- Lehnardt, S., S. Lehmann, D. Kaul, K. Tschimmel, O. Hoffmann, S. Cho, C. Krueger, R. Nitsch, A. Meisel and J. R. Weber (2007). "Toll-like receptor 2 mediates CNS injury in focal cerebral ischemia." J Neuroimmunol **190**(1-2): 28-33.
- Li, W., Y. Luo, F. Zhang, A. P. Signore, G. T. Gobbel, R. P. Simon and J. Chen (2006). "Ischemic preconditioning in the rat brain enhances the repair of endogenous oxidative DNA damage by activating the base-excision repair pathway." J Cereb Blood Flow Metab **26**(2): 181-198.
- Liesz, A., E. Suri-Payer, C. Veltkamp, H. Doerr, C. Sommer, S. Rivest, T. Giese and R. Veltkamp (2009). "Regulatory T cells are key cerebroprotective immunomodulators in acute experimental stroke." Nat Med **15**(2): 192-199.
- Lin, H., J. P. Lu, P. Laflamme, S. Qiao, B. Shayegan, I. Bryskin, L. Monardo, B. C. Wilson, G. Singh and J. H. Pinthus (2010). "Inter-related in vitro effects of androgens, fatty acids and oxidative stress in prostate cancer: a mechanistic model supporting prevention strategies." Int J Oncol **37**(4): 761-766.
- Liu, H., R. G. Sadygov and J. R. Yates, 3rd (2004). "A model for random sampling and estimation of relative protein abundance in shotgun proteomics." Anal Chem **76**(14): 4193-4201.
- Lloyd-Jones, D., R. J. Adams, T. M. Brown, M. Carnethon, S. Dai, G. De Simone, T. B. Ferguson, E. Ford, K. Furie, C. Gillespie, A. Go, K. Greenlund, N. Haase, S. Hailpern, P. M. Ho, V. Howard, B. Kissela, S. Kittner, D. Lackland, L. Lisabeth, A. Marelli, M. M. McDermott, J. Meigs, D. Mozaffarian, M. Mussolino, G. Nichol, V. L. Roger, W. Rosamond, R. Sacco, P. Sorlie, T. Thom, S. Wasserthiel-Smoller, N. D. Wong and J. Wylie-Rosett (2010). "Heart disease and stroke statistics--2010 update: a report from the American Heart Association." Circulation **121**(7): e46-e215.
- Lu, G. W., S. Yu, R. H. Li, X. Y. Cui and C. Y. Gao (2005). "Hypoxic preconditioning: a novel intrinsic cytoprotective strategy." Mol Neurobiol **31**(1-3): 255-271.
- Lu, P., C. Vogel, R. Wang, X. Yao and E. M. Marcotte (2007). "Absolute protein expression profiling estimates the relative contributions of transcriptional and translational regulation." Nat Biotechnol **25**(1): 117-124.
- Lu, S., Z. Tan, M. Wortman, S. Lu and Z. Dong (2010). "Regulation of heat shock protein 70-1 expression by androgen receptor and its signaling in human prostate cancer cells." Int J Oncol **36**(2): 459-467.
- Makarov, A. (2000). "Electrostatic axially harmonic orbital trapping: a high-performance technique of mass analysis." Anal Chem **72**(6): 1156-1162.
- Manwani, B. and L. D. McCullough (2013). "Function of the master energy regulator adenosine monophosphate-activated protein kinase in stroke." J Neurosci Res.
- March, R. E. (2009). "Quadrupole ion traps." Mass Spectrom Rev **28**(6): 961-989.

- Martin, E., R. E. Rosenthal and G. Fiskum (2005). "Pyruvate dehydrogenase complex: metabolic link to ischemic brain injury and target of oxidative stress." J Neurosci Res **79**(1-2): 240-247.
- Masada, T., Y. Hua, G. Xi, S. R. Ennis and R. F. Keep (2001). "Attenuation of ischemic brain edema and cerebrovascular injury after ischemic preconditioning in the rat." J Cereb Blood Flow Metab **21**(1): 22-33.
- Matsuki, A., T. Nozawa, A. Igawa, N. Igarashi, T. Nakadate, N. Fujii and H. Inoue (2009). "Ischemic preconditioning accelerates the fatty acid oxidation of rat hearts." Int J Cardiol **132**(3): 405-410.
- Meehan, K. L. and M. D. Sadar (2003). "Androgens and androgen receptor in prostate and ovarian malignancies." Front Biosci **8**: d780-800.
- Meller, R., S. J. Thompson, T. A. Lusardi, A. N. Ordonez, M. D. Ashley, V. Jessick, W. Wang, D. J. Torrey, D. C. Henshall, P. R. Gafken, J. A. Saugstad, Z. G. Xiong and R. P. Simon (2008). "Ubiquitin proteasome-mediated synaptic reorganization: a novel mechanism underlying rapid ischemic tolerance." J Neurosci **28**(1): 50-59.
- Millea, K. M., I. S. Krull, S. A. Cohen, J. C. Gebler and S. J. Berger (2006). "Integration of multidimensional chromatographic protein separations with a combined "top-down" and "bottom-up" proteomic strategy." J Proteome Res **5**(1): 135-146.
- Miller, A., O. Lider and H. L. Weiner (1991). "Antigen-driven bystander suppression after oral administration of antigens." J Exp Med **174**(4): 791-798.
- Mitchell, L., F. Piovella, F. Ofosu and M. Andrew (1991). "Alpha-2-macroglobulin may provide protection from thromboembolic events in antithrombin III-deficient children." Blood **78**(9): 2299-2304.
- Moncayo, J., G. R. de Freitas, J. Bogousslavsky, M. Altieri and G. van Melle (2000). "Do transient ischemic attacks have a neuroprotective effect?" Neurology **54**(11): 2089-2094.
- Murry, C. E., R. B. Jennings and K. A. Reimer (1986). "Preconditioning with ischemia: a delay of lethal cell injury in ischemic myocardium." Circulation **74**(5): 1124-1136.
- Namura, S., J. Zhu, K. Fink, M. Endres, A. Srinivasan, K. J. Tomaselli, J. Yuan and M. A. Moskowitz (1998). "Activation and cleavage of caspase-3 in apoptosis induced by experimental cerebral ischemia." J Neurosci **18**(10): 3659-3668.
- Nawashiro, H., D. Martin and J. M. Hallenbeck (1997). "Neuroprotective effects of TNF binding protein in focal cerebral ischemia." Brain Res **778**(2): 265-271.
- Nesvizhskii, A. I., A. Keller, E. Kolker and R. Aebersold (2003). "A statistical model for identifying proteins by tandem mass spectrometry." Anal Chem **75**(17): 4646-4658.
- Nordstrom, A., E. Want, T. Northen, J. Lehtio and G. Siuzdak (2008). "Multiple ionization mass spectrometry strategy used to reveal the complexity of metabolomics." Anal Chem **80**(2): 421-429.
- O'Farrell, P. H. (1975). "High resolution two-dimensional electrophoresis of proteins." J Biol Chem **250**(10): 4007-4021.
- Obrenovitch, T. P. (2008). "Molecular physiology of preconditioning-induced brain tolerance to ischemia." Physiol Rev **88**(1): 211-247.
- Offner, H., S. Subramanian, S. M. Parker, C. Wang, M. E. Afentoulis, A. Lewis, A. A. Vandenbark and P. D. Hurn (2006). "Splenic atrophy in experimental stroke is accompanied by increased regulatory T cells and circulating macrophages." J Immunol **176**(11): 6523-6531.
- Ohtaki, H., T. Fujimoto, T. Sato, K. Kishimoto, M. Fujimoto, M. Moriya and S. Shioda (2006). "Progressive expression of vascular endothelial growth factor (VEGF) and angiogenesis after chronic ischemic hypoperfusion in rat." Acta Neurochir Suppl **96**: 283-287.
- Old, W. M., K. Meyer-Arendt, L. Aveline-Wolf, K. G. Pierce, A. Mendoza, J. R. Sevinsky, K. A. Resing and N. G. Ahn (2005). "Comparison of label-free methods for quantifying human proteins by shotgun proteomics." Mol Cell Proteomics **4**(10): 1487-1502.
- Oliva, A. A., Jr., Y. Kang, J. Sanchez-Molano, C. Furones and C. M. Atkins (2012). "STAT3 signaling after traumatic brain injury." J Neurochem **120**(5): 710-720.
- Oliver, S. G., M. K. Winson, D. B. Kell and F. Baganz (1998). "Systematic functional analysis of the yeast genome." Trends Biotechnol **16**(9): 373-378.

- Olsson, I., K. Larsson, R. Palmgren and B. Bjellqvist (2002). "Organic disulfides as a means to generate streak-free two-dimensional maps with narrow range basic immobilized pH gradient strips as first dimension." Proteomics **2**(11): 1630-1632.
- Omenn, G. S., D. J. States, M. Adamski, T. W. Blackwell, R. Menon, H. Hermjakob, R. Apweiler, B. B. Haab, R. J. Simpson, J. S. Eddes, E. A. Kapp, R. L. Moritz, D. W. Chan, A. J. Rai, A. Admon, R. Aebersold, J. Eng, W. S. Hancock, S. A. Hefta, H. Meyer, Y. K. Paik, J. S. Yoo, P. Ping, J. Pounds, J. Adkins, X. Qian, R. Wang, V. Wasinger, C. Y. Wu, X. Zhao, R. Zeng, A. Archakov, A. Tsugita, I. Beer, A. Pandey, M. Pisano, P. Andrews, H. Tammen, D. W. Speicher and S. M. Hanash (2005). "Overview of the HUPO Plasma Proteome Project: results from the pilot phase with 35 collaborating laboratories and multiple analytical groups, generating a core dataset of 3020 proteins and a publicly-available database." Proteomics **5**(13): 3226-3245.
- Ong, S. E., B. Blagoev, I. Kratchmarova, D. B. Kristensen, H. Steen, A. Pandey and M. Mann (2002). "Stable isotope labeling by amino acids in cell culture, SILAC, as a simple and accurate approach to expression proteomics." Mol Cell Proteomics **1**(5): 376-386.
- Ong, S. E., L. J. Foster and M. Mann (2003). "Mass spectrometric-based approaches in quantitative proteomics." Methods **29**(2): 124-130.
- Otori, T., T. Katsumata, H. Muramatsu, F. Kashiwagi, Y. Katayama and A. Terashi (2003). "Long-term measurement of cerebral blood flow and metabolism in a rat chronic hypoperfusion model." Clin Exp Pharmacol Physiol **30**(4): 266-272.
- Ottens, A. K., L. Bustamante, E. C. Golden, C. Yao, R. L. Hayes, K. K. Wang, F. C. Tortella and J. R. Dave (2010). "Neuroproteomics: a biochemical means to discriminate the extent and modality of brain injury." J Neurotrauma **27**(10): 1837-1852.
- Ow, S. Y., M. Salim, J. Noirel, C. Evans, I. Rehman and P. C. Wright (2009). "iTRAQ underestimation in simple and complex mixtures: "the good, the bad and the ugly"." J Proteome Res **8**(11): 5347-5355.
- Papadakis, M., G. Hadley, M. Xilouri, L. C. Hoyte, S. Nagel, M. M. McMenamin, G. Tsaknakis, S. M. Watt, C. W. Drakesmith, R. Chen, M. J. Wood, Z. Zhao, B. Kessler, K. Vekrellis and A. M. Buchan (2013). "Tsc1 (hamartin) confers neuroprotection against ischemia by inducing autophagy." Nat Med **19**(3): 351-357.
- Paschen, W. and G. Mies (1999). "Effect of induced tolerance on biochemical disturbances in hippocampal slices from the gerbil during and after oxygen/glucose deprivation." Neuroreport **10**(7): 1417-1421.
- Patel, V. J., K. Thalassinos, S. E. Slade, J. B. Connolly, A. Crombie, J. C. Murrell and J. H. Scrivens (2009). "A comparison of labeling and label-free mass spectrometry-based proteomics approaches." J Proteome Res **8**(7): 3752-3759.
- Patti, G. J., O. Yanes and G. Siuzdak (2012). "Innovation: Metabolomics: the apogee of the omics trilogy." Nat Rev Mol Cell Biol **13**(4): 263-269.
- Patton, W. F. (2002). "Detection technologies in proteome analysis." J Chromatogr B Analyt Technol Biomed Life Sci **771**(1-2): 3-31.
- Peng, L., L. Gu, H. Zhang, X. Huang, E. Hertz and L. Hertz (2007). "Glutamine as an energy substrate in cultured neurons during glucose deprivation." J Neurosci Res **85**(15): 3480-3486.
- Perez-Pinzon, M. A. and J. G. Born (1999). "Rapid preconditioning neuroprotection following anoxia in hippocampal slices: role of the K+ ATP channel and protein kinase C." Neuroscience **89**(2): 453-459.
- Perez-Pinzon, M. A., G. P. Xu, W. D. Dietrich, M. Rosenthal and T. J. Sick (1997). "Rapid preconditioning protects rats against ischemic neuronal damage after 3 but not 7 days of reperfusion following global cerebral ischemia." J Cereb Blood Flow Metab **17**(2): 175-182.
- Pietrzkowski, Z., G. Mulholland, L. Gomella, B. A. Jameson, D. Wernicke and R. Baserga (1993). "Inhibition of growth of prostatic cancer cell lines by peptide analogues of insulin-like growth factor 1." Cancer Res **53**(5): 1102-1106.

- Pignataro, G., D. Capone, G. Polichetti, A. Vinciguerra, A. Gentile, G. Di Renzo and L. Annunziato (2011). "Neuroprotective, immunosuppressant and antineoplastic properties of mTOR inhibitors: current and emerging therapeutic options." Curr Opin Pharmacol **11**(4): 378-394.
- Rappsilber, J., U. Ryder, A. I. Lamond and M. Mann (2002). "Large-scale proteomic analysis of the human spliceosome." Genome Res **12**(8): 1231-1245.
- Relton, J. K., D. Martin, R. C. Thompson and D. A. Russell (1996). "Peripheral administration of Interleukin-1 Receptor antagonist inhibits brain damage after focal cerebral ischemia in the rat." Exp Neurol **138**(2): 206-213.
- Roepstorff, P. and J. Fohlman (1984). "Proposal for a common nomenclature for sequence ions in mass spectra of peptides." Biomed Mass Spectrom **11**(11): 601.
- Ross, P. L., Y. N. Huang, J. N. Marchese, B. Williamson, K. Parker, S. Hattan, N. Khainovski, S. Pillai, S. Dey, S. Daniels, S. Purkayastha, P. Juhasz, S. Martin, M. Bartlet-Jones, F. He, A. Jacobson and D. J. Pappin (2004). "Multiplexed protein quantitation in Saccharomyces cerevisiae using amine-reactive isobaric tagging reagents." Mol Cell Proteomics **3**(12): 1154-1169.
- Rudolphi, K. A., P. Schubert, F. E. Parkinson and B. B. Fredholm (1992). "Adenosine and brain ischemia." Cerebrovasc Brain Metab Rev **4**(4): 346-369.
- Ruscher, K., N. Isaev, G. Trendelenburg, M. Weih, L. Iurato, A. Meisel and U. Dirnagl (1998). "Induction of hypoxia inducible factor 1 by oxygen glucose deprivation is attenuated by hypoxic preconditioning in rat cultured neurons." Neurosci Lett **254**(2): 117-120.
- Sadygov, R. G., D. Cociorva and J. R. Yates, 3rd (2004). "Large-scale database searching using tandem mass spectra: looking up the answer in the back of the book." Nat Methods **1**(3): 195-202.
- Santoni, V., M. Molloy and T. Rabilloud (2000). "Membrane proteins and proteomics: un amour impossible?" Electrophoresis **21**(6): 1054-1070.
- Sarwar, M., S. Sandberg, P. A. Abrahamsson and J. L. Persson (2013). "Protein kinase A (PKA) pathway is functionally linked to androgen receptor (AR) in the progression of prostate cancer." Urol Oncol.
- Saugstad, J. A. (2010). "MicroRNAs as effectors of brain function with roles in ischemia and injury, neuroprotection, and neurodegeneration." J Cereb Blood Flow Metab **30**(9): 1564-1576.
- Schaller, B. (2005). "Ischemic preconditioning as induction of ischemic tolerance after transient ischemic attacks in human brain: its clinical relevance." Neurosci Lett **377**(3): 206-211.
- Schaller, J. and S. S. Gerber (2011). "The plasmin-antiplasmin system: structural and functional aspects." Cell Mol Life Sci **68**(5): 785-801.
- Scheler, C., S. Lamer, Z. Pan, X. P. Li, J. Salnikow and P. Jungblut (1998). "Peptide mass fingerprint sequence coverage from differently stained proteins on two-dimensional electrophoresis patterns by matrix assisted laser desorption/ionization-mass spectrometry (MALDI-MS)." Electrophoresis **19**(6): 918-927.
- Schenk, S., G. J. Schoenhals, G. de Souza and M. Mann (2008). "A high confidence, manually validated human blood plasma protein reference set." BMC Med Genomics **1**: 41.
- Schroeter, M., S. Jander, O. W. Witte and G. Stoll (1994). "Local immune responses in the rat cerebral cortex after middle cerebral artery occlusion." J Neuroimmunol **55**(2): 195-203.
- Schurr, A. (2006). "Lactate: the ultimate cerebral oxidative energy substrate?" J Cereb Blood Flow Metab **26**(1): 142-152.
- Schurr, A., K. H. Reid, M. T. Tseng, C. West and B. M. Rigor (1986). "Adaptation of adult brain tissue to anoxia and hypoxia in vitro." Brain Res **374**(2): 244-248.
- Schwanhausser, B., D. Busse, N. Li, G. Dittmar, J. Schuchhardt, J. Wolf, W. Chen and M. Selbach (2011). "Global quantification of mammalian gene expression control." Nature **473**(7347): 337-342.
- Schwartz, J. C., M. W. Senko and J. E. Syka (2002). "A two-dimensional quadrupole ion trap mass spectrometer." J Am Soc Mass Spectrom **13**(6): 659-669.
- Shen, H. Y., T. A. Lusardi, R. L. Williams-Karnesky, J. Q. Lan, D. J. Poulsen and D. Boison (2011). "Adenosine kinase determines the degree of brain injury after ischemic stroke in mice." J Cereb Blood Flow Metab **31**(7): 1648-1659.

- Sheng, R., L. S. Zhang, R. Han, X. Q. Liu, B. Gao and Z. H. Qin (2010). "Autophagy activation is associated with neuroprotection in a rat model of focal cerebral ischemic preconditioning." Autophagy **6**(4): 482-494.
- Shenhar-Tsarfaty, S., E. Ben Assayag, I. Bova, L. Shopin, M. Cohen, S. Berliner, I. Shapira and N. M. Bornstein (2008). "Persistent hyperfibrinogenemia in acute ischemic stroke / transient ischemic attack (TIA)." Thromb Haemost **99**(1): 169-173.
- Shimazaki, K., T. Nakamura, K. Nakamura, K. Oguro, T. Masuzawa, Y. Kudo and N. Kawai (1998). "Reduced calcium elevation in hippocampal CA1 neurons of ischemia-tolerant gerbils." Neuroreport **9**(8): 1875-1878.
- Silva, J. C., R. Denny, C. Dorschel, M. V. Gorenstein, G. Z. Li, K. Richardson, D. Wall and S. J. Geromanos (2006). "Simultaneous qualitative and quantitative analysis of the Escherichia coli proteome: a sweet tale." Mol Cell Proteomics **5**(4): 589-607.
- Sommer, C. (2009). "Neuronal plasticity after ischemic preconditioning and TIA-like preconditioning ischemic periods." Acta Neuropathol **117**(5): 511-523.
- Stapels, M., C. Piper, T. Yang, M. Li, C. Stowell, Z. G. Xiong, J. Saugstad, R. P. Simon, S. Geromanos, J. Langridge, J. Q. Lan and A. Zhou (2010). "Polycomb group proteins as epigenetic mediators of neuroprotection in ischemic tolerance." Sci Signal **3**(111): ra15.
- Steen, H. and M. Mann (2004). "The ABC's (and XYZ's) of peptide sequencing." Nat Rev Mol Cell Biol **5**(9): 699-711.
- Stenzel-Poore, M. P., S. L. Stevens, J. S. King and R. P. Simon (2007). "Preconditioning reprograms the response to ischemic injury and primes the emergence of unique endogenous neuroprotective phenotypes: a speculative synthesis." Stroke **38**(2 Suppl): 680-685.
- Stenzel-Poore, M. P., S. L. Stevens, Z. Xiong, N. S. Lessov, C. A. Harrington, M. Mori, R. Meller, H. L. Rosenzweig, E. Tobar, T. E. Shaw, X. Chu and R. P. Simon (2003). "Effect of ischaemic preconditioning on genomic response to cerebral ischaemia: similarity to neuroprotective strategies in hibernation and hypoxia-tolerant states." Lancet **362**(9389): 1028-1037.
- Stetler, R. A., F. Zhang, C. Liu and J. Chen (2009). "Ischemic tolerance as an active and intrinsic neuroprotective mechanism." Handb Clin Neurol **92**: 171-195.
- Stevens, S. L., T. M. Ciesielski, B. J. Marsh, T. Yang, D. S. Homen, J. L. Boule, N. S. Lessov, R. P. Simon and M. P. Stenzel-Poore (2008). "Toll-like receptor 9: a new target of ischemic preconditioning in the brain." J Cereb Blood Flow Metab **28**(5): 1040-1047.
- Stevens, S. L. and M. P. Stenzel-Poore (2006). "Toll-like receptors and tolerance to ischaemic injury in the brain." Biochem Soc Trans **34**(Pt 6): 1352-1355.
- Stoll, G., C. Kleinschnitz and B. Nieswandt (2008). "Molecular mechanisms of thrombus formation in ischemic stroke: novel insights and targets for treatment." Blood **112**(9): 3555-3562.
- Sumner, L.W., A. Amberg, D. Barrett, M.H. Beale, R. Beger, C.A. Daykin, T.W. Fan, O. Fiehn, R. Goodacre, J.L. Griffin, T. Hankemeier, N. Hardy, J. Harnly, R. Higashi, J. Kopka, A.N. Lane, J.C. Lindon, P. Marriott, A.W. Nicholls, M.D. Reily, J.J. Thaden, M.R.Viant (2007). "Proposed minimum reporting standards for chemical analysis Chemical Analysis Working Group (CAWG) Metabolomics Standards Initiative (MSI)." Metabolomics **3**(3):211-221.
- Tang, S. C., T. V. Arumugam, X. Xu, A. Cheng, M. R. Mughal, D. G. Jo, J. D. Lathia, D. A. Siler, S. Chigurupati, X. Ouyang, T. Magnus, S. Camandola and M. P. Mattson (2007). "Pivotal role for neuronal Toll-like receptors in ischemic brain injury and functional deficits." Proc Natl Acad Sci U S A **104**(34): 13798-13803.
- Tang, Y., E. Pacary, T. Freret, D. Divoux, E. Petit, P. Schumann-Bard and M. Bernaudin (2006). "Effect of hypoxic preconditioning on brain genomic response before and following ischemia in the adult mouse: identification of potential neuroprotective candidates for stroke." Neurobiol Dis **21**(1): 18-28.
- Tixier, E., C. Leconte, O. Touzani, S. Roussel, E. Petit and M. Bernaudin (2008). "Adrenomedullin protects neurons against oxygen glucose deprivation stress in an autocrine and paracrine manner." J Neurochem **106**(3): 1388-1403.

- Tong da, Y., X. Wu, H. Sun, Y. Jin, Z. Liu and F. Zhou (2012). "Expression changes and regulation of AR and IGF-1 in PC3 prostate cancer cells treated with sexual hormones and flutamide." Tumour Biol **33**(6): 2151-2158.
- Tracy, K. and K. F. Macleod (2007). "Regulation of mitochondrial integrity, autophagy and cell survival by BNIP3." Autophagy **3**(6): 616-619.
- Tripodi, A., V. Chantarangkul, V. De Stefano and P. Mannucci (2000). "Alpha(2)-macroglobulin levels are high in adult patients with congenital antithrombin deficiency." Thromb Res **98**(2): 117-122.
- Turck, C. W., A. M. Falick, J. A. Kowalak, W. S. Lane, K. S. Lilley, B. S. Phinney, S. T. Weintraub, H. E. Witkowska and N. A. Yates (2007). "The Association of Biomolecular Resource Facilities Proteomics Research Group 2006 study: relative protein quantitation." Mol Cell Proteomics **6**(8): 1291-1298.
- Tyers, M. and M. Mann (2003). "From genomics to proteomics." Nature **422**(6928): 193-197.
- Uchida, M., J. M. Palmateer, P. S. Herson, A. C. DeVries, J. Cheng and P. D. Hurn (2009). "Dose-dependent effects of androgens on outcome after focal cerebral ischemia in adult male mice." J Cereb Blood Flow Metab **29**(8): 1454-1462.
- Unlü, M., M.E. Morgan, J.S. Minden (1997) "Difference gel electrophoresis: a single gel method for detecting changes in protein extracts." Electrophoresis **18**(11):2071-7.
- Valsecchi, V., G. Pignataro, A. Del Prete, R. Sirabella, C. Matrone, F. Boscia, A. Scorziello, M. J. Sisalli, E. Esposito, N. Zambrano, G. Di Renzo and L. Annunziato (2011). "NCX1 is a novel target gene for hypoxia-inducible factor-1 in ischemic brain preconditioning." Stroke **42**(3): 754-763.
- Vandenbogaert, M., S. Li-Thiao-Te, H. M. Kaltenbach, R. Zhang, T. Aittokallio and B. Schwikowski (2008). "Alignment of LC-MS images, with applications to biomarker discovery and protein identification." Proteomics **8**(4): 650-672.
- Villas-Boas, S. G., S. Mas, M. Akesson, J. Smedsgaard and J. Nielsen (2005). "Mass spectrometry in metabolome analysis." Mass Spectrom Rev **24**(5): 613-646.
- Villas-Boas, S. G., S. Rasmussen and G. A. Lane (2005). Metabolomics or metabolite profiles? Trends Biotechnol. England. **23:** 385-386.
- Violante, S., L. Ijlst, H. Te Brinke, I. Tavares de Almeida, R. J. Wanders, F. V. Ventura and S. M. Houten (2013). "Carnitine palmitoyltransferase 2 and carnitine/acylcarnitine translocase are involved in the mitochondrial synthesis and export of acylcarnitines." Faseb j **27**(5): 2039-2044.
- Virmani, A. and Z. Binienda (2004). "Role of carnitine esters in brain neuropathology." Mol Aspects Med **25**(5-6): 533-549.
- Vlasov, T. D., D. E. Korzhevskii and E. A. Polyakova (2005). "Ischemic preconditioning of the rat brain as a method of endothelial protection from ischemic/repercussion injury." Neurosci Behav Physiol **35**(6): 567-572.
- Voyksner, R. D. and H. Lee (1999). "Investigating the use of an octupole ion guide for ion storage and high-pass mass filtering to improve the quantitative performance of electrospray ion trap mass spectrometry." Rapid Commun Mass Spectrom **13**(14): 1427-1437.
- Wacker, B. K., T. S. Park and J. M. Gidday (2009). "Hypoxic preconditioning-induced cerebral ischemic tolerance: role of microvascular sphingosine kinase 2." Stroke **40**(10): 3342-3348.
- Wainwright, M. S., R. Kohli, P. F. Whitington and D. H. Chace (2006). "Carnitine treatment inhibits increases in cerebral carnitine esters and glutamate detected by mass spectrometry after hypoxia-ischemia in newborn rats." Stroke **37**(2): 524-530.
- Wang, Q., X. N. Tang and M. A. Yenari (2007). "The inflammatory response in stroke." J Neuroimmunol **184**(1-2): 53-68.
- Washburn, M. P., D. Wolters and J. R. Yates, 3rd (2001). "Large-scale analysis of the yeast proteome by multidimensional protein identification technology." Nat Biotechnol **19**(3): 242-247.
- Weaver, C. T., L. E. Harrington, P. R. Mangan, M. Gavrieli and K. M. Murphy (2006). "Th17: an effector CD4 T cell lineage with regulatory T cell ties." Immunity **24**(6): 677-688.
- Wegener, S., B. Gottschalk, V. Jovanovic, R. Knab, J. B. Fiebach, P. D. Schellinger, T. Kucinski, G. J. Jungehulsing, P. Brunecker, B. Muller, A. Banasik, N. Amberger, K. D. Wernecke, M. Siebler, J. Rother, A. Villringer and M. Weih (2004). "Transient ischemic attacks before ischemic stroke:

preconditioning the human brain? A multicenter magnetic resonance imaging study." Stroke **35**(3): 616-621.

- Weih, M., K. Kallenberg, A. Bergk, U. Dirnagl, L. Harms, K. D. Wernecke and K. M. Einhaupl (1999). "Attenuated stroke severity after prodromal TIA: a role for ischemic tolerance in the brain?" Stroke **30**(9): 1851-1854.
- Wenger, C. D. and J. J. Coon (2013). "A proteomics search algorithm specifically designed for high-resolution tandem mass spectra." J Proteome Res **12**(3): 1377-1386.
- Westerhuis J. A.,Hefsloot H. C. J., Smit S., Vis D. J., Smilde A. K., van Velzen E. J. J., van Duijnhoven D. J., van Dorsten F. A.(2008). "Assessment of PLSDA cross validation." Metabolomics **4**: 81–89.
- Wick, A., W. Wick, J. Waltenberger, M. Weller, J. Dichgans and J. B. Schulz (2002). "Neuroprotection by hypoxic preconditioning requires sequential activation of vascular endothelial growth factor receptor and Akt." J Neurosci **22**(15): 6401-6407.
- Wiegand, F., W. Liao, C. Busch, S. Castell, F. Knapp, U. Lindauer, D. Megow, A. Meisel, A. Redetzky, K. Ruscher, G. Trendelenburg, I. Victorov, M. Riepe, H. C. Diener and U. Dirnagl (1999). "Respiratory chain inhibition induces tolerance to focal cerebral ischemia." J Cereb Blood Flow Metab **19**(11): 1229-1237.
- Wilkins, M. R., C. Pasquali, R. D. Appel, K. Ou, O. Golaz, J. C. Sanchez, J. X. Yan, A. A. Gooley, G. Hughes, I. Humphery-Smith, K. L. Williams and D. F. Hochstrasser (1996). "From proteins to proteomes: large scale protein identification by two-dimensional electrophoresis and amino acid analysis." Biotechnology (N Y) **14**(1): 61-65.
- Wolburg, H. and A. Lippoldt (2002). "Tight junctions of the blood-brain barrier: development, composition and regulation." Vascul Pharmacol **38**(6): 323-337.
- Wold, S. (1991). "Chemometrics, why, what and where to next?" J Pharm Biomed Anal **9**(8): 589-596.
- Wysocki, V. H., K. A. Resing, Q. Zhang and G. Cheng (2005). "Mass spectrometry of peptides and proteins." Methods **35**(3): 211-222.
- Xia, J. and D. S. Wishart (2011). "Metabolomic data processing, analysis, and interpretation using MetaboAnalyst." Curr Protoc Bioinformatics **Chapter 14**: Unit 14.10.
- Yan, W. and S. S. Chen (2005). "Mass spectrometry-based quantitative proteomic profiling." Brief Funct Genomic Proteomic **4**(1): 27-38.
- Yang, W., Q. Ma, G. B. Mackensen and W. Paschen (2009). "Deep hypothermia markedly activates the small ubiquitin-like modifier conjugation pathway; implications for the fate of cells exposed to transient deep hypothermic cardiopulmonary bypass." J Cereb Blood Flow Metab **29**(5): 886-890.
- Yarmush, M. L. and A. Jayaraman (2002). "Advances in proteomic technologies." Annu Rev Biomed Eng **4**: 349-373.
- Yates, J. R., D. Cociorva, L. Liao and V. Zabrouskov (2006). "Performance of a linear ion trap-Orbitrap hybrid for peptide analysis." Anal Chem **78**(2): 493-500.
- Yenari, M., K. Kitagawa, P. Lyden and M. Perez-Pinzon (2008). "Metabolic downregulation: a key to successful neuroprotection?" Stroke **39**(10): 2910-2917.
- Yoshida, S., K. Aihara, Y. Ikeda, Y. Sumitomo-Ueda, R. Uemoto, K. Ishikawa, T. Ise, S. Yagi, T. Iwase, Y. Mouri, M. Sakari, T. Matsumoto, K. Takeyama, M. Akaike, M. Matsumoto, M. Sata, K. Walsh and S. Kato "Androgen receptor promotes sex-independent angiogenesis in response to ischemia and is required for activation of vascular endothelial growth factor receptor signaling." Circulation **128**(1): 60-71.
- Zhang, F. Y., X. C. Chen, H. M. Ren and W. M. Bao (2006). "Effects of ischemic preconditioning on blood-brain barrier permeability and MMP-9 expression of ischemic brain." Neurol Res **28**(1): 21-24.
- Zhang, H. X., G. H. Du and J. T. Zhang (2003). "Ischemic pre-conditioning preserves brain mitochondrial functions during the middle cerebral artery occlusion in rat." Neurol Res **25**(5): 471-476.

- Zhang, Y. B., S. X. Li, X. P. Chen, L. Yang, Y. G. Zhang, R. Liu and L. Y. Tao (2008). "Autophagy is activated and might protect neurons from degeneration after traumatic brain injury." Neurosci Bull **24**(3): 143-149.
- Zhu, W., J. W. Smith and C. M. Huang (2010). "Mass spectrometry-based label-free quantitative proteomics." J Biomed Biotechnol **2010**: 840518.
- Zwingmann, C. and D. Leibfritz (2003). "Regulation of glial metabolism studied by 13C-NMR." NMR Biomed **16**(6-7): 370-399.

CHAPTER 7

APPENDIX

7. PUBLICATIONS

Parts of the results of this thesis, were published in:

Scornavacca Giacomo, Gesuete Raffaella, Orsini Franca, Pastorelli Roberta , Fanelli Roberto, de Simoni Maria-Grazia, Airoldi Luisa. "Proteomic analysis of mouse brain cortex identifies metabolic down-regulation as a general feature of ischemic pre-conditioning"; J Neurochem. 2012 Sep;122(6):1219-29.

ACKNOWLEDGEMENTS

I would like to thank all the people who helped me during these years to grow up not only from a professional point of view but also from a human one.

First of all, I would like to express my deepest gratitude to my director of studies, Dr. Roberta Pastorelli for her constant guidance, expertise and encouragement.

I gratefully acknowledge Dr. Luisa Airoldi for her great support and Prof. David O'Connor for his supervision and valuable advices.

Special thanks to: Dr. Maria Grazia de Simoni and Raffaella Gesuete for their helpful collaboration in this research; Luigi Cappellini and Dr. Renzo Bagnati for their technical and instrumental assistance; Dr. Roberto Fanelli for the precious support.

I thank the IRCCS-Istituto di Ricerche Farmacologiche Mario Negri for giving me the opportunity to undertake my PhD.

Thanks also to all my colleagues and friends, in particular: Giorgio, Laura, Matteo, Miky, Roby and Rudy for the enjoyable time spent together.

Thanks to the Metal music that supports me in every moment of my life.

I dedicate this thesis to all my family (especially to Pippo, Fernanda and Davide) and Erika for offering me unconditional love, support and to put up with my bad temper...thanks.